2014

# Advanced Control of Small-Scale Power Systems with Penetration of Renewable Energy Sources

Shaghayegh Kazemlou
*Louisiana State University and Agricultural and Mechanical College*, skazem3@tigers.lsu.edu

# ADVANCED CONTROL OF SMALL-SCALE POWER SYSTEMS WITH PENETRATION OF RENEWABLE ENERGY SOURCES

A Dissertation

Submitted to the Graduate Faculty of the
Louisiana State University and
Agricultural and Mechanical College
in partial fulfillment of the
requirements for the degree of
Master of Science in Electrical Engineering

in
Department of Electrical and Computer Engineering

by
Shaghayegh Kazemlou
B.S., Sharif University of Technology, 2007
M.S., Sharif University of Technology, 2010
M.S., Louisiana State University, 2013
May 2015

# ACKNOWLEDGEMENTS

I would like to express my sincere gratitude to my advisor Dr. Shahab Mehraeen, for his encouragement and invaluable guidance throughout the research.

I would also like to acknowledge the invaluable help and assistance from the members of the committee, Dr. Leszek S. Czarnecki, Dr. Hsiao-Chun Wu, Dr. John R Smith, and also my general exam committee Dr. Ernest Mendrela. I express gratitude to all ECE staff specially Ms. Beth Cochran for being always supportive and helpful. I would also like to thank all my friends, colleagues and everyone from Louisiana State University who helped me throughout my dissertation research.

# TABLE OF CONTENTS

ACKNOWLEDGEMENTS ii

ABSTRACT v

CHAPTER 1. INTRODUCTION 1
1.1 Introduction 1
1.2 Past Work 4
1.3 Research Objective and Contributions 4
1.4 Definitions 7
1.5 References 8

CHAPTER 2. DECENTRALIZED DISCRETE-TIME ADAPTIVE NEURAL NETWORK CONTROL OF INTERCONNECTED DC DISTRIBUTION SYSTEM 11
2.1 Introduction 11
2.2 DC Grid Model 14
2.3 Buck Converter Discrete-Time Model 17
2.4 Discrete-Time Interconnected System Background 22
2.5 Nonlinear Discrete-Time Controller Design and Stability Analysis 25
2.6 Simulation Results 30
2.7 Conclusion 38
2.8 References 39

CHAPTER 3. DECENTRALIZED DISCRETE-TIME OUTPUT FEEDBACK CONTROL OF INTERCONNECTED DC DISTRIBUTION SYSTEM 43
3.1 Introduction 43
3.2 Interconnected DC Microgrid 44
3.3 Buck Converter Model 45
3.4 Output Feedback Controller Design 47
3.5 Simulation Results 53
3.6 Conclusion 59
3.7 References 60

CHAPTER 4. NOVEL DECENTRALIZED CONTROL OF POWER SYSTEMS WITH PENETRATION OF RENEWABLE ENERGY SOURCES IN SMALL-SCALE POWER SYSTEMS 61
4.1 Introduction 61
4.2 Renewable Generator Model 64
4.3 Decentralized Controller Design 71
4.4 Simulation Results 79
4.5 Conclusion 86
4.6 References 87

CHAPTER 5. CONCLUSIONS AND FUTURE WORK....90
5.1 Conclusions....90
5.2 Recommendation of Future Work....91

APPENDIX A....93

APPENDIX B....96

APPENDIX C....101

VITA....104

# ABSTRACT

Stability, protection, and operational restrictions are important factors to be taken into account in a proper integration of distributed energy. The objective of this research is presenting advanced controllers for small-scale power systems with penetration of renewable energy sources resources to ensure stable operation after the network disturbances.

Power systems with distributed energy resources are modeled and controlled through applying nonlinear control methods to their power electronic interfaces in this research. The stability and control of both ac and dc systems have been studied in a multi-source framework.

The dc distribution system is represented as a class of interconnected, nonlinear discrete-time systems with unknown dynamics. It comprises several dc sources, here called subsystems, along with resistive and constant-power loads (which exhibit negative resistance characteristics and reduce the system stability margins.) Each subsystem includes a dc-dc converter (DDC) and exploits distributed energy resources (DERs) such as photovoltaic, wind, etc. Due to the power system frequent disturbances this system is prone to instability in the presence of the DDC dynamical components and constant-power loads. On the other hand, designing a centralized controller may not be viable due to the distance between the subsystems (dc sources.) In this research it is shown that the stability of an interconnected dc distribution system is enhanced through decentralized discrete-time adaptive nonlinear controller design that employs neural networks (NNs) to mitigate voltage and power oscillations after disturbances have occurred.

The ac power system model is comprised of conventional synchronous generators (SGs) and renewable energy sources, here, called renewable generators (RGs,) via grid-tie inverters (GTI.) A novel decentralized adaptive neural network (NN) controller is proposed for the GTI that makes the device behave as a conventional synchronous generator. The advantage of this

modeling is that all available damping controllers for synchronous generator, such as AVR (Automatic Voltage Regulator) + PSS (Power System Stabilizer), can be applied to the renewable generator.

Simulation results on both types of grids show that the proposed nonlinear controllers are able to mitigate the oscillations in the presence of disturbances and adjust the renewable source power to maintain the grid voltage close to its reference value. The stability of the interconnected grids has been enhanced in comparison to the conventional methods.

# CHAPTER 1
# INTRODUCTION

## 1.1 Introduction

There has been an increasing trend towards the integration of renewable energy resources into the power networks in recent years, in order to address increasing electricity demands and reduce environmental pollution due to the widespread utilization of fossil fuels. The power grid components interaction and the impact of renewable energy sources including solar, hydro, biogas, biomass and wind, have been of the most important and challenging subjects of the power industry during the past few years, especially in micro grids [1]-[6]. Important factors to be taken into account in a proper integration of distributed energy resources include stability, protection, and operational restrictions to ensure stable operation after faults, load changes, and other network disturbances. High penetration levels of wind and solar energy can change power system dynamic characteristics, significantly affecting the stability of the system [2]-[4]. Excitation control, FACTS devices, and other power system controllers can play important roles in improving dynamic performance and maintaining the power system stability and reliability [4].

Many distributed energy resources (DERs) such as photovoltaic (PV,) variable-speed wind turbines, and storage devices can be connected to the dc grid through dc-dc converters (DDCs.) Therefore, the dc distribution system has attracted much attention as there is only one voltage conversion mechanism (i.e., dc-dc converter) between the power generators and the grid. This reduces system costs, as opposed to ac grids that require an additional dc-ac conversion. However, the dc distribution system employs constant power loads, which reduce grid stability margins by exhibiting negative resistance characteristics in the system.

Both ac and dc grids take advantage of power electronic interfaces that interface the renewable energy sources to the grid.

Each subsystem in dc distribution system, represents a distributed energy resource (such as photovoltaic source) connected to the grid through a dc-dc buck converter as shown in Fig. 1.1.

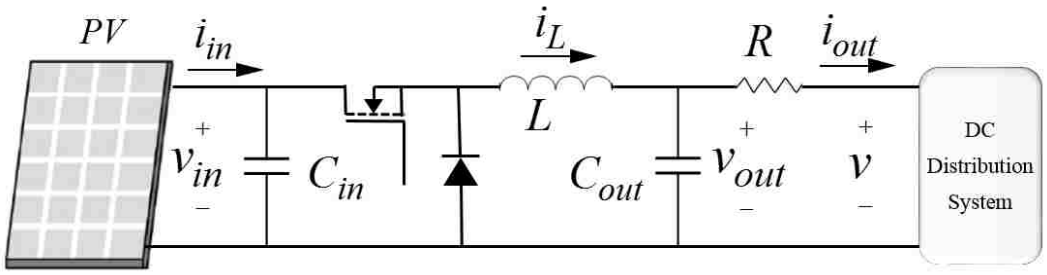


Fig. 1.1 photovoltaic source connected to dc grid through dc-dc buck converter.

Ac grids include distributed energy resources including conventional synchronous generators and renewable energy sources, here called renewable generators. Each renewable generator comprises a photovoltaic source connected to an inverter via a dc-dc converter as represented in Fig. 1.2.

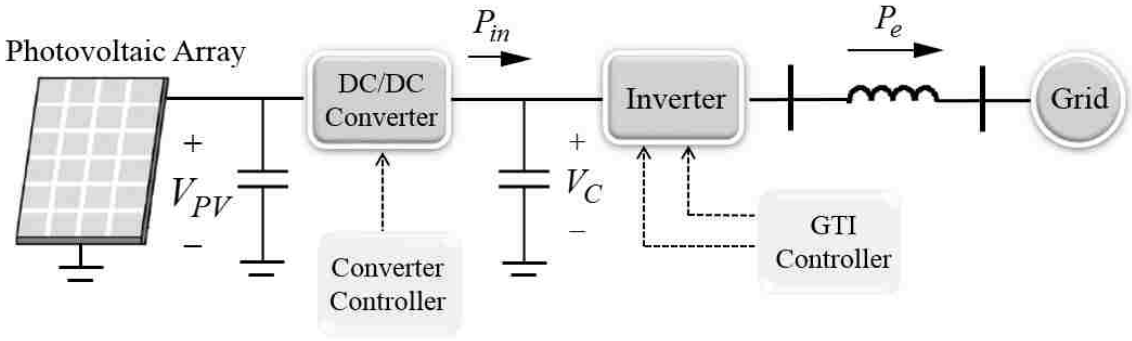


Fig. 1.2 Grid-connected renewable generator.

The existence of dynamic elements in DDC, such as capacitor and inductor as well as low-inertia power resources, such as photovoltaic (PV) systems, can cause undesired oscillatory

behaviors when disturbances occur in both ac and dc power systems. Particularly, in micro grids, faults, load changes, and other network disturbances affect the entire system more severely than in larger grids. Moreover, the frequent changes in the renewable power and loads can potentially aggravate the grid's stability.

On the other hand, a variety of control mechanisms may be applied to the grids with penetration of renewable energy sources to improve the stability of the grid. In order to design a linear controller the small signal model should be driven by linearization around an operating point. Linear controllers are easier to design and realize while nonlinear controllers are more advanced and can potentially lead to better performance and accuracy. These mechanisms can be implemented in centralized or decentralized forms. A centralized controller requires the information of the entire system while in decentralized controller only the local information in each subsystem is needed. In an interconnected system, a decentralized controller is usually preferred because it permits reduced amount of information exchange between subsystems, which leads to less time delays and computational burden. In addition, the controllers can be discrete-time or continuous-time. In discrete-time control, the controller is applied in certain time steps, which is usually equal to the sampling time while in continuous-time domain the controller is assumed to be applied continuously. The discrete-time controller is preferred for computer implementation because it considers the discrete-time natures of the hardware.

Advanced controllers can take advantage of adaptive mechanisms as opposed to fixed controller designs. In fixed controllers, the operational range is limited and relies on system's nature and operator expertise. In adaptive controllers, the controller adjusts automatically as needed during operation and can accommodate a wider range of operational conditions without much human interference.

## 1.2 Past Work

Several methods have been proposed aiming at a stabilized grid and often rely on small signal analysis [7]-[11] using linear systems control approaches; that is, they are only valid around a small neighborhood of an operating point. Also, they have not considered the interconnected nature of general dc grids where several loads and generations interact. The cases of a multi-load system have been studied in [5]-[6] and a large-signal stability method is proposed to ensure the entire system's stability. However, these methods rely on a constant voltage dc bus (Fig. 1.1), an assumption that may not be realized in many grids such as micro grids. The main drawback of the method presented in [5] is its centralized controller that requires obtaining the information from all subsystems.

Most of decentralized control schemes have been developed for nonlinear continuous-time systems [12]-[14] with less work in discrete-time systems [15]-[16] while the latter is preferred for computer implementation. For example, it is well-known that a stabilizing proportional controller for strictly proper plants can be unstable if discretized for the computer implementation [17]. Hence, the discrete-time natures of the system and the controller are explicitly taken into account in dc grid modeling and control design.

## 1.3 Research Objective and Contributions

This work aims at addressing aforementioned issues presenting novel decentralized nonlinear controllers for both interconnected ac and dc grids. In contrast with the conventional approaches, the proposed method considers the nonlinear nature of the entire grid. The proposed controllers are designed in decentralized forms and thus require minimal data acquisition. Specifically, component interactions and nonlinearities of the interconnected grid and low-inertia distributed energy resources (such as solar arrays) have been considered in the control design.

For all the proposed control methods, the stability of the entire grid is proven through thorough math.

Fig 1.3 explains this research that comprises two major parts; modeling and control. In modeling, the grid components including renewable sources (photovoltaic cells,) loads, and network are modeled in both ac and dc systems. Nonlinear nature of the components is considered in the modeling. Next, decentralized adaptive neural network controllers are designed for both continuous- and discrete-time systems. State and output feedback controller designs in decentralized framework are proposed to stabilize the grids.

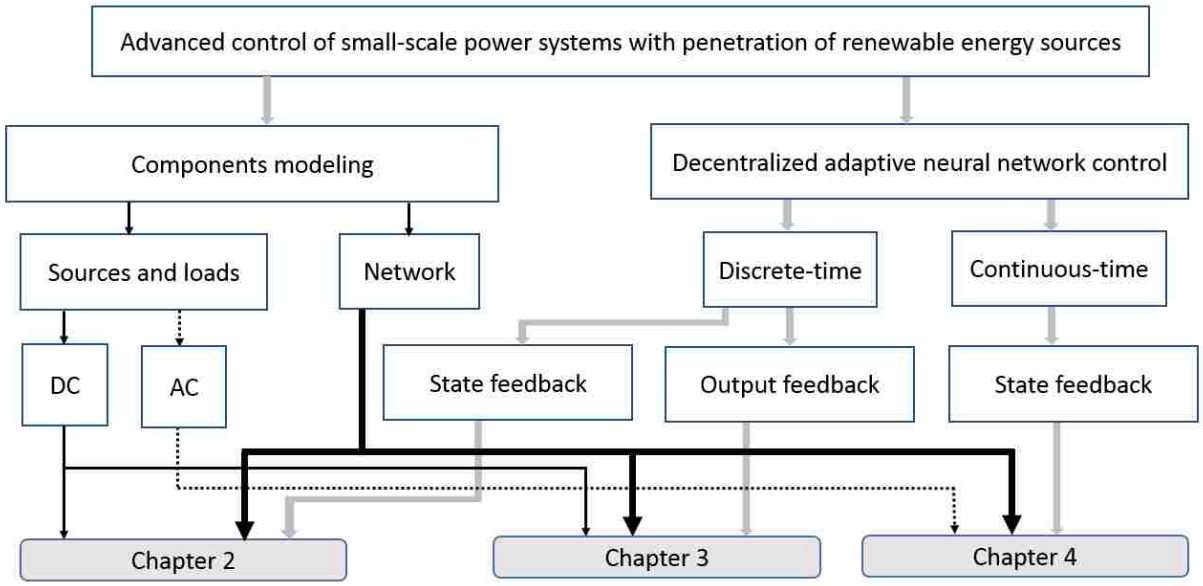


Fig 1.3 Research aspects flowchart

Each dc-dc converter in dc grid is modeled as a dynamical subsystem and the stability of the entire grid is investigated. The decentralized controller achieves transient stability and steady-state requirements based only on local information and measurements and the adaptive neural networks (NNs) are employed to approximate the unknown nonlinearities.

The renewable generator (RG) in the ac grid is modeled to behave as a synchronous generator (SG) with similar dynamics where the dc-link capacitor acts as the energy storage similar to the rotor of a SG. With the proposed modeling, the GTI resembles a synchronous generator with excitation control. The advantage of this modeling is that all available excitation control methods for synchronous generator can be applied to the renewable generator equipped with the proposed GTI excitation-like mechanism. Thus, the GTI can be controlled by excitation-like mechanisms such as AVR (Automatic Voltage Regulator) and PSS (Power System Stabilizer), as well as their nonlinear counterparts.

The contributions of this dissertation are:

- Nonlinear modeling and decentralized control of dc grids through adaptive neural network state feedback controller in discrete-time with proven stability
- Nonlinear modeling and decentralized control of dc grids through adaptive neural network output feedback controller in discrete-time with proven stability
- Nonlinear modeling and decentralized control of ac grids through adaptive neural network state feedback controller in continuous-time with proven stability

The rest of the dissertation is arranged in the following sequence. In Chapter 2 a dc interconnected network has been modeled in discrete-time domain and a decentralized neural network controller with state feedback method is proposed. This kind of controller can utilize output feedback method as proposed in Chapter 3. In Chapter 4 an ac network has been considered in continues-time domain and has been stabilized by a decentralized neural network controller using state feedback method. Chapter 5 includes the conclusion and suggestions for the future work.

### 1.4 Definitions

Neural network (NN) approximation [18]

A general function $f(x) \in \Re$ where $x \in \Re^m$ can be written as $f(x) = W^T \Phi(\bar{V}^T x) + \varepsilon(x)$ [14-15] in the compact set $\Lambda \in \Re^m$ (neural network approximation domain) with $\varepsilon(x)$ denotes neural network functional reconstruction error vector, $W \in R^{N \times 1}$ and $\bar{V} \in R^{m \times N}$ represent target neural network weight matrices.

Mean-value theorem [19]

Given an arc (differentiable) between two endpoints, there is at least one point at which the tangent to the arc is parallel to the secant through its endpoints: $f'(c) = \dfrac{f(b) - f(a)}{b - a}$

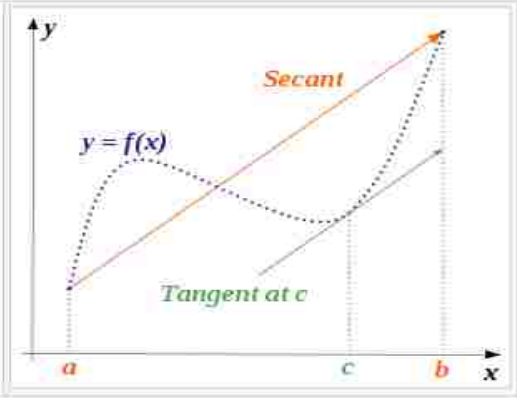


Fig 1.4 Arc and secant between two endpoints a and b

Uniform ultimate bounded (UUB) [18]

Consider the dynamical system $x(k+1) = f(x)$ with $x \in \Re^n$ being a state vector. Let the initial time step be $k_0$ and initial condition be $x_0 = x(k_0)$. Then, the equilibrium point $x_e$ is said

to be UUB if there exists a compact set $S \subset \Re^n$ so that for all $x_0 \in S$ there exists a bound B and a time step $K(B, x_0)$ such that $\|x(t) - x_e\| \leq B$ for $\forall k > k_0 + K$.

Constant power loads (CPLs) [7]

Power electronic converters when tightly regulated, behave as constant power loads (CPLs), which exhibit negative impedance characteristics and consequently reduce the grid stability margins.

**1.5 References**


[1] A. Bidram, A. Davoudi, and R. S. Balog, "Control and circuit techniques to mitigate partial shading effects in photovoltaic arrays," IEEE Journal of Photovoltaics, vol. 2, no. 4, pp. 532–546, 2012.

[2] Y. C. Chen and A. D. Garcia, "A method to study the effect of renewable resource variability on power system dynamics," IEEE Transaction Power Systems, vol. 27, no. 4, pp. 1978–1989, 2012.

[3] D. Gautam, V. Vittal, and T. Harbour, "Impact of increased penetration of DFIG-based wind turbine generators on transient and small signal stability of power systems," IEEE Transaction Power Systems, vol. 24, no. 3,pp. 1426–1434, 2009.

[4] S. Mehraeen, S. Jagannathan, and M. L. Crow, "Power system stabilization using adaptive neural network-based dynamic surface control," IEEE Transaction Power Systems, vol. 26, no. 2, pp. 669–680, 2011.

[5] P. Magne, B. Nahid-Mobarakeh, and S. Pierfederici, "General active global stabilization of multiloads dc-power networks," *IEEE Trans. Power Electronic*s, vol. 27, no. 4, pp. 1788–1798, 2012.

[6] P. Magne, B. Nahid-Mobarakeh, and S. Pierfederici, "Active stabilization of dc microgrids without remote sensors for more electric aircraft," *IEEE Trans. Industry Applications*, vol. 49, no. 5, pp. 2352–2360, 2013.

[7] A. Emadi, A. Khaligh, C. H. Rivetta, and G. A. Williamson, "Constant power loads and negative impedance instability in automotive systems: Definition, modeling, stability, and

control of power electronic converters and motor drives," *IEEE Trans. Vehicle Technology.*, vol. 55, no. 4, pp. 1112–1125, 2006.

[8] P. Liutanakul, A. Awan, S. Pierfederici, B. Nahid-Mobarakeh, and F. Meibody-Tabar, "Linear stabilization of a dc bus supplying a constant power load: A general design approach," *IEEE Trans. Power Electronics*, vol. 25, no. 2, pp. 475–488, 2010.

[9] A. M. Rahimi and A. Emadi, "Active damping in dc/dc power electronic converters: A novel method to overcome the problems of constant power loads," *IEEE Trans. Industrial Electronics*, vol. 56, no. 5, pp. 1428–1439, 2009.

[10] X. Liu, N. Fournier, and A. J. Forsyth, "Active stabilization of an HVDC distribution system with multiple constant power loads," in *Proc. IEEE VPPC*, Hei Longjiang, China, Sep. 2008, pp. 1–6.

[11] X.Liu, A.J. Forsyth, and A.M.Cross, "Negative input-resistance compensator for a constant power load," *IEEE Trans. Industrial Electronics*, vol. 54, no. 6, pp. 3188–3196, 2007.

[12] S. Jain and F. Khorrami, "Decentralized adaptive control of a class of large-scale interconnected nonlinear systems," *IEEE Trans. Automatic Control*, vol. 42, no. 2, pp. 136–154, 1997.

[13] B. Karimi, M.B. Menhaj, M. Karimi-Ghartemani, and I. Saboori, "Decentralized adaptive control of large-scale affine and nonaffine nonlinear systems," *IEEE Trans. Instrumentation and Measurement*, vol. 58, no. 8, pp. 2459–2467, 2009.

[14] J.T. Spooner and K.M. Passino, "Adaptive control of a class of decentralized nonlinear systems," *IEEE Trans. Automatic Control*, vol. 4 , no. 2, pp. 280–284, 1996.

[15] S. Jagannathan, "Decentralized discrete-time neural network controller for a class of nonlinear systems with unknown interconnections," in *Proc. IEEE International Symposium on Intelligent Cont.*, Limassol, Cyprus, June 2005, pp. 268–273.

[16] E. Gyurkovics and T. Takacs, "Stabilization of discrete-time interconnected systems under control constraints," *IEE Proceedings-Control Theory and Applications*, vol. 147, no. 2, pp. 137–144, 2000.

[17] K. J. Astrom and B. Wittenmark, "Computer Controlled Systems. Theory and Practice," 3rd ed., Prentice-Hall, Inc., Upper Saddle River, NJ,1997.

[18] F. L. Lewis, S. Jagannathan, and A. Yesildirek, “Neural network control of robot. manipulators and nonlinear systems,” Taylor & Francis, 1998.

[19] P.K. Sahoo and T. Riedel, “Mean Value Theorems and Functional Equations,” World Scientific Publishing Co., 1998.

# CHAPTER 2
# DECENTRALIZED DISCRETE-TIME ADAPTIVE NEURAL NETWORK CONTROL OF INTERCONNECTED DC DISTRIBUTION SYSTEM

## 2.1 Introduction

Many distributed energy resources (DERs) such as photovoltaic (PV,) variable-speed wind turbines, and storage devices can be connected to the dc grid through dc-dc converters (DDCs.) Therefore, the dc distribution system has attracted much attention [1]-[7], as there is only one voltage conversion mechanism (i.e., dc-dc converter) required between the power generators and the grid. This reduces system costs, as opposed to ac grids that require an additional dc-ac conversion. However, the dc distribution system employs constant power loads, which reduce grid stability margins [2]-[9]. Also, the existence of dynamic elements in DDC, such as capacitor and inductor as well as low-inertia power resources, such as photovoltaic (PV) systems, can produce undesired oscillatory behaviors when disturbances occur. Particularly, in micro grids, faults, load changes, and other network disturbances affect the entire system more severely than larger grids. Moreover, the frequent changes in the renewable power and loads can potentially aggravate the grid's stability. The main idea in [2]-[6] is to stabilize the system by "reshaping" the load impedance or the source impedance to improve the stability margins. These studies often rely on small signal analysis; that is, they are only valid around a small neighborhood of an operating point. Some other studies have looked into system stability using large signal analysis [7]-[11] and proposed nonlinear stabilization techniques. In [7], loop cancellation technique is applied to all converters loaded by CPLs to cancel the nonlinearity and obtain a stable system. However, the method relies on the existence of resistive loads. Also, synergetic and sliding-mode control techniques have been proposed in [12].

The aforementioned techniques present approaches to overcome the system instability; however, they have not considered the interconnected nature of general dc grids where several loads and generators interact. Examples of such systems include medium-size dc distributed generation systems and micro grids that employ multiple DERs.

The cases of a multi-load system have been studied in [13]-[14] and a large-signal stability method is proposed to ensure the entire system's stability. In these methods, a stabilizing power, which is determined by the relevant controller, must be absorbed by each load. However, the method relies on a constant voltage dc bus, an assumption that may not be realized in many dc power systems. The main drawback of the method presented in [13] is its centralized controller that requires obtaining the information from all subsystems. In an interconnected system, a decentralized control is usually preferred because it permits reduced amount of information exchange between subsystems, which leads to less time delays and reduces computational burden.

In recent years, there has been a continuous trend towards the decentralized control of interconnected nonlinear systems [15]-[19] for their increased reliability over the centralized control structure as mentioned earlier. The decentralized control schemes have been developed primarily for nonlinear continuous-time systems [15]-[17] with less work in discrete-time systems [18]-[19]. In discrete-time control, the controller is applied in certain time steps, which is usually equal to the sampling time while in continuous-time domain the controller is assumed to be applied continuously. The discrete-time controller is preferred for computer implementation [20] because it considers the discrete-time natures of the hardware. For example, it is well-known that a stabilizing proportional controller for strictly proper plants can

be unstable if discretized for the computer implementation [21]. Hence, the discrete-time natures of the system and the controller have to be explicitly taken into account in the design.

Limited work has been reported in the literature for decentralized control of dc systems to enhance a grid's stability. In [22] a decentralized predictive controller in discrete-time is developed and applied to dc-dc converters connected in parallel branches; however, interactions and nonlinearities of the interconnected dc grid and low-inertia DERs (such as solar arrays) are not considered in the control design. In [23] a decentralized controller approach is proposed for coordinated supplementary control of active and reactive power in high-voltage dc links in ac grids using linear controller design techniques. Finally, voltage droop control is proposed based on load sharing and linear system theory to stabilize the dc voltage [24]-[25].

A novel decentralized nonlinear neural network controller is proposed in this chapter for the interconnected dc grid in discrete-time. The dc grid is modeled as an interconnection of DERs connected to constant-power and resistive loads through DDCs. Then, adaptive NN controllers with online learning capabilities are employed to overcome uncertainties in the DDCs' dynamics and stabilize the output voltages in the event disturbances occur in the grid. Each DDC is modeled as a discrete-time dynamical subsystem and the stability of the entire dc grid is investigated. Though the proposed modeling and controller design can be applied to a variety of DERs, specific attention is paid to solar arrays to address low-inertia distribution systems and micro grids. Through the Lyapunov stability method the stability of all the DDCs' output voltages in the interconnected dc grid is proven using local states measurement.

In this chapter, first, the dc distribution grid topology is presented in section 2.2 followed by the developed DDC discrete-time model. In section 2.3, dynamic model of the buck converter is derived in canonical form. The dc network is then presented in the form of a nonlinear

interconnected discrete-time system in section 2.4, while it's associated decentralized NN controller development using state feedback is proposed in section 2.5. Simulation results on a low-voltage distribution grid and concluding remarks are presented in sections 2.6 and 2.7, respectively.

## 2.2 DC Grid Model

The *N*-bus interconnected dc grid comprising *n* subsystems (dc-dc converters) and "*N* - *n*" load buses is depicted in Fig. 2.1. Each subsystem represents a distributed energy resource connected to the grid through a dc-dc converter that is modeled by dynamical equations. The subsystems interconnect through the dc network that is governed by algebraic load-flow equations. Thus, the dc grid can be represented by, generally nonlinear, differential-algebraic equations. When converted to discrete-time model, the dc grid is modeled by difference-algebraic equations. In this section, the buck converter in continuous-current mode (CCM) operation is considered; however, other types of DDCs can be utilized and modeled in a similar way.

It is important to mention that boost converters are more attractive due to their ability to increase the output voltage that requires lower solar array voltage leading to fewer panels; however, their operating range is very limited [26],[27]. The advantage of the buck converter is its greater stability since unlike in the boost converter, output voltage in the buck converter is proportional to the duty cycle and does not grow exponentially, and thus, the duty cycle has a greater control range. In low-voltage applications, solar voltage connected through a step-down buck converter is conventional. Also, solar voltages up to 600V [28] are feasible through stacking the solar panels which in turn reduces the wiring connection losses in the panels due to lower currents [26]. On the other hand, if needed, voltage magnification can be provided by

using the forward converter that takes advantage of both transformer action and buck converter voltage adjustment. The forward converter can be modeled in a similar manner to the buck converter where the output voltage/current is multiplied/divided by the forward transformer's turns ratio.

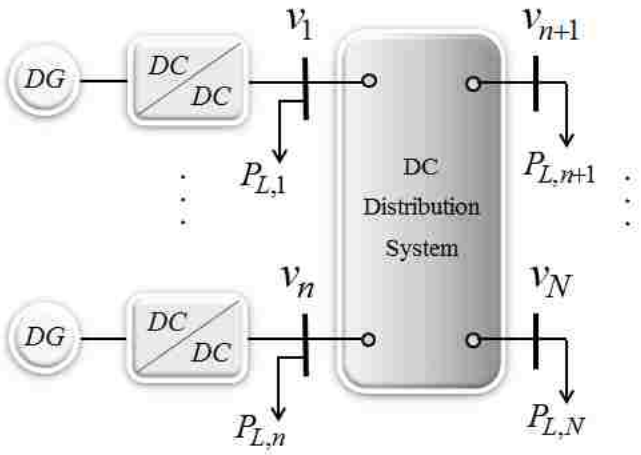


Fig. 2.1 *N*-bus dc distribution system, *n* generator buses and *N*-*n* non-generator buses, with load $P_{L,i}$ on bus '*i*'.

A typical buck converter topology that can interface a DER with the dc grid is represented in Fig. 2.2. Consider the converter's input and output capacitors' voltages, $v_{in,i}$ and $v_{out,i}$, and the inductor's current $i_{L,i}$ (Fig. 2.2) as the subsystem's state variables. Then, the dynamical equations describing the *i*-th subsystem (i.e., the *i*-th DDC) at time step *kT* (discretized in the switching period $T$) can be shown by

$$v_{in,i}((k+1)T) = C_{in,i}^{-1}[\int_{kT}^{(k+1)T} i_{in,i}(t)\,dt - \int_{kT}^{(k+d_i)T} i_{L,i}(t)\,dt] + v_{in,i}(kT)$$

$$i_{L,i}((k+1)T) = L_i^{-1}[\int_{kT}^{(k+d_i)T} v_{in,i}(t)\,dt - \int_{kT}^{(k+1)T} v_{out,i}(t)\,dt] + i_{L,i}(kT)$$

$$v_{out,i}((k+1)T) = C_{out,i}^{-1}\int_{kT}^{(k+1)T} (i_{L,i}(t) - i_{out,i}(t))\,dt + v_{out,i}(kT) \qquad (1)$$

where index $1 \le i \le n$ represents the subsystem (DDC) number, $n$ is the total number of subsystems , $T$ and $d_i$ are the converter switching period and duty cycle, respectively, and $L_i$, $C_{in,i}$ and $C_{out,i}$, are the converter's inductor, input capacitor, and output capacitor values, respectively. In addition, $i_{in,i}$ is the input current provided by the DER, and $k$ is the discrete step ($k \in Z^+$.)

*Remark 1*. Note that in the conventional DDC modeling the effects of the voltage and current variations during each switching cycle are ignored leading to the simplified equations

$$v_{in,i}((k+1)T) = T/C_{in,i} \times [i_{in,i}(kT) - d_i\, i_{L,i}(kT)] + v_{in,i}(kT)$$

$$i_{L,i}((k+1)T) = T/L_i \times [d_i\, v_{in,i}(kT) - v_{out,i}(kT)] + i_{L,i}(kT)$$

$$v_{out,i}((k+1)T) = T/C_{out,i} \times [i_{L,i}(kT) - i_{out,i}(kT)] + v_{out,i}(kT)\,. \qquad (2)$$

From now on, the switching time $T$ is removed from the time index for simplicity; for instance, $v_{in,i}(kT)$ is shown by $v_{in,i}(k)$.

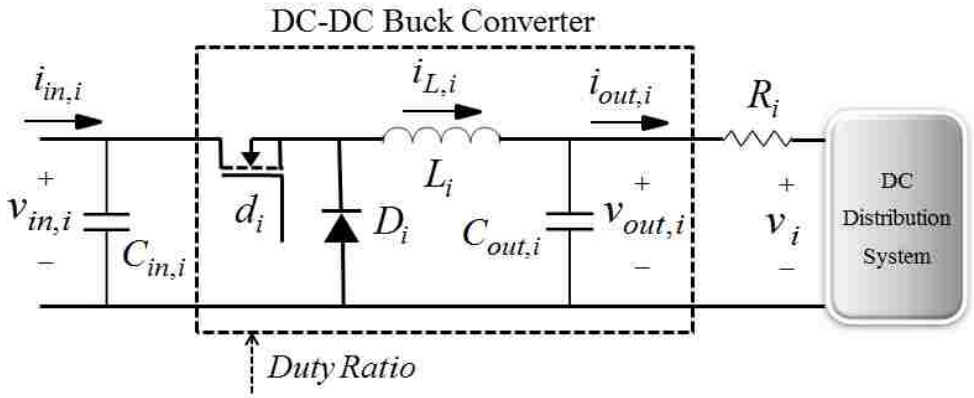


Fig. 2.2 Dc-dc buck converter.

*Remark 2*. Output current $i_{out,i}(k)$ in (1) generally depends on the grid's bus voltage vector $[v_{out,1},\ldots,v_{out,n},v_1,v_2,\ldots,v_N]^T$. However, grid voltages $[v_1,v_2,\ldots,v_N]^T$ can be obtained from

DDC output voltage vector $[v_{out,1}, v_{out,2}, \ldots, v_{out,n}]^T$ by solving the load-flow equations for $[v_1, v_2, \ldots, v_N]^T$.

In the next section, the discrete-time interconnected dc grid model will be obtained.

**2.3 Buck Converter Discrete-Time Model**

In this section, the buck converter discrete-time model (1) is represented in Brunovsky canonical form [29]. The presented modeling and proposed controller aim at stabilizing the buck converter output voltage in an interconnected dc network and in the presence of PV power generators as the source of electric power. Thus, no storage is considered in the system model to avoid extra costs to the network. Also, no high-power constant dc source, such as rectified ac-dc power, is assumed in the grid to include isolated micro grids. As the network undergo faults and disturbances, the dc voltage fluctuates in the network affecting the solar power generation in a nonlinear fashion which could potentially lead to the entire network instability and voltage collapse. Thus, in this work the goal is to stabilize the converter output voltages through an adaptive control scheme by using the learning capability of the NNs leading to an enhanced stability of such interconnected dc grids. The proposed controller alters the converter's duty cycle to attain the stability through an adaptive scheme while taking the converter input and output voltages and currents as the only measurable states to the selected converter; thus, no communications are assumed between the converters to simplify the controller structure.

In this section, several steps are carried out to convert dynamics (1) to a standard controllable representation. First, error dynamics are derived around the steady-state operating points. Next, the unknown functions in the error dynamics are expanded and elaborated. Subsequently, new converter dynamic representation is presented by assigning the converter

output voltage as the controlled variable and a supplementary duty cycle as the control input. Finally, a discussion on the stability of the converter unobservable state is carried out.

Recall that each DDC, which connects a DER to the dc grid, is considered as a subsystem. Equations (1) model buck converter '*i*' dynamics as functions of subsystem state variables $x_i(k) = [v_{in,i}(k), i_{L,i}(k), v_{out,i}(k)]^T$ (values defined at the beginning of the switching interval.) Subtracting the steady-state values $x_{oi} = [v_{ino,i}, i_{Lo,i}, v_{outo,i}]^T$ from the actual values, the state error vector can be calculated as $\hat{x}_i(k) = x_i(k) - x_{oi} = [\hat{v}_{in,i}(k), \hat{i}_{L,i}(k), \hat{v}_{out,i}(k)]^T$. Also, $\hat{i}_{in,i}(k) = i_{in,i}(k) - i_{ino,i}$ and $\hat{i}_{out,i}(k) = i_{out,i}(k) - i_{outo,i}$ are the converter input and output current errors, respectively.

In this work, the errors are aimed to be made zero that in turn makes the converter output voltage approach its steady-state value. This procedure is conducted through synthesizing an additional duty cycle $\hat{d}_i$ (defined later) to be added to the steady-state duty cycle $d_{o,i}$ mitigating the errors. The scheme stabilizes the network around the nominal converter output voltage in the presence of the grid disturbances.

Dynamics $\hat{v}_{in,i}((k+1)T)$, $\hat{i}_{L,i}((k+1)T)$, and $\hat{v}_{out,i}((k+1)T))$ in (1) are in general functions of the state error vector $\hat{x}_i(k)$ and output current error $\hat{i}_{out,i}(k)$; however, it is difficult to obtain closed-form representations of these dynamics, and thus, these functions are unknown. Subsequently, the error dynamics are represented as unknown functions of the errors

$$\hat{v}_{in,i}((k+1)) = h_1(\hat{x}_i(k), d_i)$$

$$\hat{i}_{L,i}((k+1)) = h_2(\hat{x}_i(k), d_i)$$

$$\hat{v}_{out,i}((k+1)) = h_3(\hat{x}_i(k)) + \vartheta_i(\hat{i}_{out,i}(k)). \quad (3)$$

As mentioned earlier, since the integrals in (1) cannot be easily converted to closed-form functions of the states without simplification mentioned in Remark 1, functions $h_{1,i}(.)$, $h_{2,i}(.)$, $h_{3,i}(.)$, and $\vartheta_i(.)$ are unknown. While, $h_{1,i}(.)$, $h_{2,i}(.)$ and $h_{3,i}(.)$ are functions of the converter state errors $\hat{x}_i(k)$ (available at converter '$i$' location,) $\vartheta_i(.)$ is a function of the entire grid state errors since $\hat{i}_{out,i}(k)$ depends on the other converters states, as explained in Remark 2. These states are not available at converter '$i$' location due to the controllers' decentralized structure.

Next, for the convenience of control design, dynamics (3) are presented in canonical form. One can take $\hat{v}_{out,i}(k)$ along with its next step value as new state variables $\xi_i = [\xi_{1,i}, \xi_{2,i}]^T$ for converter '$i$' and perform input-output feedback linearization [29] as follows

$$\xi_{1,i}(k) = \hat{v}_{out,i}(k)$$

$$\xi_{1,i}(k+1) = \hat{v}_{out,i}(k+1) = \xi_{2,i}(k)$$

$$\xi_{2,i}(k+1) = \hat{v}_{out,i}(k+2). \quad (4)$$

According to (1) (and (2),) in obtaining $\hat{v}_{out,i}(k+2)$ it is noted that the future step of output current ($\hat{i}_{out,i}(k+1)$) is needed that cannot be measured. As explained earlier (Remark 2,) the output current can be obtained as a function of all subsystems' output voltages; i.e., $\hat{i}_{out,i}(k+1) = \vartheta_i(\hat{v}_{out,1}(k+1),\ldots,\hat{v}_{out,n}(k+1))$. Thus, $\hat{i}_{out,i}(k+1)$ is a function of $\xi(k) = [\xi_1(k),\ldots,\xi_n(k)]^T$ according to (4). Consequently, $\xi_{2,i}(k+1)$ in (4) can be expressed as

$\xi_{2,i}(k+1) = h_{4,i}(\hat{x}_i(k), d_i) + \Delta_i(\xi(k))$ where $h_{4,i}(\hat{x}_i(k), d_i) = h_{3,i}(\hat{x}_i(k+1))$ is obtained from the last equation in (3).

Output current $\hat{i}_{out,i}(k+1)$ (and thus, function $\Delta_i(\xi(k))$) cannot be computed since other DDCs' states are not available at subsystem '*i*' location. Function $\Delta_i(\xi(k))$ depends on the entire system state vector $\xi(k)$ and is called the interconnection term [30] that is a function of all the converters' states, some of which are unavailable.

Next, by utilizing mean-value theorem [31] around $d_i = d_{o,i}$, function $h_{4,i}(\hat{x}_i(k), d_i)$ can be rewritten as

$$h_{4,i}(\hat{x}_i(k), d_i) = f_i(\hat{x}_i(k)) + g_i(\hat{x}_i(k))u_i(\hat{x}_i(k)) \tag{5}$$

where $d_{o,i}$ is the steady-state duty cycle, $u_i = \hat{d}_i$ is the state feedback control input, $\hat{d}_i = d_i - d_{o,i}$, $f_i(\hat{x}_i(k)) = h_{4,i}(\hat{x}_i(k), d_{o,i})$, and $g_i(\hat{x}_i(k)) = \partial h_{4,i} / \partial d_i \big|_{d_{o,i} + \bar{d}_i(\hat{d}_i)}$ with $\bar{d}_i$ being an appropriate function of $\hat{d}_i$. Therefore, according to (4) and (5), converter state-space equations can be rewritten in canonical form as

$$\xi_{1,i}(k+1) = \xi_{2,i}(k)$$

$$\xi_{2,i}(k+1) = f_i(\hat{x}_i(k)) + g_i(\hat{x}_i(k))u_i(k) + \Delta_i(\xi(k)) \tag{6}$$

with $u_i = \hat{d}_i$ as the subsystem's input and unknown nonlinear functions $f_i(\hat{x}_i(k))$, $g_i(\hat{x}_i(k))$, and $\Delta_i(\xi)$.

In summary, new representation (6) is presented that involves local states $\xi_{1,i}(k)$, $\xi_{2,i}(k)$, and state error vector $\hat{x}_i(k)$ as well as generally unavailable grid states $\xi_{2,j}(k)$ for

$j = 1,\ldots,n; j \neq i$. Also, due to unknown functions involved in dynamic representation (1), $f_i(\hat{x}_i(k))$, $g_i(\hat{x}_i(k))$, and $\Delta_i(\xi)$ are unknown.

Dynamics represented in (4) are only of order two while the converter original dynamics (1) are of order three. That is, one of the dynamics has been neglected in this procedure. With respect to the design variable $\hat{v}_{out,i}(k)$, the additional dynamic is *unobservable* and is known as *internal dynamics* [29]. The internal dynamics constitute the *zero dynamics* when the designed observable states (here $\xi_i = [\xi_{1,i}, \xi_{2,i}]^T$) tend to zero and must be stable to assure the overall network stability (*minimum-phase* system [29].) In the proposed design, $\hat{v}_{in,i}(k)$ is taken as the subsystem zero dynamic, that is,

$$\hat{v}_{in,i}((k+1)) = h_1(\hat{x}_i(k)). \tag{7}$$

Input current $i_{in,i}$ is fed to the converter from a DER and can be considered as a function of converter input voltage $i_{in,i} = \Psi_i(v_{in,i})$. The characteristics of function $\Psi_i(.)$ play an important role in attaining stable internal dynamic, which will be discussed in section V. In order to achieve stable internal dynamic, the DER requires certain design considerations, as will be explained.

*Remark 3.* In order to assure system stability, the following DDC properties are elaborated and utilized. First, it is worthwhile to mention that $v_{in,i}(k)$ (DER interface voltage) has a maximum. Also, as this work investigates the voltage and power fluctuations, it is reasonable to assume that $v_{in,i}(k)$ stays away from zero. These result in $0 < g_{i,\min} \leq g_i(\hat{x}_i(k)) \leq g_{i,\max}$. For convenience, if the simplified model of Remark 1 is considered, $g_i(\hat{x}_i(k))$ is bounded between

$g_{i,\min} = T^2 / (L_i\, C_{out,i}) \times v_{in,i,\min}$ and $g_{i,\max} = T^2 / (L_i\, C_{out,i}) \times v_{in,i,\max}$. Second, according to (3) in all subsystems the interconnection terms $\Delta_i(\xi)$ are functions of output current errors and consequently have small values as long as the step time (or equivalently DDC switching time) is small. For example, using the simplified model, a switching frequency of 10 kHz and output capacitor of 10 mF introduces a factor of 0.01 to the output current error. Further reduction in the step time *T* and/or an increase in the output capacitor size reduces $\Delta_i(\xi)$.

It is noteworthy that the buck converter model in discontinuous-current mode (DCM) can be represented in a similar manner to dynamics (1) as

$$v_{in,i}((k+1)T) = C_{in,i}^{-1}[\int_{kT}^{(k+1)T} i_{in,i}(t)\,dt - \int_{kT}^{(k+d_i)T} i_{L,i}(t)\,dt] + v_{in,i}(kT)$$

$$v_{out,i}((k+1)T) = C_{out,i}^{-1}\int_{kT}^{(k+1)T} (i_{L,i}(t) - i_{out,i}(t))\,dt + v_{out,i}(kT).$$

Note that the discrete inductor current is zero at all sampling times (beginning of switching cycle) and can be removed from the states since one may solve for the current using input and output voltages at discrete steps. Also, the unknown dynamics from the DCM operation can be represented in the form of equations (6). Though the focus is only on the converter CCM operation, the NN controller developed in the next section may be applied to both continuous and discontinuous system representations since the utilized approximation property of the NN holds for both types of systems [29] as will be

**2.4 Discrete-Time Interconnected System Background**

A class of discrete-time interconnected systems consisting of *n* subsystems (DDCs) can be represented in canonical form as

$$\xi_{p,i}(k+1) = \xi_{p+1,i}(k);\ 1 \le p \le l-1)$$

$$\xi_{l,i}(k+1) = f_i(\hat{x}_i(k)) + g_i(\hat{x}_i(k))u_i(k) + \Delta_i(\xi(k))$$

$$y_i(k) = \xi_{1,i}(k) \tag{8}$$

for $1 \le i \le n$ where $\xi_i = [\xi_{1,i}, \ldots, \xi_{l,i}]^T$ is the state error vector of subsystem '$i$' after conducting input-output feedback linearization, $l$ is the order of the subsystem ($l = 2$ according to model (4),) $f_i(\hat{x}_i(k))$ denotes internal dynamics, $g_i(\hat{x}_i(k))$ is the input gain and $\Delta_i(\xi(k))$ represents the interconnection effects with $\xi = [\xi_1^T, \ldots, \xi_n^T]^T$ and $\hat{x}_i$ is the original subsystem states errors from which the input-output feedback linearization was derived as explained in (4) and (6). Functions $f_i(\hat{x}_i(k))$ and $g_i(\hat{x}_i(k))$ can in general be nonlinear functions of states. It is desired to design a controller that stabilizes $\xi$ at the origin ($\xi = 0$.) Thus, filtered error is defined as

$$r_i(k) = [\lambda_i \ 1]^T \xi_i(k) \tag{9}$$

where $\lambda_i = [\lambda_{1,i}, \ldots, \lambda_{l-1,i}]^T$ and $\lambda_{1,i}$ through $\lambda_{l-1,i}$ are chosen in such a way that place the poles of the characteristic equation $\kappa(s) = \lambda_{1,i} + \lambda_{2,i}s + \cdots + \lambda_{l-1,i}s^{l-2} + s^{l-1}$ inside the unit disc. In constructing filtered error $r_i(k)$ in (9) for the DDC an estimate of state $\xi_{2,i}(k)$ maybe used by employing simplified model of Remark 1 as illustrated in Fig. 2.3. This doesn't affect the convergence of the DDC output voltage since filtered error utilizes state $\xi_{1,i}(k)$ as well. The design proceeds by two assumptions and one definition.

*Assumption 1*- Functions $g_i(x_i(k))$ are bounded and away from zero for $1 \le i \le n$. That is,

$$0 < g_{i,\min} \le g_i(\hat{x}_i(k)) \le g_{i,\max} \tag{10}$$

where $g_{i,\min}$ and $g_{i,\max}$ are positive real constants. This is a valid assumption for the dc grid as discussed in Remark 3 and is less restrictive than unity control gain ($g_i(\hat{x}_i(k)) = 1$) in the past literature [18].

*Assumption 2 [29]-* The interconnection terms are bounded by a function of the states such that $\Delta_i(\xi) \le \sigma_{0i} + \sum_{j=1}^{N} \eta_{ij} \left\| \xi_j \right\|_2$ where $\sigma_{0i}$ and $\eta_{ij}$ are positive constants for $1 \le i \le n$. The filtered error $r_j(k)$ converges to zero whenever states $\xi_j(k)$ converge to zero. Similar to continuous-time systems [30] this further implies that

$$\Delta_i(\xi) \le \sum_{j=1}^{n} \delta_{ij}(r_j) \le \delta_{0i} + \sum_{j=1}^{n} \gamma_{ij} \left| r_j \right| \tag{11}$$

where $\delta_{ij}$ is a positive function while $\delta_{0i}$ and $\gamma_{ij}$ are positive constants for $1 \le i \le n$ and $1 \le j \le l$. In addition, the effects of the interconnection terms are assumed weak compared to the subsystem dynamics. That is, $\delta_{0i}$ and $\gamma_{ij}$ are small values, which is valid in the dc grid as explained in Remark 3. This assumption is less stringent than that of [18] with constant bounds on the interconnection terms.

*Definition.* **(**Uniform Ultimate Bounded (UUB)) [29]. Consider the dynamical system $x(k+1) = f(x)$ with $x \in \Re^n$ being a state vector. Let the initial time step be $k_0$ and initial condition be $x_0 = x(k_0)$. Then, the equilibrium point $x_e$ is said to be UUB if there exists a compact set $S \subset \Re^n$ so that for all $x_0 \in S$ there exists a bound $B$ and a time step $K(B, x_0)$ such that $\|x(k) - x_e\| \le B$ for $\forall k > k_0 + K$.

## 2.5 Nonlinear Discrete-Time Controller Design and Stability Analysis

In this section, a state feedback controller for the discrete-time interconnected system (1) is presented and NN function approximation [29] is employed to overcome the unknown dynamics of each subsystem. The NN controller utilizes an adaptive NN weight tuning scheme which is conducted online with no need to utilize large data sets as in offline training schemes.

A. Nonlinear Controller Design

The filtered error dynamic in (9) can be derived using (8) as

$$r_i(k+1) = [\lambda_i \ \ 1]^T \xi_i(k+1)$$

$$= g_i(\hat{x}_i(k))\left( \frac{f_i(\hat{x}_i(k)) + [0 \ \ \lambda_i]^T \xi_i}{g_i(\hat{x}_i(k))} + u_i + \frac{\Delta_i(\xi_i(k))}{g_i(\hat{x}_i(k))} \right). \tag{12}$$

The goal is to achieve asymptotically stable filtered error dynamics in the form of $r_i(k+1) = K_i g_i(x_i(k)) r_i(k)$ (with $0 < K_i < 1/g_{i,\max}$) in the absence of the interconnection terms. Thus, one can define the stabilizing control as

$$u_i = u_i^* = u_{id} + K_i \, r_i(k) \tag{13}$$

where

$$u_{id} = -g_i(\hat{x}_i(k))^{-1}\left( f_i(\hat{x}_i(k)) + [0 \ \ \lambda_i]^T \xi_i(k) \right). \tag{14}$$

In practice, the internal dynamics $f_i(\hat{x}_i(k))$ and input gain $g_i(\hat{x}_i(k))$ may be uncertain or difficult to obtain as explained in Section 2.3, and thus, $u_{id}$ is unavailable. Thus, NN function approximation property is employed to approximate $u_{id}$ [29] using the available states as

$$u_{id} = -g_i(\hat{x}_i(k))^{-1}\left( f_i(\hat{x}_i(k)) + [0 \ \ \lambda_i]^T \xi_i(k) \right) = \theta_i^T \mu_i(\hat{x}_i(k), \xi_i(k)) - \varepsilon_i(\hat{x}_i(k), \xi_i(k)) \tag{15}$$

where $\theta_i$ is the target NN weight matrix, $\mu_i(.)$ is the activation function and a basis function [31], and $\varepsilon_i(.)$ is the NN function approximation error that satisfies $\|\varepsilon_i(.)\| \le \varepsilon_{i,\max}$ [29] in a compact set $\Lambda$ comprising all possible variations of variables $\hat{x}_i = [\hat{v}_{in,i}, \hat{i}_{L,i}, \hat{v}_{out,i}]$. In practice, only an estimation of the target NN weights $\theta_i$ is available.

From now on, for simplicity, $\mu_i$ and $\varepsilon_i$ are utilized to represent $\mu_i(\hat{x}_i(k))$ and $\varepsilon_i(\hat{x}_i(k))$, respectively. Thus, $u_{id}$ is approximated as $\hat{u}_{id}$, which renders controller $u_i$ in (13) as

$$u_i = \hat{u}_{id} + K_i r_i(k) = \hat{\theta}_i^T(k)\mu_i + K_i r_i(k) \tag{16}$$

where $\hat{\theta}_i^T(k)$ is the NN weight estimation matrix. The block diagram of the converter's NN controller is depicted in Fig. 2.3. In the figure all the input variables are discretized at the sample time *k*T.

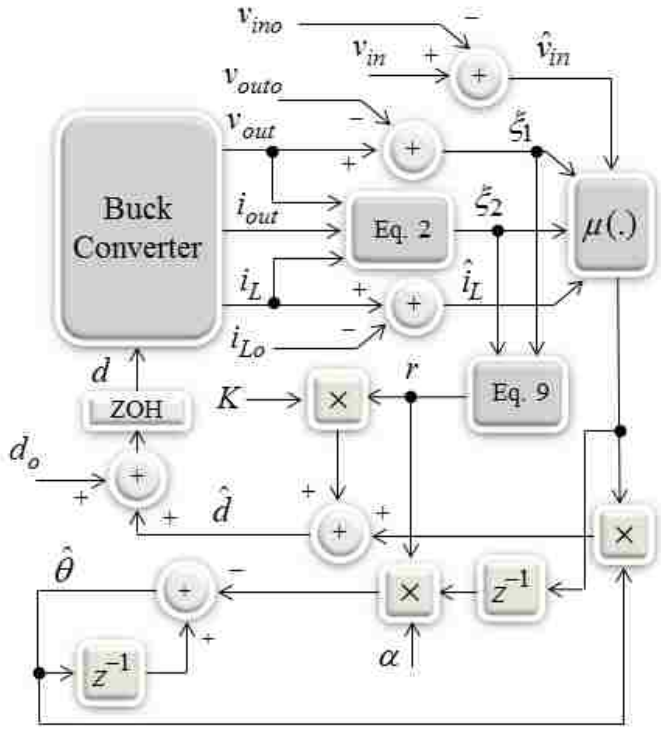


Fig. 2.3 Converter NN controller.

B. Stability Analysis

By replacing $u_i$ from (16) in (12), the filtered error dynamic becomes

$$r_i(k+1) = [\lambda_i \ \ 1]^T \xi_i(k+1) = f_i(\hat{x}_i(k)) + [0 \ \ \lambda_i]^T \xi_i(k)$$

$$+ g_i(\hat{x}_i(k))\left(\hat{\theta}_i^T(k)\mu_i + K_i r_i(k)\right) + \Delta_i(\xi(k)). \tag{17}$$

The weight estimation error is defined as $\tilde{\theta}_i = \hat{\theta}_i - \theta_i$, and thus, by adding and subtracting $u_{id}$, (17) can be rewritten as

$$r_i(k+1) = g_i(x_i(k))\left(\tilde{\theta}_i^T \mu_i + \varepsilon_i + K_i r_i(k)\right) + \Delta_i(\xi(k). \tag{18}$$

Next, define the NN weight update law [32] as

$$\hat{\theta}_i^T(k+1) = \hat{\theta}_i(k) - \alpha_i \mu_i r_i(k+1) \tag{19}$$

where $0 < \alpha_i < 1$ is a positive design constant. Subtracting the target weights from (19), one has

$$\tilde{\theta}_i^T(k+1) = \tilde{\theta}_i(k) - \alpha_i \mu_i r_i(k+1). \tag{20}$$

Provided that the NN weight update is obtained by (19) and control gains $K_i$ and $\alpha_i$ in (16) and (19) are chosen properly, the states $\xi_{p,i}$ approach zero for all $1 \le i \le n$ and $1 \le p \le l$ in UUB fashion; i.e, they stay in close proximity of the origin. Unknown nonlinearities in the subsystems are approximated by NNs whose weights are calculated using (19).

The stability of the nonlinear discrete-time interconnected system (1) in the presence of unknown dynamics $f_i(\hat{x}_i(k))$ and input gain $g_i(\hat{x}_i(k))$, and unknown interconnection terms $\Delta_i(\xi(k))$ for $1 \le i \le n$ is proven by showing the stability of weight estimation errors $\tilde{\theta}_i(k)$ and the filtered errors $r_i(k)$ for all $1 \le i \le n$ and is given in Appendix A. The filtered error $r_i(k)$, and consequently $\xi_i(k)$, converge to zero for all $1 \le i \le n$ as explained.

Next, one should assure that zero dynamics $\hat{v}_{in,i}(k)$ (as described in Section 2.3) are stable for $1 \le i \le n$ when the observable states $\xi_i = [\xi_{1,i}\ ,\ \xi_{2,i}]^T$ are zero. In order to prove the stability of the zero dynamic, here the simplified model of Remark 1 is used for convenience.

According to Remark 1, the zero dynamic is driven by

$$\hat{v}_{in,i}(k+1) = T/C_{in,i} \times [\Psi_i(v_{in,i}(k)) - d_i\, i_{L,i}(k)] + \hat{v}_{in,i}(k)\ . \tag{21}$$

When the output variable $\hat{v}_{out,i}(k)$ is zero, the controlled system (4) is at the equilibrium; that is, $v_{out,i}(k) = v_{outo,i}$, $i_{L,i}(k) = i_{Lo,i}$, and $d_i(k) = d_{o,i}$, and thus, observable states $\xi_i(k) = 0$. Consequently, at equilibrium, (21) becomes

$$\hat{v}_{in,i}(k+1) = T/C_{in,i} \times [\Psi_i(v_{in,i}(k)) - d_{o,i}\, i_{Lo,i}] + \hat{v}_{in,i}(k)\ . \tag{22}$$

Consider the Lyapunov function candidate $\Gamma = \hat{v}_{in,i}{}^2(k)$. Then, the first difference of the Lyapunov function is

$$\Delta\Gamma = \hat{v}_{in,i}{}^2(k+1) - \hat{v}_{in,i}{}^2(k)\,. \tag{23}$$

By using (22), (23) can be calculated as

$$\begin{aligned}\Delta\Gamma &= (T/C_{in,i})^2 \times [\Psi_i(v_{in,i}(k)) - d_{o,i}\, i_{Lo,i}]^2 + \hat{v}_{in,i}{}^2(k) \\ &+ 2T/C_{in,i} \times [\Psi_i(v_{in,i}(k)) - d_{o,i}\, i_{Lo,i}]\hat{v}_{in,i}(k) - \hat{v}_{in,i}{}^2(k)\end{aligned} \tag{24}$$

which results in

$$\begin{aligned}\Delta\Gamma &= (T/C_{in,i})^2 \times [\Psi_i(v_{in,i}(k)) - d_{o,i}\, i_{Lo,i}]^2 \\ &+ 2T/C_{in,i} \times [\Psi_i(v_{in,i}(k)) - d_{o,i}\, i_{Lo,i}]\hat{v}_{in,i}(k)\,.\end{aligned} \tag{25}$$

For photovoltaic source considered here, $i_{in,i}(k)$ is a nonlinear function of $v_{in,i}(k)$ in the form of

$$i_{in,i}(k) = \Psi(v_{in,i}(k)) = n_{pi}\,(I_{sc} - I_{rs}(e^{\,v_{in,i}(k)/(V_T\,n_{si})} - 1)) \tag{26}$$

where $n_{pi}$ and $n_{si}$ are the numbers of the parallel strings and series panels forming the PV generator [33], respectively, $V_T$ is thermal voltage, $I_{sc}$ is the short circuit current and $I_{rs}$ denotes the reverse saturation current [28].

The derivative of the solar current with respect to the panel voltage is negative. That means, for an increase in the voltage the current decreases. In other words, one has

$$\Psi_i(v_{in,i}(k)) < \Psi_i(v_{ino,\,i}) = d_{o,i}\,i_{Lo,i} \qquad \text{for} \quad \hat{v}_{in,i}(k) > 0\,,$$

$$\Psi_i(v_{in,i}(k)) > \Psi_i(v_{ino,\,i}) = d_{o,i}\,i_{Lo,i} \qquad \text{for} \quad \hat{v}_{in,i}(k) < 0$$

where $v_{ino,i}$ is the input capacitor steady state voltage. Therefore, the second term in (25) is negative. In order to prove $\Delta\Gamma \le 0$ in (25), it is enough to show that

$$\left|\,\Psi_i(v_{in,i}(k)) - d_{o,i}\,i_{Lo,i}\right| \le 2\,C_{in,i}/T \times \left|\hat{v}_{in,i}(k)\right|. \tag{27}$$

The term on the left hand side of (27) is the solar current derivative with respect to $\hat{v}_{in}(k)$ that satisfies

$$\left|\,\Psi_i(v_{in,i}(k)) - d_{o,i}\,i_{Lo,i}\right| \le \left|\partial\Psi_i/\partial v_{in,i}\right|_{\max} \left|\hat{v}_{in,i}(k)\right|. \tag{28}$$

As (26) suggests, $\left|\partial\Psi_i/\partial v_{in,i}\right|$ has its maximum value at $v_{in} = V_{op}$ (solar open circuit voltage,) and thus, from (27) and (28), stability criterion becomes

$$\left|\partial\Psi_i/\partial v_{in,i}\right|_{v_{in,i}=V_{op}} \le 2\,C_{in,i}/T\,. \tag{29}$$

Finally, using (26) and (29), one concludes that

$$(n_{pi}\,I_{rs}/V_T\,n_{si})\,e^{\,V_{op}/(V_T\,n_{si})} \le 2\,C_{in,i}/T\,. \tag{30}$$

By assuring (30) in the solar and dc-dc converter system design, $\Delta L \leq 0$ and stability of $\hat{v}_{in}(k)$ are obtained.

**2.6 Simulation Results**

In order to confirm the theoretical analysis and the proposed adaptive NN controller design, the interconnected dc grid shown in Fig. 2.4 is tested using the Matlab/Simulink environment. The dc grid comprises four DDCs fed by PV sources and connected to the dc network comprising CPLs and resistive loads whose data are given in Table 2.1. The total load in the grid is 23.1 kW, of which $74\%$ is CPL. Each DDC is a step-down buck converter of Fig. 2.2, equipped with NN controller (16) accompanied by NN weight update law (19). The goal is to stabilize the all DDC output voltages despite grid disturbances. The simulations are performed in multiple cases in order to evaluate the transient response and robustness of the controller.

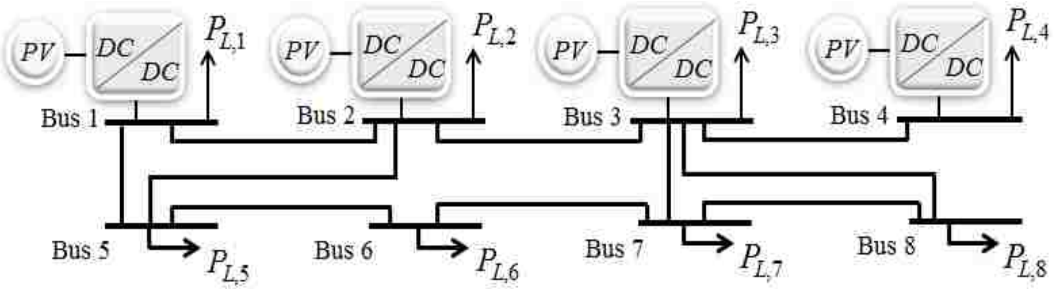


Fig. 2.4. Test interconnected dc network.

In the first three scenarios, load changes are applied to the system at t=0.9 s and removed at t=1 s in 3 locations. Also, the transient response of the system to the intermittent solar generation is evaluated.

*Case 1.* A disturbance occurs at bus 1 as a result of a load change from 2 kW to 5 kW causing a sudden increase in the grid power consumption.

*Case 2.* Load $P_{L,6}$ on bus 6 increases from 4.2 kW to 8.2 kW.

*Case 3.* Load $P_{L,8}$ on bus 8 is disconnected which causes a sudden reduction of 3.5 kW in power consumption.

Table 2.1. Grid parameters

| DDC Parameters | DDC Parameters |
|---|---|
| - PV series and parallel cells & arrays $n_s$=1000 ; $n_p$=20 | $P_{L,1}$ 2kW-(Resistive:1kW;CPL:1kW) |
| - PV short circuit current $I_{sc}$ =1 A | $P_{L,2}$ 2 kW-Resistive |
| - PV maximum power $P_{max}$ =8.7 kW | $P_{L,3}$ 1 kW- Resistive |
| - DDC capacitors $C_{in}$=$C_{out}$=10 mF | $P_{L,4}$ 2 kW- Resistive |
| - DDC inductance $L$=150 mH | $P_{L,5}$ 3.4kW-CPL |
| - Switching frequency $f_s$=10 kHz | $P_{L,6}$ 4.2kW-CPL |
| - Line resistances (Fig. 2.4) $R_{Line}$= 0.01 Ohm | $P_{L,7}$ 5 kW-CPL |
| | $P_{L,8}$ 3.5kW-CPL |

Figures 2.5 to 2.8 show that the DDC output and grid voltages are controlled and maintained close to the reference value while the input solar power and voltage undergo transient changes and are finally stabilized as predicted. Voltages and powers are shown in volts and watts, respectively. As the photovoltaic system operates in voltage higher than maximum power point voltage ($v_{in} > V_{mpp}$,) an increase in input power $p_{in}$ necessitates a reduction in the DDC input voltage $v_{in}$, as Figs. 2.6 and 2.7 confirm. Selected grid voltages are depicted in Fig. 2.8 and imply stable voltages in the entire dc grid.

*Case 4.* In this case, solar arrays 1 (i.e., connected to bus 1) undergo a drop in the power production due to a moving object passing over the PV panels. As a result, some of the parallel arrays are disconnected and the solar power reduces by 80%. Figure 2.9 shows that the DDC

input voltage and solar power of bus 1 drop, significantly; however, the proposed adaptive controller is able to maintain the output voltage and stabilize the DDC both when the obstacle blocks the arrays and when it is removed. Note that, the other solar panels compensate for the load-generation power mismatch through maintained nominal output voltage.

*Case 5*. In order to further demonstrate the ability of the controller to automatically adjust to different operating points, in this case the load level of bus 7 has been altered. Load $P_{L,7}$ (bus 7, in Fig. 2.4) increases from 5 kW to 8 kW at t=0.9 s and goes back to 5 kW at t=1.2 s. Then, it decreases to 3 kW at t=1.5 s and reaches to 6 kW at t=1.8 s. The results are depicted in Figs. 2.10 to 2.12 where good tracking performance of the controller is observed.

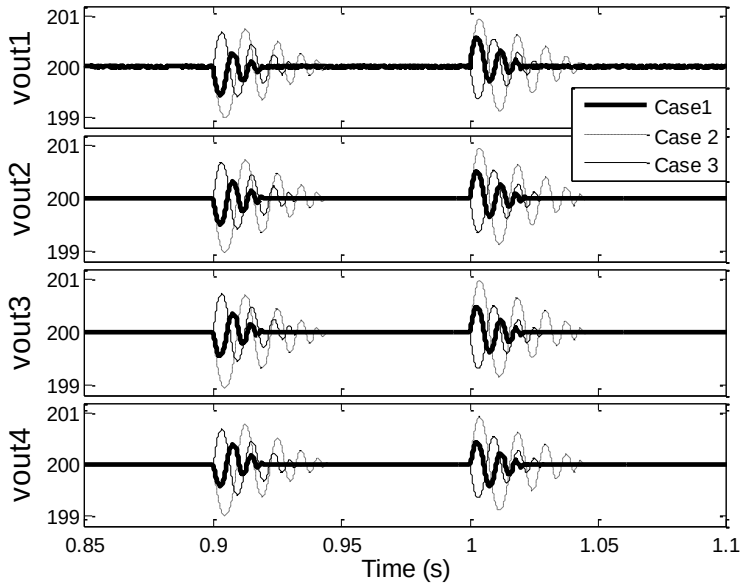


Fig. 2.5 DDC output voltages after the load changes in cases 1, 2, and 3.

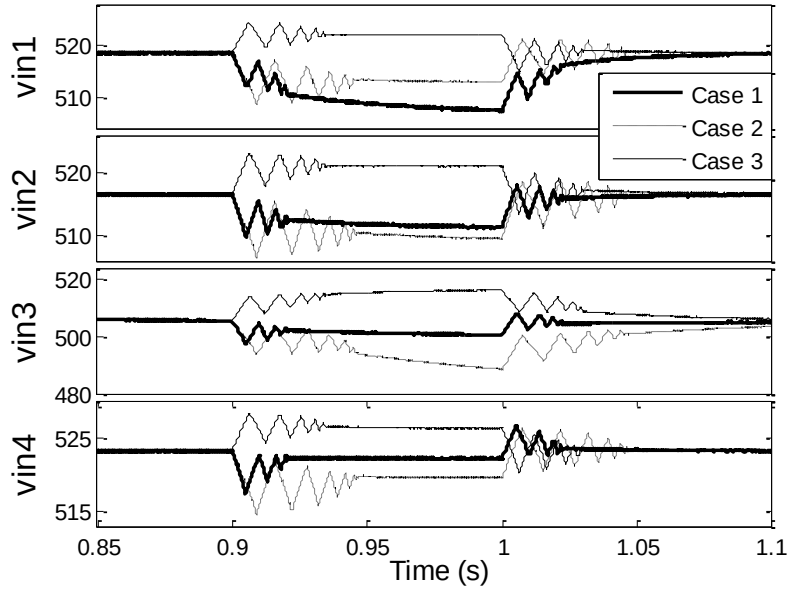


Fig. 2.6 DDC input voltages after the load changes in cases 1, 2, and 3.

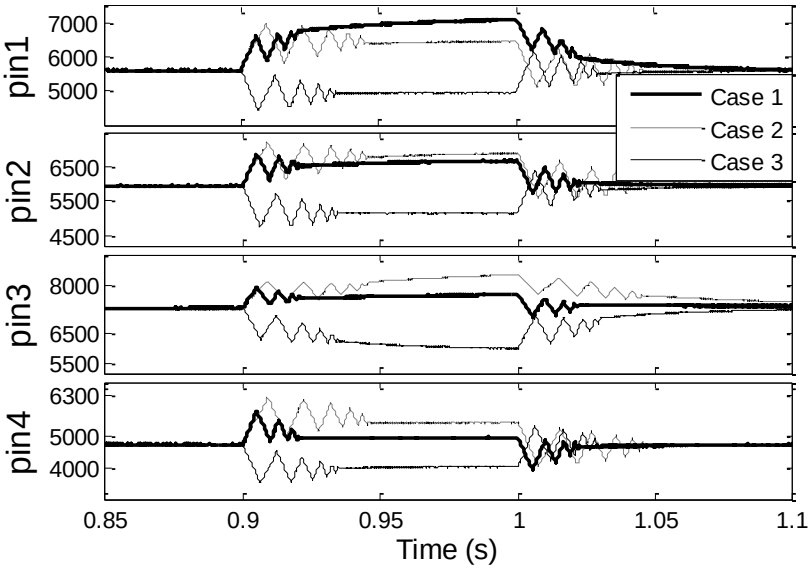


Fig. 2.7 DDC input powers after the load changes in cases 1, 2, and 3.

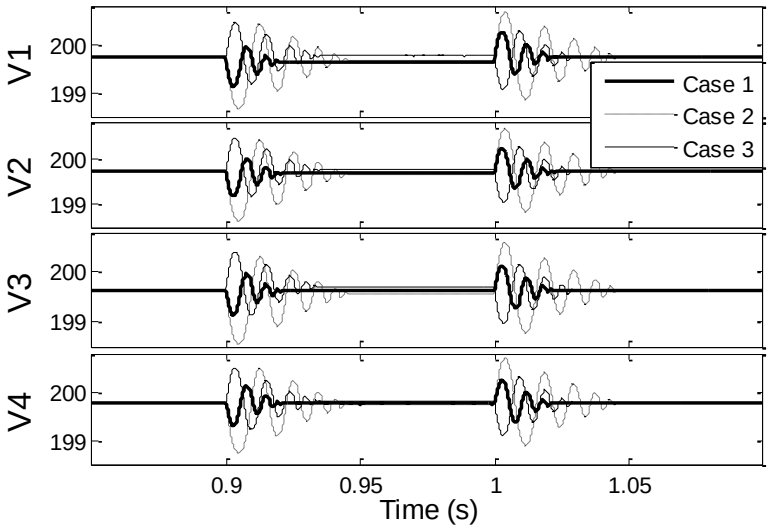


Fig. 2.8 Bus voltages after the load changes in cases 1, 2, and 3.

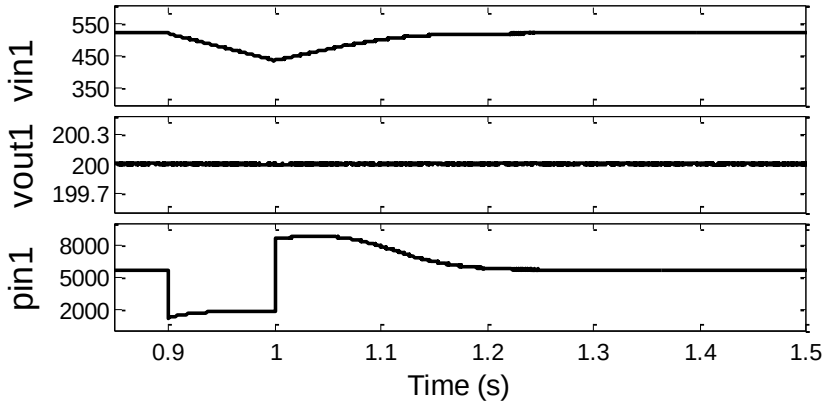


Fig. 2.9 Proposed controller's performance in the presence of intermittent solar power in case 4.

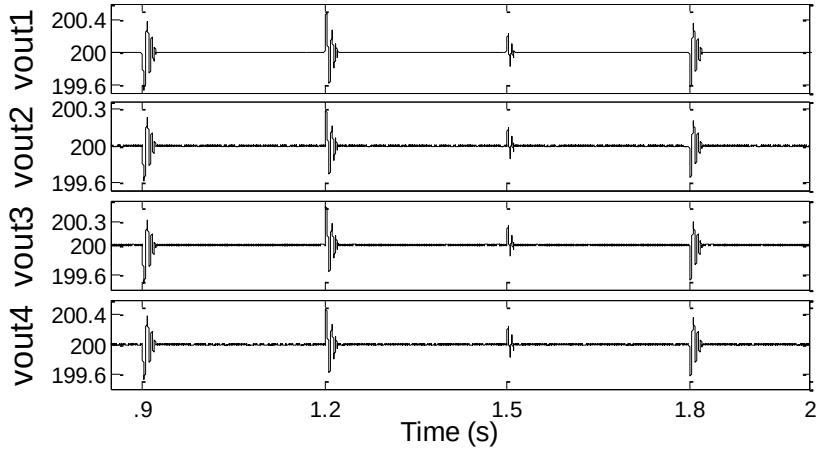


Fig. 2.10 DDC output voltages in load changes of case 5.

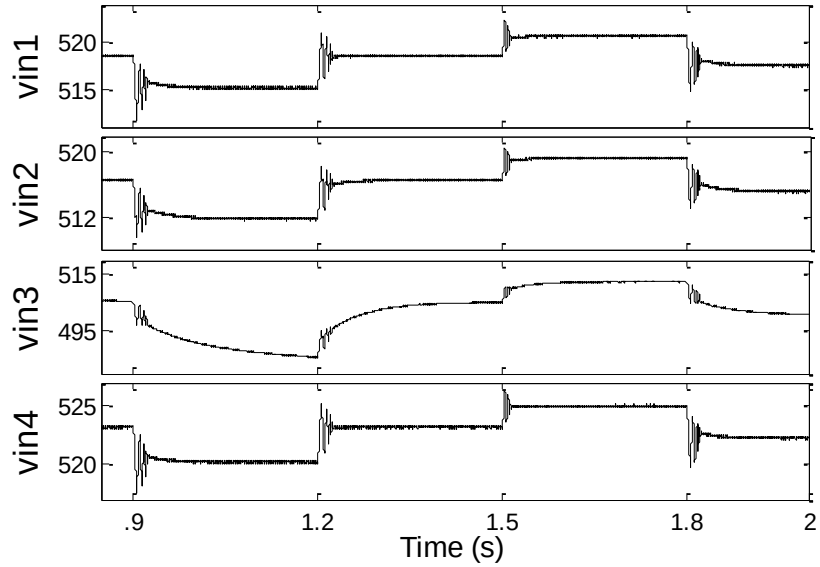

Fig. 2.11 DDC input voltages in load changes of case 5.

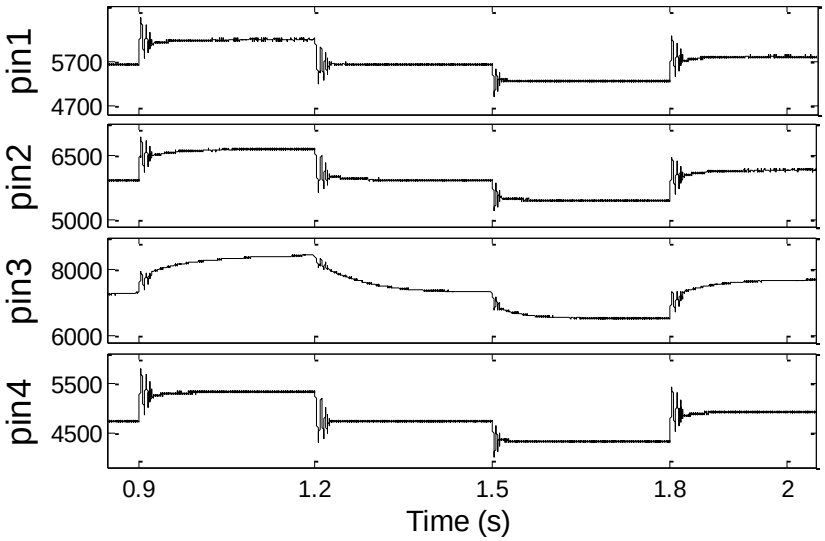

Fig. 2.12 DDC input powers in load changes of case 5.

*Case 6.* The performance of the proposed controller is evaluated under a line-break scenario where the line connecting busses 1 and 5 is subject to a fault and disconnects at t=0.9 s. The results are illustrated in Figs. 2.13 through 2.15 showing that the voltages are kept in acceptable ranges while the solar generators experience changes in their delivered power.

*Case 7.* The performance of the proposed controller is compared against the droop-based decentralized controller proposed in [25]. The droop controller is designed and tuned to track the

converter nominal output voltage with $K_P = 30$ and $K_I = 1$. In this scenario, load $P_{L,7}$ decreases from 5 kW to 3 kW at t=0.9 s and then to 1 kW at t=1 s. As Fig. 2.16 implies, as opposed to the proposed controller's precise voltage tracking, the droop controller has an overall steady state error. The droop controller's transients are slightly shorter and have smaller voltage variations than that of the proposed adaptive controller; however, it leads to larger steady-state errors in the output voltage. Next, in order to evaluate both controllers robustness, a sinusoidal measurement noise of 1 kHz frequency and 2 V (peak-peak) amplitude is added to all the output voltage measurements. Results of Fig. 2.17 show an improved performance and better noise rejection of the proposed adaptive controller over the droop controller.

Overall, the simulation results show a good control performance provided by the proposed adaptive NN controller in stabilizing the interconnected dc grid.

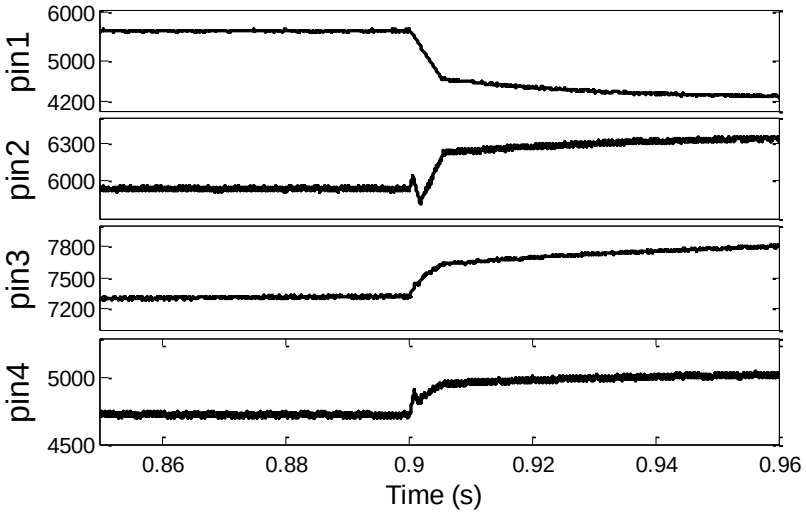

Fig. 2.13 Line disconnect scenario; DDCs' input powers, in case 6.

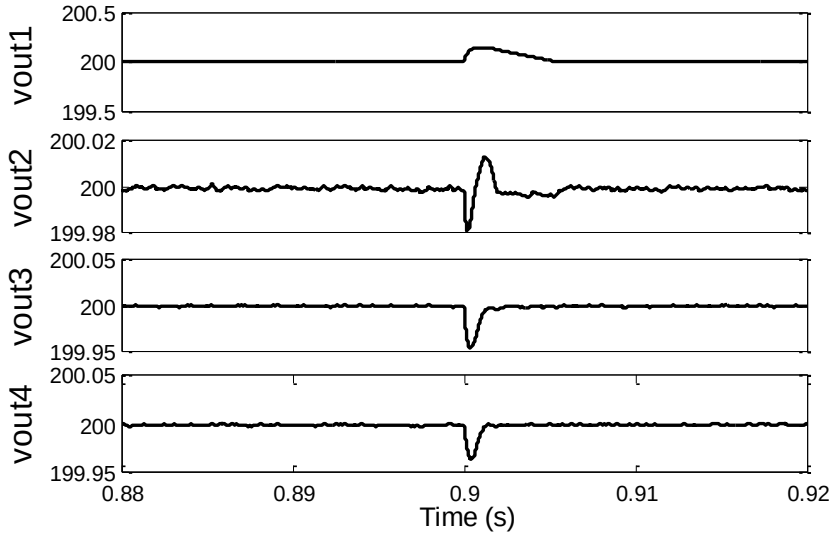


Fig. 2.14 Line disconnect scenario; DDCs' output voltages, in case 6.

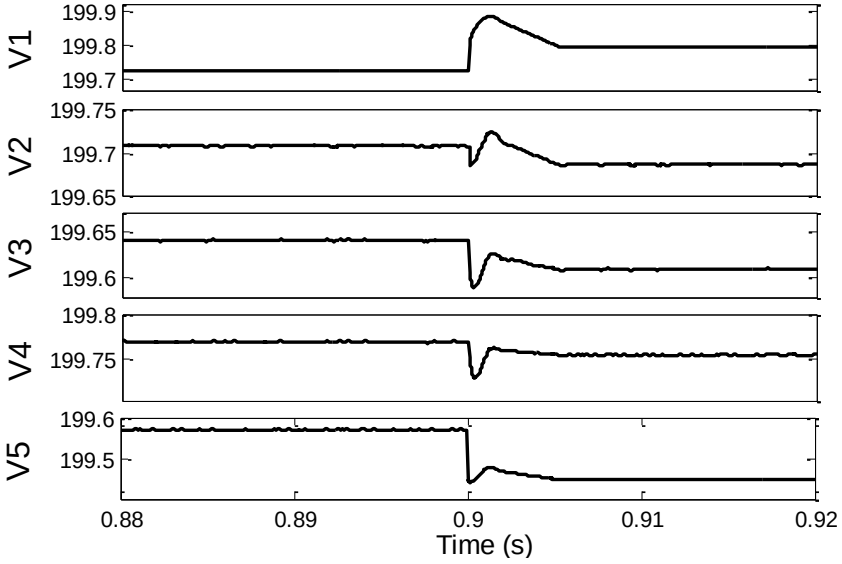


Fig. 2.15 Line disconnect scenario; grid voltages, in case 6.

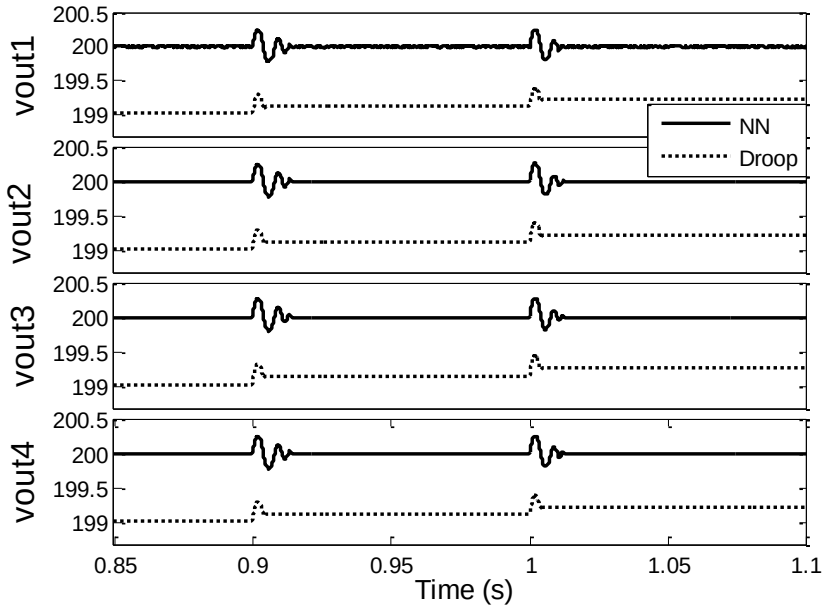


Fig. 2.16 Comparison of the proposed NN and droop controllers under the load change of case 7.

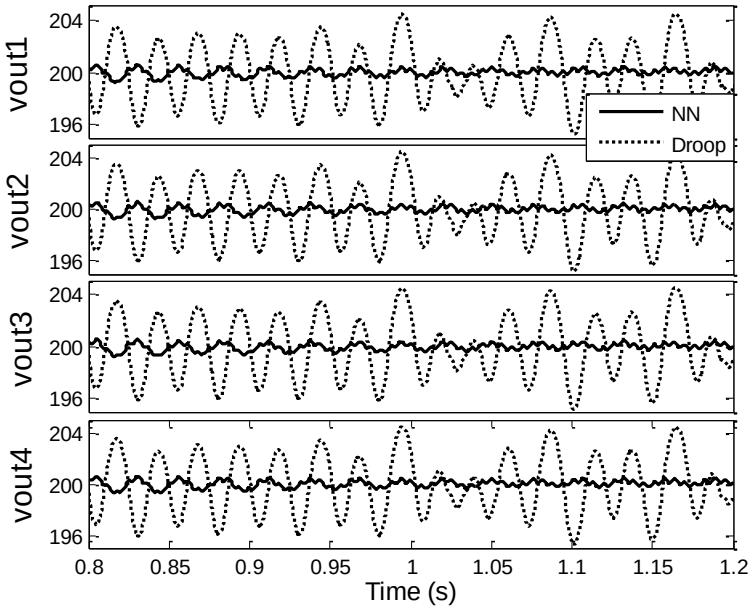


Fig. 2.17 Comparison of the proposed NN and droop controllers in response to measurement noise in case 7.

## 2.7 Conclusions

In this chapter, a nonlinear discrete-time model of the interconnected dc grid is presented in controllable form and grid stability is achieved through an adaptive state feedback neural network controller design. The neural networks with online learning are utilized to approximate

unknown nonlinear functions in the grid's dynamic representation. Through Lyapunov stability criterion, stability of the interconnected dc grid is proven in the presence of unknown dynamics of the dc-dc converters. Simulation results show the effectiveness of the proposed adaptive discrete-time NN controller in the presence of the power system disturbances. The theoretical conjectures and simulation results of the proposed NN controller imply that the converter input voltages and powers as well as the output voltages are stabilized desirably in the entire dc grid using local data in a decentralized control scheme.

### 2.8 References


[1] S. Anand, B. G. Fernandes, and J. M. Guerrero, "Distributed control to ensure proportional load sharing and improve voltage regulation in low voltage dc microgrids," *IEEE Trans. Power Electronics*, vol. 28, no. 4, pp. 1900–1913, 2013.

[2] A. Emadi, A. Khaligh, C. H. Rivetta, and G. A. Williamson, "Constant power loads and negative impedance instability in automotive systems: Definition, modeling, stability, and control of power electronic converters and motor drives," *IEEE Trans. Vehicle Technology.*, vol. 55, no. 4, pp. 1112–1125, 2006.

[3] P. Liutanakul, A. Awan, S. Pierfederici, B. Nahid-Mobarakeh, and F. Meibody-Tabar, "Linear stabilization of a dc bus supplying a constant power load: A general design approach," *IEEE Trans. Power Electronics*, vol. 25, no. 2, pp. 475–488, 2010.

[4] A. M. Rahimi and A. Emadi, "Active damping in dc/dc power electronic converters: A novel method to overcome the problems of constant power loads," *IEEE Trans. Industrial Electronics*, vol. 56, no. 5, pp. 1428–1439, 2009.

[5] X. Liu, N. Fournier, and A. J. Forsyth, "Active stabilization of an HVDC distribution system with multiple constant power loads," in *Proc. IEEE VPPC*, Hei Longjiang, China, Sep. 2008, pp. 1–6.

[6] X.Liu, A.J. Forsyth, and A.M.Cross, "Negative input-resistance compensator for a constant power load," *IEEE Trans. Industrial Electronics*, vol. 54, no. 6, pp. 3188–3196, 2007.

[7] A. M. Rahimi, G. A. Williamson, and A. Emadi, "Loop-cancellation technique: A novel nonlinear feedback to overcome the destabilizing effect of constant-power loads," *IEEE Trans. Veh. Technol.*, vol. 59, no. 2, pp. 650–661, 2010.

[8] C. N. Onwuchekwa and A. Kwasinski, "Analysis of boundary control for buck converters with instantaneous constant-power loads," *IEEE Trans. Power Electronics*, vol. 25, no. 8, pp. 2018–2032, 2010.

[9] P. Magne, B. Nahid-Mobarakeh, and S. Pierfederci, "Large-signal stabilization of a dc-link supplying a constant power load using a virtual capacitor: impact on the domain of attraction," *IEEE Trans. Industrial Applications*, vol. 48, no. 3, pp. 878–887, 2012.

[10] D. Marx, P. Magne, B. Nahid-Mobarakeh, S. Pierfederci, and B. Davat, "Large signal stability analysis tools in dc power systems with constant power loads and variable power loads-a review," *IEEE Trans. Power Electronics*, vol. 27, no. 4, pp. 1773–1787, 2012.

[11] C. Rivetta and G. A. Williamson, "Large-signal analysis and control of buck converters loaded by dc–dc converters," in *Proc. IEEE Power Electron. Spec. Conf.*, Aachen, Germany, June 2004, vol. 5, pp. 3675–3680.

[12] E. Santi, D. Li, A. Monti, and A. M. Stankovic, "A geometric approach to large-signal stability of switching converters under sliding mode control and synergetic control," in *Proc. IEEE Power Electron. Spec. Conf.*, Recife, Brazil, Jun. 2005, pp. 1389–1395.

[13] P. Magne, B. Nahid-Mobarakeh, and S. Pierfederici, "General active global stabilization of multiloads dc-power networks," *IEEE Trans. Power Electronic*s, vol. 27, no. 4, pp. 1788–1798, 2012.

[14] P. Magne, B. Nahid-Mobarakeh, and S. Pierfederici, "Active stabilization of dc microgrids without remote sensors for more electric aircraft," *IEEE Trans. Industry Applications*, vol. 49, no. 5, pp. 2352–2360, 2013.

[15] S. Jain and F. Khorrami, "Decentralized adaptive control of a class of large-scale interconnected nonlinear systems," *IEEE Trans. Automatic Control*, vol. 42, no. 2, pp. 136–154, 1997.

[16] B. Karimi, M.B. Menhaj, M. Karimi-Ghartemani, and I. Saboori, "Decentralized adaptive control of large-scale affine and nonaffine nonlinear systems," *IEEE Trans. Instrumentation and Measurement*, vol. 58, no. 8, pp. 2459–2467, 2009.

[17] J.T. Spooner and K.M. Passino, "Adaptive control of a class of decentralized nonlinear systems," *IEEE Trans. Automatic Control*, vol. 4 , no. 2, pp.280–284, 1996.

[18] S. Jagannathan, "Decentralized discrete-time neural network controller for a class of nonlinear systems with unknown interconnections," in *Proc. IEEE International Symposium on Intelligent Cont.*, Limassol, Cyprus, June 2005, pp. 268–273.

[19] E. Gyurkovics and T. Takacs, "Stabilization of discrete-time interconnected systems under control constraints," IEE Proceedings-Control Theory and Applications, vol. 147, no. 2, pp. 137–144, 2000.

[20] Y. H. Lin and K. S. Narendra, "A new error model for adaptive systems," IEEE Trans. Automatic Control, vol. 25, no. 3, pp. 585–587, 1980.

[21] K. J. Astrom and B. Wittenmark, "Computer Controlled Systems. Theory and Practice," 3rd ed., Prentice-Hall, Inc., Upper Saddle River, NJ,1997.

[22] A. G. Beccuti, M. Kvasnica, G. Papafotiou, and M. Morari, "A decentralized explicit predictive control paradigm for parallelized dc-dc circuits," *IEEE Trans. Control Systems Technology*, vol. 21, no. 1, pp. 136–148, 2013.

[23] Y. Pipelzadeh, B. Chaudhuri, and T. C. Green, "Control coordination within a VSC HVDC link for power oscillation damping: a robust decentralized approach using homotopy," *IEEE Trans. Control Systems Technology*, vol. 21, no. 4, pp. 1270–1279, 2013.

[24] X. Lu, J. M. Guerrero, K. Sun, and J. C. Vasquez, "An improved droop control method for dc microgrids based on low bandwidth communication with dc bus voltage restoration and enhanced current sharing accuracy," *IEEE Trans. Power Electronics*, vol. 29, no. 4, pp. 1800–1812, 2014.

[25] S. Anand and B. G. Fernandes, "Reduced-order model and stability analysis of low-voltage dc microgrid," *IEEE Trans. Industrial Electronics*, vol. 60, no. 11, pp. 5040–5049, 2013.

[26] R. C. N. Pilawa-Podgurski, and D. J. Perreault, "Submodule integrated distributed maximum power point tracking for solar photovoltaic applications," *IEEE Trans. Power Electronics*, vol. 28, no. 6, pp. 2957–2967, 2013.

[27] G. R. Walker and P. C. Sernia, "Cascaded dc–dc converter connection of photovoltaic modules," *IEEE Trans. Power Electronics*, vol. 19, no. 4, pp. 1130–1139, 2004.

[28] A. Keyhani, "*Design of Smart Power Grid Renewable Energy Systems,*" John Wiley, 2011.

[29] F. L. Lewis, S. Jagannathan, and A. Yesildirek, "*Neural Network Control of Robot.* Manipulators and Nonlinear Systems," Taylor & Francis, 1998.

[30] S. Huang, K.K. Tan, and T.H. Lee, "Decentralized control design for large-scale systems with strong interconnections using neural networks," IEEE Trans. Automatic Control, vol. 48, no. 5, pp. 805–810, 2003.

[31] P.K. Sahoo and T. Riedel, "Mean Value Theorems and Functional Equations," World Scientific Publishing Co., 1998.

[32] S. Mehraeen, S. Jagannathan, and M. L. Crow, "Decentralized adaptive neural network state and output feedback control of a class of interconnected nonlinear discrete-time systems," Proc. of American Control Conference (ACC), Montreal, Canada, June 2012, pp. 6406–6411.

[33] H. De Battista and R. J. Mantz, "Variable structure control of a photovoltaic energy converter," IEE Proceedings-Control Theory and Applications, vol. 149, no. 4, pp. 303–310, 2002.

[34] J. M. Steele, "The Cauchy-Schwarz Master Class: An Introduction to the Art of Mathematical Inequalities," Maa Problem Books Series, The Mathematical Association of America, 2004.

[35] F. L Lewis, D. M. Dawson, and C. T. Abdallah, "Robot manipulator control: Theory and practice," CRC Press. 2003.

# CHAPTER 3
# DECENTRALIZED DISCRETE-TIME OUTPUT FEEDBACK CONTROL OF INTERCONNECTED DC DISTRIBUTION SYSTEM

## 3.1 Introduction

A novel decentralized nonlinear controller is proposed in this chapter, for the interconnected dc grid in discrete-time using output feedback mechanism. The dc grid is an interconnection of DERs connected to resistive and constant-power loads through DDCs. The adaptive NN-based controller is employed to overcome the unknown dynamics of each subsystem's converter and stabilize the entire grid, assuming that only part of the local measurements are available to each converter. Here the photovoltaic arrays are employed as DERs and their nonlinear characteristics is taken into account. Through the Lyapunov stability method the stability of all the DDCs' output voltages in the interconnected dc grid is proven using some local states measurement. In Chapter 2 a decentralized nonlinear controller for the interconnected dc grid was proposed. In that method a state feedback controller is utilized in each subsystem which requires obtaining all state variables of each subsystem. However all state variables might not be available or measurable in some systems. In this chapter an output feedback controller is utilized instead of state feedback. As the output feedback controller needs only partial knowledge of subsystem states, the controller is viable even if some of the states are not available and also the number of measure points is reduced [1].

The rest of the chapter is organized as follows. In the next section the dc distribution grid topology is presented. In Section 3.3, the DDC discrete-time model is developed and presented in the form of a nonlinear interconnected discrete-time system. The decentralized NN controller is developed in Section 3.4 using output. Simulation results on a low-voltage distribution grid are shown in Section 3.5 followed by the concluding remarks in Section 3.6.

### 3.2 Interconnected DC Microgrid

In this section, the dynamical model along with the control mechanism of the DERs is represented. Though the proposed modeling and controller design can be applied to a variety of DERs, specific attention is paid to photovoltaic source here to address the low-inertia distribution systems and micro grids. Fig. 3.1 shows the interconnected dc grid comprising *N* buses with *n* DER buses and *N*-*n* load buses.

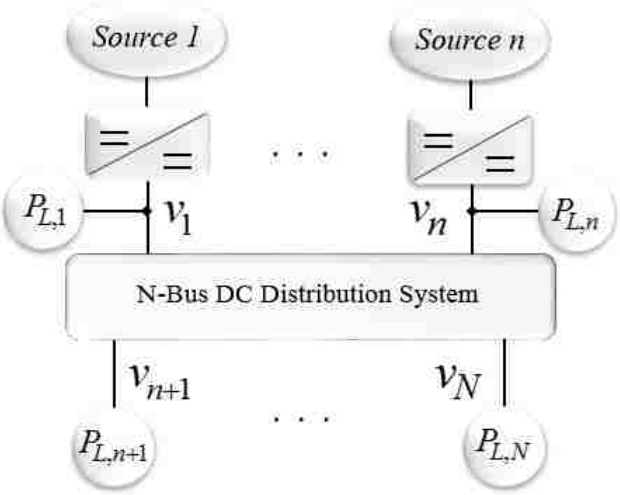


Fig. 3.1 *N*-bus dc distribution system, *n* distributed generation sources and *N*-*n* non-generator buses, with load $P_{L,i}$ on bus '*i*'.

Each DER is a photovoltaic source connected to a dc-dc converter as depicted in Fig. 3.2. Each dc-dc converter is modeled as a discrete-time dynamical subsystem and the stability of the entire dc grid is investigated. In this chapter, the buck converter in continuous-current mode (CCM) operation is considered. As explained in Chapter 2 boost converters are more commonly used in photovoltaic systems due to their ability to increase the output voltage that requires lower solar array voltage leading to fewer panels; however, the boost converter output voltage grows exponentially and therefore its operating range is very limited [2]. Unlike the boost converter, output voltage in the buck converter is proportional to the duty cycle and thus, the duty cycle has

a greater control range and stability [2]. In photovoltaic energy applications if voltage magnification is needed, forward converter can be utilized that takes advantage of both transformer action and buck converter voltage adjustment.

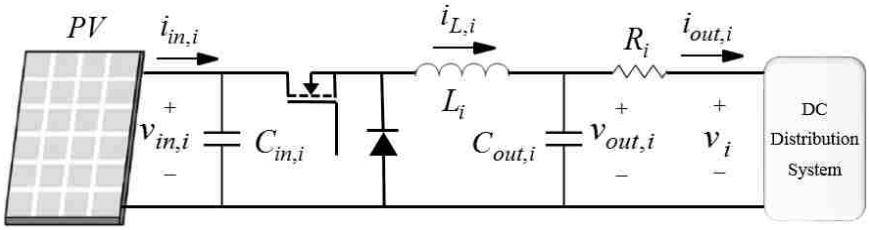


Fig. 3.2 dc-dc buck converter.

As any fault and disturbance occurs in the network, the dc voltage fluctuates affecting the photovoltaic power generation in which could potentially lead to the entire network instability. The goal is modeling and designing an adaptive controller to stabilize the buck converter output voltage in an interconnected dc network. The proposed controller in [2] adjusts the converter's duty cycle to attain the stability through a decentralized scheme while taking the converter input and output voltages and currents as the only measurable states to the selected converter.

### 3.3 Buck Converter Model

A discrete-time model for the buck converter Fig. 3.2 is represented in this section in Brunovsky canonical form [2],[3]. The converter output voltage and duty cycle are assigned as the controlled variable and the control input, respectively.

Figure 3.2 represents the *i*th subsystem of the dc microgrid of Fig. 3.1 which is a buck converter interfacing a DER with the dc grid. This subsystem state variables are the converter's input and output capacitors' voltages, $v_{in,i}$ and $v_{out,i}$, and the inductor's current $i_{L,i}$ (Fig. 3.2).

Subtracting the states steady-state values $x_{oi}$ from the actual values, the state error vector can be considered as $\bar{x}_i(k) = x_i(k) - x_{oi} = [\bar{v}_{in,i}(k), \bar{i}_{L,i}(k), \bar{v}_{out,i}(k)]^T$. Also, $\bar{i}_{in,i}(k) = i_{in,i}(k) - i_{ino,i}$ and $\bar{i}_{out,i}(k) = i_{out,i}(k) - i_{outo,i}$ are the converter input and output current errors, respectively.

The controller aims to make the errors zero and equivalently (making the converter output voltage approach its steady-state value) by synthesizing an additional duty cycle $\hat{d}_i$ to be added to the steady-state duty cycle $d_{o,i}$. The scheme stabilizes the network around the converter output voltage reference value in the presence of the grid disturbances

According to [2] the error dynamics are represented as unknown functions of the errors

$$\bar{v}_{in,i}((k+1)) = h_1(\bar{x}_i(k), d_i)$$

$$\bar{i}_{L,i}((k+1)) = h_2(\bar{x}_i(k), d_i)$$

$$\bar{v}_{out,i}((k+1)) = h_3(\bar{x}_i(k)) + \vartheta_i(\bar{i}_{out,i}(k)). \quad (1)$$

Since the integrals in (1) cannot be easily converted to closed-form functions of the states, functions $h_{1,i}(.)$, $h_{2,i}(.)$, $h_{3,i}(.)$, and $\vartheta_i(.)$ are unknown. As $\bar{i}_{out,i}(k)$ depends on the other converters states, $\vartheta_i(.)$ is a function of the entire grid state errors which are not available at converter '*i*' location due to the controllers' decentralized structure.

In order to present dynamics (1) in canonical form define new state variables $\xi_i = [\xi_{1,i}, \xi_{2,i}]^T$. Take $\bar{v}_{out,i}(k)$ along with its next step as follows

$$\xi_{1,i}(k) = \bar{v}_{out,i}(k)$$

$$\xi_{1,i}(k+1) = \bar{v}_{out,i}(k+1) = \xi_{2,i}(k)$$

$$\xi_{2,i}(k+1) = \bar{v}_{out,i}(k+2). \quad (2)$$

As explained in [2] the converter state-space equations can be rewritten in canonical form as

$$\xi_{1,i}(k+1) = \xi_{2,i}(k)$$

$$\xi_{2,i}(k+1) = f_i(\bar{x}_i(k)) + g_i(\bar{x}_i(k))u_i(k) + \Delta_i(\xi(k)) \quad (3)$$

with $u_i = \hat{d}_i$ as the subsystem's input and unknown nonlinear functions $f_i(\bar{x}_i(k)), g_i(\bar{x}_i(k))$, and $\Delta_i(\xi)$. Function $\Delta_i(\xi(k))$ depends on the entire system state vector $\xi(k)$ and is called the interconnection term [4] that is a function of all the converters' states, some of which are unavailable.

Dynamics represented in (4) are of order two while the converter original dynamics (1) are of order three. That is, one of the dynamics known as *internal dynamics* [2] has been shown to be stable when the observable states (here $\xi_i = [\xi_{1,i}, \xi_{2,i}]^T$) tend to zero.

In the next section the proposed discrete-time control design is discussed.

**3.4 Output Feedback Controller Design**

In this section, the decentralized output feedback controller proposed in [1] is applied to system (3) using partial knowledge of subsystem states.

A. Discrete-Time Interconnected System Background

A class of discrete-time interconnected systems consisting of *n* subsystems (DDCs) is represented in canonical form as

$$\xi_{p,i}(k+1) = \xi_{p+1,i}(k);\ 1 \le p \le m-1$$

$$\xi_{m,i}(k+1) = f_i(\bar{x}_i(k)) + g_i(\bar{x}_i(k))u_i(k) + \Delta_i(\xi(k)) \quad (4)$$

$$y_i(k) = \xi_{1,i}(k)$$

for $1 \le i \le n$ where $\xi_i = [\xi_{1,i}, \ldots, \xi_{m,i}]^T$ is the state error vector of subsystem '*i*' , $m$ is the order of the subsystem ( $m = 2$ according to model (3)), $\Delta_i(\xi(k))$ denotes the interconnection effects with $\xi = [\xi_1{}^T, \ldots, \xi_n{}^T]^T$ and $\bar{x}_i$ is the original subsystem states errors from which the feedback linearization was derived. The internal dynamics $f_i(\bar{x}_i(k))$ and the input gain $g_i(\bar{x}_i(k))$ in general are nonlinear functions of states. It is desired to design a controller that stabilizes $\xi$ at the origin ( $\xi = 0$.)

Define the tracking error as

$$z_{p,i}(k) = \xi_{p,i}(k) - \xi_{pd,i}(k) \tag{5}$$

for $1 \le i \le n$ and $1 \le p \le m$, where $\xi_{pd,i}(k)$ is the desired trajectory for the state $\xi_{p,i}(k)$ , and $\xi_{p+1,d,i}(k) = \xi_{pd,i}(k+1)$ for $1 \le p \le m-1$.

Only the subsystems outputs ( $\xi_{1,i}$ for all $1 \le i \le n$ ) are considered available and so an observer is required to estimated the rest of the states. Two assumptions and one definition are presented before beginning the controller design.

*Assumption 1*- Functions $g_i(\bar{x}_i(k))$ are bounded and away from zero. That is,

$$0 < g_{i,\min} \le g_i(\bar{x}_i(k)) \le g_{i,\max} \tag{6}$$

where $g_{i,\min}$ and $g_{i,\max}$ are positive constants. This is a valid assumption for the dc grid as discussed in [2].

*Assumption 2 [3]*- The interconnection terms are bounded by a function of the states such that $\Delta_i(\xi) \le \sigma_{0i} + \sum_{j=1}^{N} \eta_{ij} \left\| \xi_j \right\|_2$ where $\sigma_{0i}$ and $\eta_{ij}$ are positive constants for $1 \le i \le n$. The tracking

error $z_j(k)$ converges to zero whenever states $\xi_j(k)$ converge to zero. Similar to continuous-time systems [4] this further implies that

$$\Delta_i(\xi) \le \sum_{j=1}^{n} \delta_{ij}(z_j) \le \delta_{0i} + \sum_{j=1}^{n} \gamma_{ij} \left| z_j \right| \tag{7}$$

where $\delta_{ij}$ is a positive function while $\delta_{0i}$ and $\gamma_{ij}$ are positive constants for $1 \le i \le n$ and $1 \le j \le m$ [2].

*Definition.* **(**Uniform Ultimate Bounded (UUB)) [3]. Consider the dynamical system $x(k+1) = f(x)$ with $x \in \Re^n$ being a state vector. Let the initial time step be $k_0$ and initial condition be $x_0 = x(k_0)$. Then, the equilibrium point $x_e$ is said to be UUB if there exists a compact set $S \subset \Re^n$ so that for all $x_0 \in S$ there exists a bound $B$ and a time step $K(B, x_0)$ such that $\left\| x(k) - x_e \right\| \le B$ for $\forall k > k_0 + K$.

B. Observer Design

Consider the observer

$$\begin{aligned} \hat{\xi}_{p,i}(k) &= \hat{\xi}_{p+1,i}(k-1)\ ;\ 1 \le p \le m-1 \\ \hat{\xi}_{m,i}(k) &= \hat{W}_{1,i}(k-1)\varphi_i({V_{1,i}}^T \hat{M}_i(k-1)) \end{aligned} \tag{8}$$

where $\hat{\xi}_i = [\hat{\xi}_{1,i}, \ldots, \hat{\xi}_{m,i}]^T$ is estimation of $\xi_i$ and $\hat{M}_i(k-1) = [\hat{\xi}_{1,i}(k-1), \hat{\xi}_{2,i}(k-1), \ldots, \hat{\xi}_{m,i}(k-1), u_i(k-1)]^T$ with state estimation error defined as $\tilde{\xi}_i = \hat{\xi}_i - \xi_i$, for all $1 \le i \le n$. $\hat{W}_{1,i} \in R^{L_{1,i} \times 1}$ is the target NN weight matrix estimation, $\varphi_i(.)$ is the activation function and $L_{1,i}$ is the number of the hidden layer neurons. The hidden layer weight

matrix $V_{1,i}$ is chosen initially at random and kept constant. In fact, the NN in observer (8) approximates the nonlinear function $f_i(\bar{x}_i(k-1)) + g_i(\bar{x}_i(k-1))u_i(k-1)$ which can be written as

$$f_i(\bar{x}_i(k-1)) + g_i(\bar{x}_i(k-1))u_i(k-1) = W_{1,i}{}^T \varphi_i(V_{1,i}{}^T M_i(k-1)) \quad + \varepsilon_{1,i}(M_i(k-1)) \tag{9}$$

where $M_i(k-1) = [\xi_{1,i}(k-1), \xi_{2,i}(k-1), ..., \xi_{m,i}(k-1), u_i(k-1)]^T$, $W_{1,i} \in R^{L_{1,i} \times 1}$ is the target NN weight matrix. For simplicity $\varphi_i(M_i(k-1))$ and $\varphi_i(\hat{M}_i(k-1))$ are used to show $\varphi_i(V_{1,i}{}^T M_i(k-1))$ and $\varphi_i(V_{1,i}{}^T \hat{M}_i(k-1))$ respectively.

Next, define the observer NN weight update law as

$$\hat{W}_{1,i}{}^T(k) = \hat{W}_{1,i}(k-1) - \alpha_{1,i}\varphi_i(\hat{M}_i(k-1))[\hat{W}_{1,i}{}^T(k-1)\varphi_i(\hat{M}_i(k-1)) + l_{1,i}\tilde{\xi}_{1,i}(k-1)] \tag{10}$$

where $0 < \alpha_{1,i} < 1$ and $l_{1,i} < 1$ are user defined positive constants.

By subtracting the target weights $W_{i1}(k) = W_{i1}(k-1)$ from (10), one obtains

$$\tilde{W}_{1,i}(k) = \tilde{W}_{1,i}(k-1) - \alpha_i\varphi_i(\hat{M}_i(k-1))[\tilde{W}_{1,i}{}^T(k-1)\varphi_i(\hat{M}_i(k-1)) + W_{1,i}{}^T\varphi_i(\hat{M}_i(k-1)) \quad + l_{1,i}\tilde{\xi}_{1,i}(k-1)] \tag{11}$$

Next, the decentralized controller development is developed.

C. Controller Design

In this section a NN-based controller is introduced to stabilize system (4) employing the estimated states calculated from the observer (8). The NN function approximates the control input.

The tracking error dynamics can be written by using (5) as $z_{m,i}(k+1) = \xi_{m,i}(k+1) - \xi_{md,i} = f_i(\bar{x}_i(k)) + g_i(\bar{x}_i(k))u_i(k) + \Delta_i(\xi(k)) - \xi_{md,i}$, where $\xi_{md,i}$ is the desired value of $\xi_{m,i}$. In order to achieve asymptotically stable dynamics for the tracking

error $z_{m,i}(k+1) = K_i g_i(\bar{x}_i(k)) z_{m,i}(k)$ with $K_i g_i(\bar{x}_i(k)) < 1$, the ideal stabilizing control input for system (4) can be defined as

$$u_{d,i} = -g_i(\bar{x}_i(k))^{-1}(f_i(\bar{x}_i(k)) - \xi_{md,i} + K_i z_{m,i}(k)$$

where $K_i$ is a positive design constant. However, in practice the internal dynamics $f_i(\bar{x}_i(k))$ and control gain $g_i(\bar{x}_i(k))$ and consequently $u_{d,i}$ are not available. Thus, the NN function approximation property is employed to approximate $u_{d,i}$ as

$$u_{d,i} = W_{2,i}^T \rho_i(V_{2,i}{}^T Y_i(k)) + \varepsilon_{2,i}(V_{2,i}{}^T Y_i(k)) + K_i z_{m,,i}(k) \tag{12}$$

where $W_{2,i}$ is the target NN weight matrix, $Y_i(k) = [\xi_{1,i}(k), \xi_{2,i}(k), ..., \xi_{m,i}(k), \xi_{md,i}(k)]^T$ and $\varepsilon_{2,i}(.)$ is the function approximation error which satisfies $\|\varepsilon_{i2}(.)\| \le \varepsilon_{i2\max}$ for all $1 \le i \le n$. Since the target NN weights $W_{2,i}$, approximation error $\varepsilon_{2,i}$, and the full subsystem state vector $\xi_i(k)$ are not available, $u_{d,i}$ is calculated using an approximation of the NN weights together with the estimated subsystem states via the nonlinear observer (8)

$$u_i = \hat{u}_{d,i} = \hat{W}_{2,i}^T \rho_i(V_{2,i}{}^T \hat{Y}_i(k)) + K_i \hat{z}_{m,i}(k) \tag{13}$$

where $\hat{W}_{2,i}$ is the NN weight estimation matrix and $\hat{Y}_i(k) = [\hat{\xi}_{1,i}(k), \hat{\xi}_{2,i}(k), ..., \hat{\xi}_{m,i}(k), \hat{\xi}_{md,i}(k)]^T$. Similar to the previous case, the hidden layer weight matrix $V_{2,i}$ is chosen initially at random and kept constant. For simplicity $\rho_i(\hat{Y}_i(k))$ is used to show $\rho_i(V_{2,i}{}^T \hat{Y}_i(k))$.

Consequently, by using (13) and adding and subtracting $u_{id}$, the tracking error dynamic becomes

$$z_{m,i}(k+1) = f_i(\bar{x}_i(k)) + \Delta_i(\xi) - \xi_{md,i}(k+1) + g_i(\bar{x}_i(k))\left(\hat{W}_{2,i}^T \rho_i(\hat{Y}_i(k)) + K_i \hat{z}_{m,i}(k) + u_{d,i} - u_{d,i}\right)$$

$$= g_i(\bar{x}_i(k))\tilde{W}_{2,i}^T \rho_i(\hat{Y}_i(k)) + S_i + g_i(\bar{x}_i(k))K_i\tilde{\xi}_{m,i} + g_i(\bar{x}_i(k))K_i z_{m,i} \tag{14}$$

where $K_i$ is the expected error damping coefficient, $S_i = g_i(\bar{x}_i(k))\left(W_{2,i}^T\tilde{\rho}_i - \varepsilon_{2,i}(Y_i(k))\right)$ and $\tilde{\rho}_i = \rho_i(\hat{Y}_i(k)) - \rho_i(Y_i(k))$.

Define the controller NN weight update law as

$$\hat{W}_{i2}(k+1) = \hat{W}_{i2}(k) - \alpha_i\rho_i(\hat{Y}_i(k))[\hat{W}_{i2}{}^T(k)\rho_i(\hat{Y}_i(k)) + l_{i2}z_{i1}] \tag{15}$$

where $0 < \alpha_{2,i} < 1$ and $l_{2,i} < 1$ are user defined positive constants.

By subtracting the target weights $W_{2,i}(k) = W_{2,i}(k-1)$ from (15), the weight estimation error $\tilde{W}_{2,i} = \hat{W}_{2,i} - W_{2,i}$ is obtained

$$\tilde{W}_{2,i}(k+1) = \tilde{W}_{2,i}(k) - \alpha_i\rho_i(\hat{Y}_i(k))[\tilde{W}_{2,i}{}^T(k)\rho_i(\hat{Y}_i(k)) + W_{i2}{}^T\rho_i(\hat{Y}_i(k) + l_{2,i}z_{1,i}] \tag{16}$$

Using (4) and (8) the state estimation error $\tilde{\xi}_i = \hat{\xi}_i - \xi_i$ dynamics can be obtained by as

$$\begin{aligned}\tilde{\xi}_{p,i}(k+1) &= \tilde{\xi}_{p+1,i}(k);\ 1 \le p \le m-1\\ \tilde{\xi}_{m,i}(k+1) &= \tilde{W}_{1,i}(k)\varphi_i(\hat{M}_i(k)) + A_i - \Delta_i(x)\end{aligned} \tag{17}$$

where $A_i = W_{i1}^T\tilde{\varphi}_i - \varepsilon_{i1}(M_i(k))$ and $\tilde{\varphi}_i = \varphi_i(\hat{M}_i(k)) - \varphi_i(\hat{M}_i(k))$. The stability of the nonlinear discrete-time interconnected system (4) is proven and given in Appendix B. The tracking errors $z_i(k)$, the state estimations errors $\tilde{\xi}_i(k)$, and NN weight estimation errors $\tilde{W}_{i1}(k)$ and $\tilde{W}_{i2}(k)$ of the individual subsystems are bounded in the presence of unknown internal dynamics $f_i(\bar{x}_i(k))$, control gain matrix $g_i(\bar{x}_i(k))$, and interconnection terms $\Delta_i(\xi)$ for $1 \le i \le n$.

### 3.5 Simulation Results

In order to demonstrate the effectiveness of the proposed adaptive NN controller design, the interconnected dc grid in the IEEE 14-bus power system configuration shown in Fig. 3.3 is tested using the Matlab/Simulink environment. The dc grid comprises five DDCs fed by PV sources and connected to the dc network. The specifications are given in Table 3.1. The total load in the grid is 24 kW, of which $42\%$ is CPL. The goal is to stabilize all of the DDC output voltages despite grid disturbances. The simulations are performed in several scenarios in order to demonstrate the effectiveness and robustness of the controller and evaluate its transient response. In all cases, the photovoltaic system operates in voltage higher than maximum power point voltage ($v_{in} > V_{mpp}$,) and thus an increase in the DDC input power $p_{in}$ necessitates a reduction in input voltage $v_{in}$.

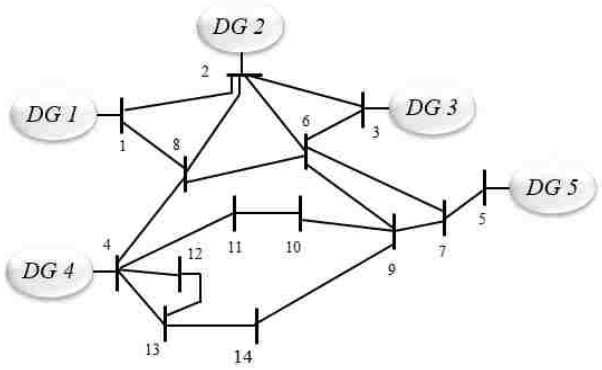


Fig. 3.3 Test interconnected dc network with 5 distributed generations (DGs) in IEEE 14-bus configuration.

In the first two scenarios, load changes are applied to the system at t=0.6 s and removed at t=0.7 s in 2 locations.

*Case 1.* A disturbance occurs at bus 6 as a result of a load change from 3 kW to 5 kW causing a sudden increase in the grid power consumption.

*Case 2.* Load $P_{L,7}$ on bus 7 is disconnected which causes a sudden reduction of CPL for 4 kW.

Table 3.1. Grid parameters

| DDC Parameters | | DDC Parameters | |
|---|---|---|---|
| - PV series cells | $n_s$=970 | $P_{L,1}$ | 2kW- Resistive |
| - PV parallel arrays | | $P_{L,2}$ | 2 kW- Resistive |
| $n_p$ = 17 for PVs 1, 2, 3 and 5 | | $P_{L,3}$ | 2 kW- Resistive |
| $n_p$ = 33 for PV 4 | | $P_{L,4}$ | 2 kW- Resistive |
| - PV short circuit current | $I_{sc}$ =1 A | $P_{L,5}$ | 2 kW- Resistive |
| - PV maximum power | | $P_{L,6}$ | 3 kW- CPL |
| $P_{max}$ =7.2 kW for PVs 1, 2, 3 and 5 | | $P_{L,7}$ | 4 kW- CPL |
| $P_{max}$ =14 kW for PV 4 | | $P_{L,8}$ | 1 kW- CPL |
| - DDC capacitors | $C_{in}$=5 mF, $C_{out}$=1 mF | $P_{L,9}$ | 0.5 kW- CPL |
| - DDC inductance | $L$=150 mH | $P_{L,10}$ | 2 kW- Resistive |
| - Switching frequency | $f_s$=10 kHz | $P_{L,11}$ | 1 kW- CPL |
| - Line resistances (Fig. 3.3) | | $P_{L,12}$ | 0.5 kW- CPL |
| $R_{Line}$= 0.01 Ohm | | $P_{L,13}$ | 1 kW- Resistive |
| | | $P_{L,14}$ | 1 kW- Resistive |

Figures 3.4 shows the DDCs output voltages response to the load changes in scenarios 1 and 2. Also the selected grid voltages are depicted in Fig. 3.5. These voltages undergo transient changes and are finally stabilized. The controller adjusts the solar power and voltage (Figs. 3.6 and 3.7) to stabilize the DDCs output voltage. This controller utilizes less information of the local system rather than the state feedback controller and estimates the unknown variables. As result, the output has more fluctuations in steady state and transient conditions in comparison to state feedback controller.

*Case 3.* In this case, the solar arrays connected to bus 3 undergo a $70\%$ drop in the power production. In this scenario a moving object passing over the PV panels causes some of the parallel arrays to be disconnected. Figure 3.8 shows that the output voltage of the DDC on bus 3

is stable in the presence of intermittent solar power. The proposed controller adjusts the generated power in each DDC when the obstacle blocks the arrays and when it is removed. That is, other solar panels compensate for the power mismatch.

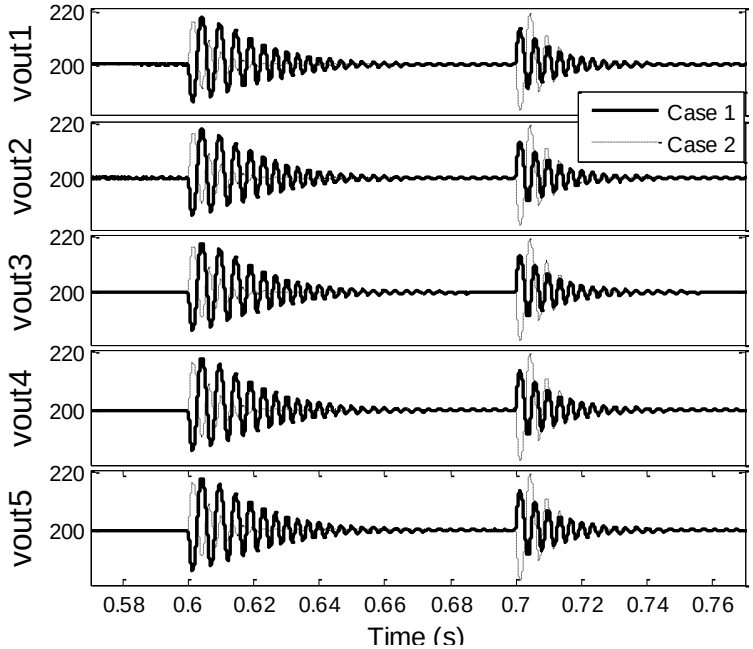


Fig. 3.4 DDC output voltages after the load changes in cases 1 and 2.

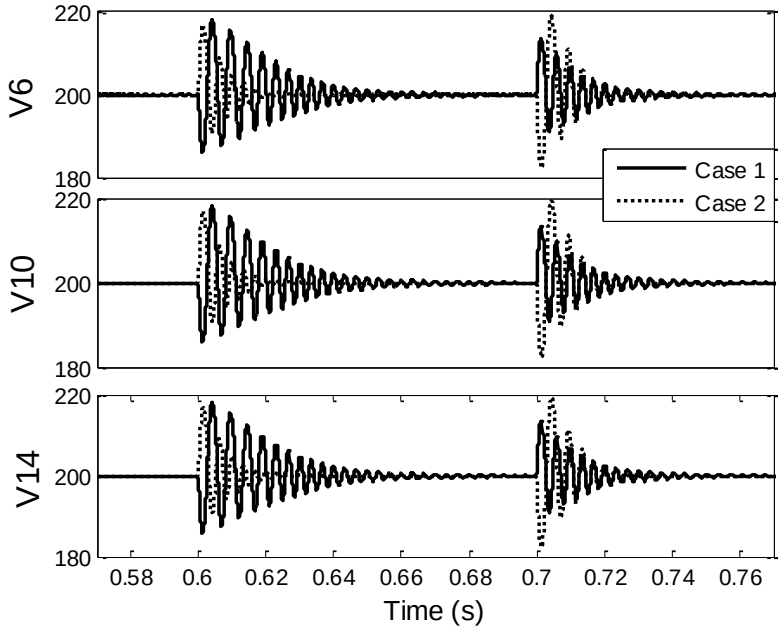


Fig. 3.5 Bus voltages after the load changes in cases 1 and 2.

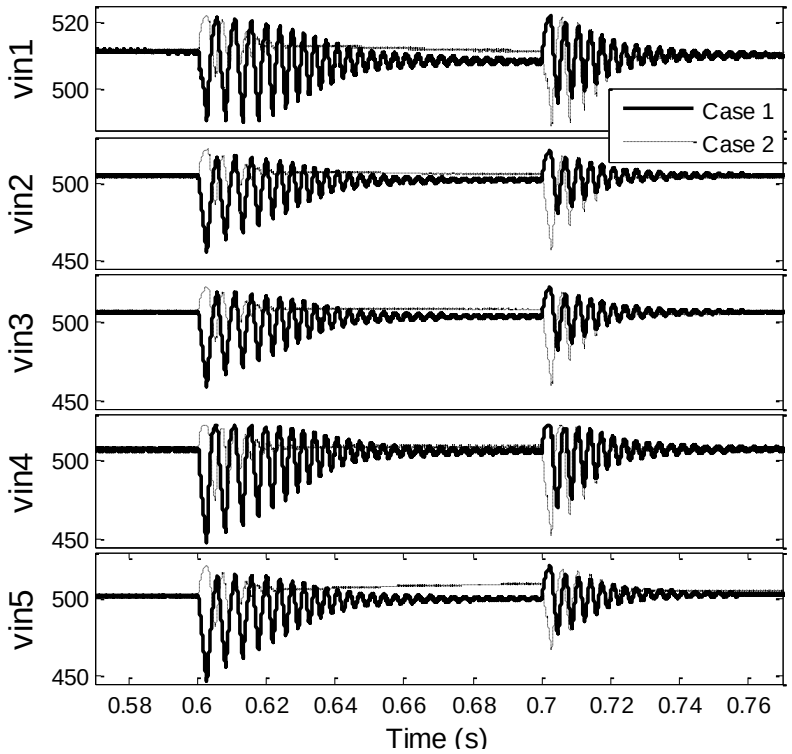

Fig. 3.6 DDC input voltages after the load changes in cases 1 and 2.

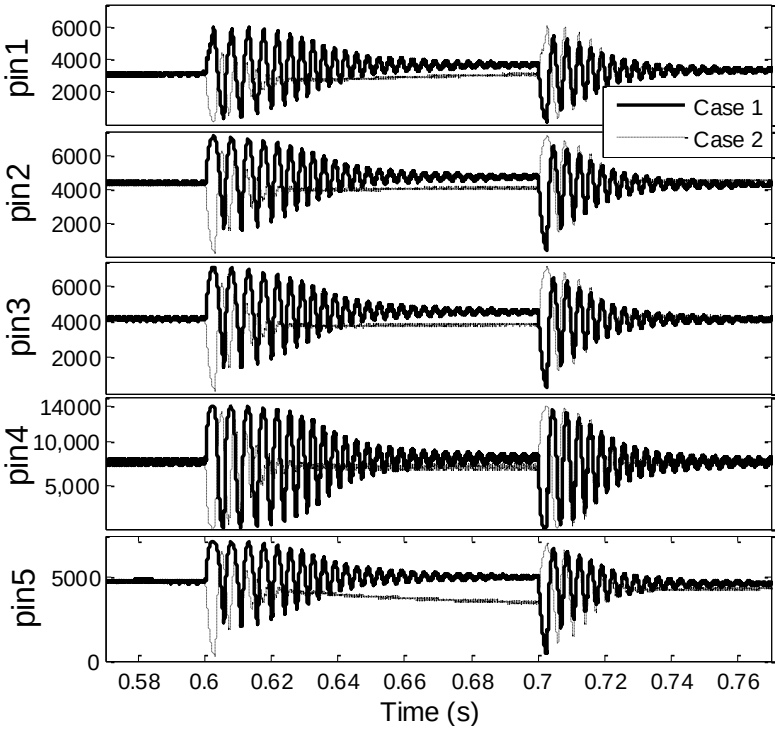

Fig. 3.7 DDC input powers after the load changes in cases 1 and 2.

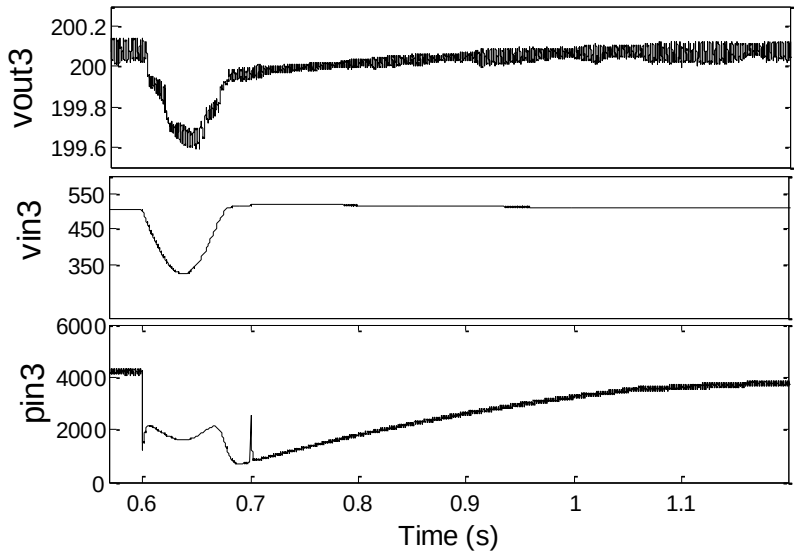


Fig. 3.8 Proposed controller's performance in the presence of intermittent solar power in case 3.

*Case 4*. The robustness of the controller is tested under a low impedance ground fault $R_{fault}=1\Omega$ condition. The fault is applied on bus 10 at t=0.6 s and removed after 5 ms at t=0.605 s. The results are depicted in Fig. 3.9 where good damping of the DDCs voltages and powers is observed.

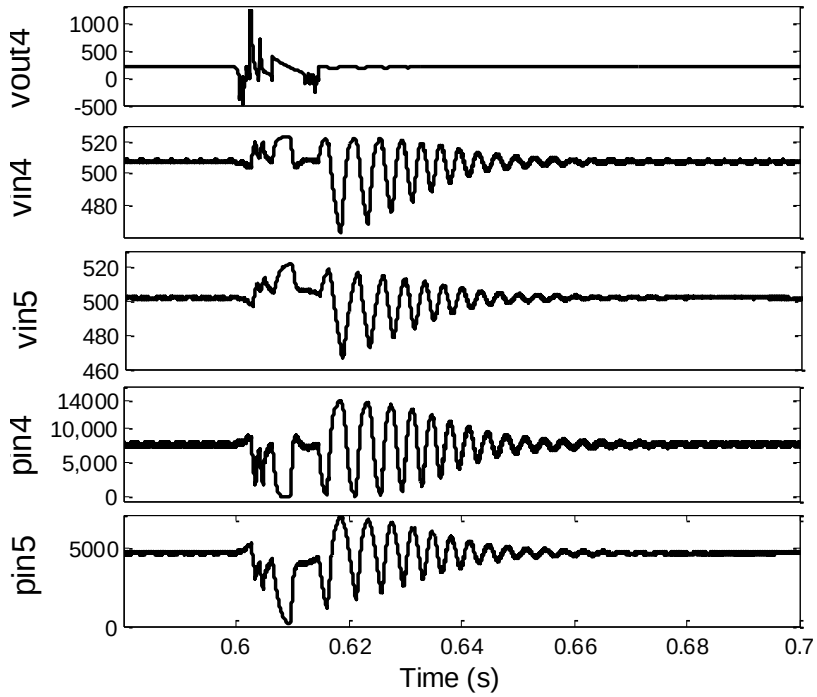


Fig. 3.9 Low impedance ground fault in case 4.

*Case 5.* The droop-based controller proposed in [5] with parameters $K_P = 30$ and $K_I = 1$ is applied to DDCs to be compared against the proposed controller. In this scenario, load $P_{L,11}$ increases from 1 kW to 2 kW at t=0.6 s and gets disconnected at t=1 s. As Fig. 3.10 implies, as opposed to the proposed controller's precise voltage tracking, the droop controller has a significant voltage fluctuations in steady state condition.

*Case 6.* Figure 3.11 compares the proposed controller with droop controller in another scenario in which there is a sinusoidal measurement noise of 1 kHz frequency and 2 V (peak-peak) in all the output voltage measurements. As the results show the proposed controller has better noise rejection over the droop controller.

In general, the proposed adaptive neural network decentralized controller makes a decent control performance in stabilizing the interconnected dc grid.

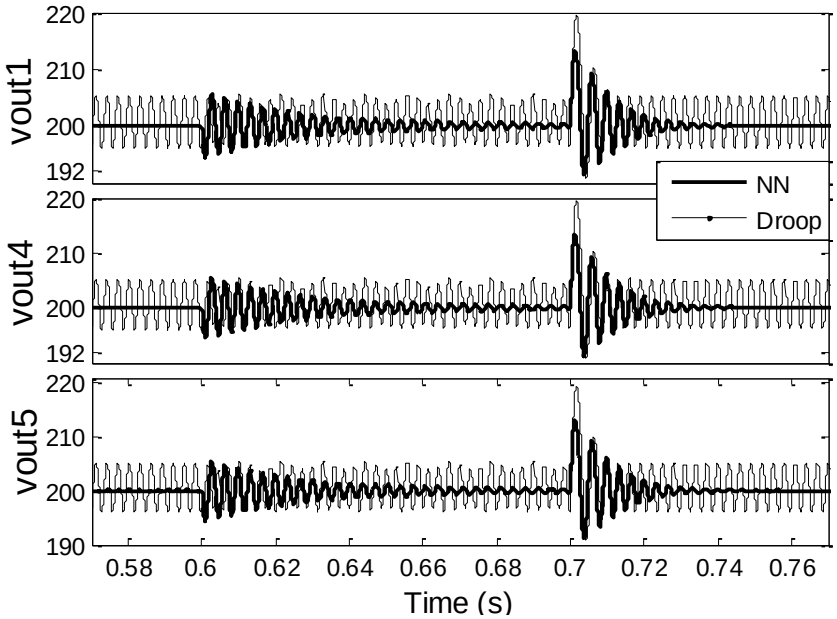

Fig. 3.10 The proposed NN and droop controllers under the load change of case 5.

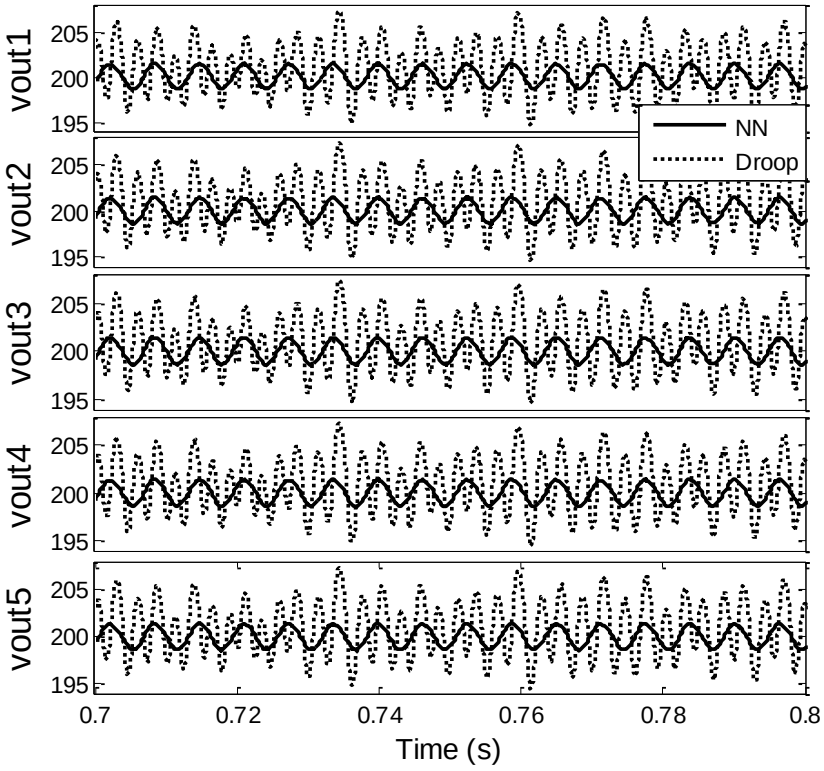


Fig. 3.11 The proposed NN and droop controllers in response to measurement noise in case 6.

### 3.6 Conclusion

In this chapter, a decentralized discrete-time model of the interconnected dc distribution system is stabilized through an adaptive output feedback neural network controller. The dc distribution system consists resistive and constant-power loads (CPLs.) and multiple dc sources which are photovoltaic sources connected to the grid via dc-dc converters. A decentralized output feedback controller design is introduced to mitigate voltage and power oscillations after disturbances. The neural networks with online learning are utilized to approximate unknown nonlinear functions in the grid's dynamic. As the output feedback controller is able to estimate some of the systems states in case they are not available. Simulation results imply that the entire dc grid is stabilized suitably through the proposed controller.

### 3.7 References

[1] S. Mehraeen, S. Jagannathan, and M. L. Crow, "Decentralized adaptive neural network state and output feedback control of a class of interconnected nonlinear discrete-time systems," *Proc. of American Control Conference (ACC)*, Montreal, Canada, June 2012, pp. 6406–6411.

[2] S. Kazemlou and S. Mehraeen, "Decentralized discrete-time adaptive neural network control of interconnected dc distribution system," *IEEE Trans. Smart Grid*, vol.5, no.5, pp. 2496–2507, Sep. 2014.

[3] F. L. Lewis, S. Jagannathan, and A. Yesildirek, "*Neural Network Control of Robot. Manipulators and Nonlinear Systems*," Taylor & Francis, 1998.

[4] S. Huang, K.K. Tan, and T.H. Lee, "Decentralized control design for large-scale systems with strong interconnections using neural networks," *IEEE Trans. Automatic Control*, vol. 48, no. 5, pp. 805–810, 2003.

[5] S. Anand and B. G. Fernandes, "Reduced-order model and stability analysis of low-voltage dc microgrid," *IEEE Trans. Industrial Electronics*, vol. 60, no. 11, pp. 5040–5049, 2013.

[6] J. M. Steele, "*The Cauchy-Schwarz Master Class: An Introduction to the Art of Mathematical Inequalities*," Maa Problem Books Series, The Mathematical Association of America, 2004.

[7] F. L Lewis, D. M. Dawson, and C. T. Abdallah, "*Robot manipulator control: Theory and practice*," CRC Press. 2003.

# CHAPTER 4
# NOVEL DECENTRALIZED CONTROL OF POWER SYSTEMS WITH PENETRATION OF RENEWABLE ENERGY SOURCES IN SMALL-SCALE POWER SYSTEMS

## 4.1 Introduction

Conventional synchronous generators have large inertia and can store a significant amount of energy in their rotating mass. When a fault or disturbance occurs in the power grid, the generators provide power balance in the network by storing or injecting power instantaneously. Therefore, the system naturally possesses some robustness against disturbances. By contrast, available distributed energy resources that are connected to the grid via grid-tie inverters (GTIs) rely only on a small amount of energy stored in their dc-link capacitor, and thus, lack these large kinetic buffers unless costly battery storage or large capacitors are employed. In order to involve the renewable generator in grid stability enhancement, the idea of modeling GTI similar to a synchronous generator has been used in many literatures [6]-[11], proposing the concept of "virtual synchronous generator" (VSG) [6] and "synchronverter" [7]. However, majority of the research in this area does not consider the dynamics of the dc-link capacitor and the stability of the overall system. In [6], the concept of "Virtual Synchronous Machine" (VSM) is presented where the power electronic interface can have virtual inertia equivalent to the rotor's inertia of a synchronous generator. Then, the inverter's reference currents are calculated from the grid voltage. However, it is assumed that the inverter has access to abundant energy and the dc-link dynamics are not considered. In [7]-[10] the inverter connecting the renewable energy source to the large grid is controlled to respond to the frequency variations while the dc-link voltage variations in small and micro grid and the stability of the entire grid are not considered. In [7], the inverter is modeled similar to a synchronous generator by considering imaginary rotor

angle and field current to provide desired active and reactive powers. In this model, the GTI phase angle mimics rotor angle. However, the dc-link dynamic has no relation to the inverter operation. In [8] and [11], a virtual inertia is attained by adding short-term energy-storage to the inverter and the required damping power proportional to the derivative of the grid frequency is supplied by the storage resulting in an increased integration cost due to storage rather than the dc-link capacitor.

On the other hand, recent advances in decentralized controllers [12]-[17] has made them attractive in power system stabilizer designs. Due to the requirement of a large amount of information exchanges between subsystems, increased need for computing capacity [12]-[14], and significant time delays [15], [16] in the centralized controllers, decentralized control is preferred to ensure the performance and stability of the power grid. Decentralized control strategies achieve transient stability and steady-state requirements based only on local information and measurements. In the past few years, much research work has been conducted on adaptive neural networks (NNs) decentralized control of nonlinear interconnected systems [17]-[19] including multi-generator power systems [12]-[16], [20]. Several authors in [16] and [18], [19] propose adaptive neural network decentralized controllers for interconnected systems and provide asymptotic stability; however, extra filters are required besides the neural network controller to provide the stability. In addition, in multi-generator transient stability the variations of the generators' input powers are neglected [12]-[16], [20]; an assumption that is not valid considering renewable energy sources such as solar arrays whose powers fluctuate with voltage.

Thus, this chapter aims at a) developing dynamical model of a renewable generator that behaves like a synchronous generator and includes both dc-dc and dc-ac conversion dynamics with a focus on the dc link energy fluctuations and stability and b) developing an adaptive

nonlinear decentralized stabilizer in continuous-time that is applied to all grid generators, regardless of their type, and assures the entire grid's stability through Lyapunov stability method.

In this chapter, the power system with penetration of renewable generators is considered where GTIs and dc-dc converters are used to interface the device to the grid in order to control the delivered power. A lot of attention has been paid to solar power in this chapter; however, the proposed approach can be used with other renewable energy sources that connect to the grid through GTI. Here, we refer to renewable energy source as the source of renewable energy such as wind, solar, etc., and renewable generator as the renewable energy system interacting with power grid that includes the source of energy as well as the pertinent power electronic and storage. In the proposed GTI model with dynamic gain and phase angle control, the renewable generator is modeled to possess similar dynamics to those of synchronous generator and the dc-link capacitor acts as the energy storage similar to the rotor of a synchronous generator. As opposed to existing VSG and synchronverter [6]-[11] models in which an imaginary inertia is considered, the energy stored in the dc-link capacitor plays the role of kinetic energy storage and appears as a dynamical state. In the proposed approach, the GTI can be controlled by excitation-like mechanisms such as AVR and PSS as well as their nonlinear counterparts. Next, the renewable generator dynamical model is extended to include the dynamics of the dc-dc converter interfacing the renewable energy source and the inverter.

Subsequently, proper nonlinear decentralized controllers are developed to stabilize the individual GTIs and the dc-dc converters. The assumption on constant input power used in the past literature is not considered. This helps integrate low-inertia renewable generators such as PV arrays into the small and micro grids. Also, much attention has been given to the multi-generator and nonlinear natures of the interconnected power grid as opposed to the past work that

considers single-machine-infinite-bus type of system [6]-[11]. Subsequently, the asymptotic stability of the overall system comprising synchronous generators and renewable generators is ensured by employing the proposed GTI and converter controllers through Lyapunov stability method. Finally, the decentralized controller is simplified. The simplified controller is easier to synthesize; however, it only assures that the states errors only stay bounded. In order to achieve this, neural networks (NNs) with quadratic neural network update law are utilized to approximate unknown interconnection effects of the grid on the synchronous generators and renewable generators and to avoid additional filters used in the previous approaches [16], [18], [19]. The proposed decentralized neural network controller is applied to both the synchronous generators excitations and the GTI excitation-like mechanisms.

The rest of the chapter is organized as follows. In the next section the model for renewable generator consisting the GTI and solar dc-dc converter is presented. Section 4.3 proposes the nonlinear decentralized controller for GTI and feedback controller for solar converter. Simulation results are shown in Section 4.4 followed by the concluding remarks in Section 4.5.

**4.2 Renewable Generator Model**

In this section, the dynamical model along with the control mechanism of the renewable generator, shown in Fig. 4.1, comprising a photovoltaic source connected to a grid-tie inverter via a dc-dc converter is represented. The entire grid comprises *n* subsystems including $n_1$ renewable generators and $n-n_1$ synchronous generators. Figure 4.1 represents one of the grid subsystems where index $1 \le i \le n_1$ indicates the subsystem number and $n_1$ is the total number of renewable generators.

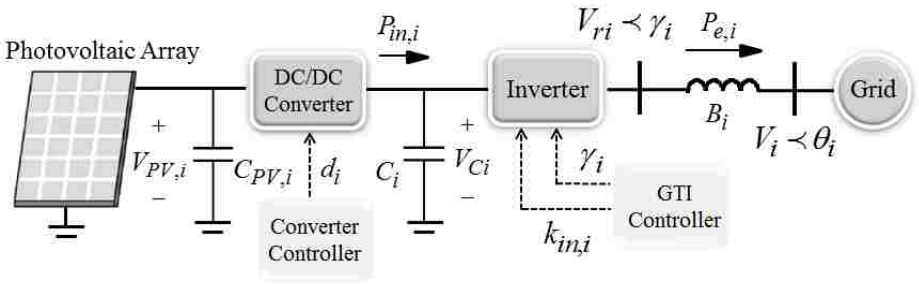


Fig. 4.1 The *i*-th renewable generator.

A. Grid-tie inverter model

The dynamic of the dc-link stored energy can be represented by the capacitor voltage driven by the power balance equation at the dc link as

$$C_i V_{Ci} \dot{V}_{Ci} = P_{in,i} - \bar{P}_{e,i} \qquad i = 1, \ldots, n_1 \tag{1}$$

where $n_1$ is the number of renewable generators, $V_{Ci}$ is the dc-link voltage of the *i*-th renewable generator, $P_{in,i}$ is the injected power to the dc-link from the dc-dc converter, and $\bar{P}_{e,i}$ is the delivered power to the grid by the *i*-th renewable generator as depicted in Fig. 4.1. The delivered power from the *i*-th GTI to the grid is given by

$$\bar{P}_{e,i} = B_i V_{ri} V_i \sin(\gamma_i - \theta_i) \qquad , \qquad i = 1, \ldots, n_1 \tag{2}$$

where $V_{ri}$ and $\gamma_i$ denote the GTI output voltage magnitude and phase angle, and $V_i$ and $\theta_i$ represent the voltage magnitude and phase angle of the grid bus connected to the GTI through admittance $B_i$.

Angle $\gamma_i$ can be altered to adjust the renewable generator output power and consequently acts similar to the rotor angle $\delta$ in the synchronous generator [21]. An auxiliary variable $\lambda_i$ is used to control $\gamma_i$ in the renewable generator as

$$\dot{\gamma}_i = \lambda_i . \tag{3}$$

Variable $\lambda_i$ mimics the rotor speed in the synchronous generator. In synchronous generators, the speed relates to the kinetic energy stored in the rotor. In order to give imaginary speed $\lambda_i$ a meaningful relationship to the stored energy in the dc-link capacitor, it is defined as

$$\dot{\lambda}_i = V_{Ci}\dot{V}_{Ci} = (1/C_i)(P_{in,i} - \bar{P}_{e,i}) . \quad (4)$$

In order to preserve the similarity to the synchronous generator, per unit values of $V_{Ci}$, $\lambda_i$, and $C_i$ are utilized in (4). From (4) it yields

$$\lambda_i = (V_{Ci}{}^2 - V_{Cio}{}^2)/2 \quad (5)$$

representing the scaled changes in the dc-link stored energy with $V_{Cio}$ as the steady-state value of $V_{Ci}$. In the renewable generator, capacitance $C_i$ plays the role of machine inertia; that is, its higher size reduces the oscillations and contributes to an enhanced dynamic stability.

Next, in order to attain excitation-like control to the renewable generator, two new auxiliary parameters are defined as $E'_{qri}$ and $E_{fdri}$, similar to the rotor flux and field voltage in the synchronous generator, introducing a third dynamic to the renewable generator; i.e.,

$$\dot{E}'_{qri} = \frac{1}{T_{dr0i}}\left(-(x_{dri}/x'_{dri})E'_{qri} + ((x_{dri} - x'_{dri})/x'_{dri})V_i \cos(\gamma_i - \theta_i) + E_{fdri}\right) \quad (6)$$

where parameters $x_{dri}$, $x'_{dri}$ and $T_{dr0i}$ are design parameters that need to be chosen for each renewable generator as opposed to those of synchronous generator that are machine parameters and fixed. $E_{fdri}$ is the applied field-voltage-like input to the GTI imaginary excitation system and can be controlled by any of the known synchronous generator excitation control methods. Equations (3), (4), and (6) represent a one-axis-like model for the renewable generator. In the one-axis model the device output power satisfies [21]

$$P_{ei} = (1/x'_{dri})V_i\,[E'_{qri}\sin(\gamma_i - \theta_i) - ((x_{qri} - x'_{dri})/(2\,x_{qri}))V_i\sin(2(\,\gamma_i - \theta_i))] \tag{7}$$

with parameter $x_{qri}$ to be a renewable generator design parameter, as opposed to synchronous generator q-axis reactance, that is a fixed machine parameter.

*Remark 1.* As mentioned earlier, angle $\gamma_i$ is a state variable that acts in a manner similar to rotor angle in the synchronous generator; that is, it varies with changes in the capacitor's stored energy. In the synchronous generator the rotor angle is not equivalent to the output voltage phase angle. Rather, the relationship between the rotor angle and the output voltage phase angle in the synchronous generator is more involved and depends on the selected synchronous generator model [22] (i.e., one-axis, two-axis, etc.) By contrast, in this work it is aimed to represent the GTI output voltage phase angle by $\gamma_i$ (unlike in the synchronous generator [7]) since it provides an easier implementation in the GTI where a phase angle and an amplitude modulation index [22] is directly generated and applied to the GTI. In order to achieve this goal it is necessary that the power from (7) (i.e., synchronous-generator-like power) is equal to the GTI power obtained from (2); thus, $\overline{P}_{e,i} = P_{e,i}$. This in turn requires inverter voltage $V_{ri}$ to be

$$V_{ri} = \frac{E'_{qri}\sin(\gamma_i - \theta_i) - \dfrac{x_{qri} - x'_{dri}}{2\,x_{qri}}V_i\sin(2(\,\gamma_i - \theta_i))}{x'_{dri}\,B_i\sin(\gamma_i - \theta_i)}. \tag{8}$$

Inverter amplitude modulation index $k_{in,i}$ can be tuned to adjust the GTI output voltage obtained in Remark 1 as

$$k_{in,i} = V_{ri}/V_{Ci}. \tag{9}$$

Adjusting amplitude modulation index $k_{in,i}$ according to (9) allows the GTI to deliver the synchronous-generator-like power governed by (7). Inverter gain $k_{in,i}$ and phase angle $\gamma_i$ are

control parameters and could be altered to adjust the renewable generator output power and enhance the individual GTI and grid stability.

Now, equations (3), (4), and (6) represent a one-axis model of the renewable generator as

$$\dot{\gamma}_i = \lambda_i; \quad \dot{\lambda}_i = (1/C_i)(P_{in,i} - P_{e,i}) \tag{10}$$

$$\dot{E}'_{qri} = \frac{1}{T_{dr0i}}\left(-(x_{dri}/x'_{dri})E'_{qri} + ((x_{dri} - x'_{dri})/x'_{dri})V_i \cos(\gamma_i - \theta_i) + E_{fdri}\right).$$

The inputs to the model are bus voltage magnitude $V_i$, angle $\theta_i$, capacitor voltage $V_{Ci}$, and control voltage $E_{fdri}$, which are all local measurements, while the outputs are inverter amplitude modulation index $k_{in,i}$ and phase angle $\gamma_i$ that are sent to the GTI power electronic switches. By using the proposed modeling and GTI control mechanism, the renewable generator can be considered as an imaginary synchronous generator and behaves similarly.

*Remark 2*. Phase angle $\gamma$ can be adjusted under constant or variable frequency. In the latter case, one can use $\lambda = 2\pi(f_{inv} - f_0)$ to find the inverter frequency $f_{inv}$ while $f_0$ is the grid (desired) frequency.

*Remark 3*. Through the synthesized states, an AVR-like mechanism can take the GTI's capacitor voltage error as input and be applied for steady-state and transient performance.

B. Solar DC-DC Converter

The renewable energy sources are often interfaced to the GTI through a dc-dc converter. The transmitted power by these PV arrays can vary dramatically with changes in the GTI dc-link voltage during grid transients. Non-linear characteristics of the renewable energy source and dynamics of the dc-dc converter must then be taken into account in the stability analysis. In this work, the buck converter is considered to interface the solar source to GTI. Although the boost

converter is more attractive for solar systems steady-state operation due to higher output voltage, its output voltage can grow exponentially with duty cycle as opposed to that of the buck converter. Thus, the operating range in the boost converter is very limited [23], [24] and it is less stable than the buck converter. Moreover, topologies such as forward converters [25] that utilize transformers can be implemented to boost the voltage while taking advantage of the buck converter performance.

For the PV system, usually the maximum power point tracking (MPPT) is carried out at the PV terminals by adjusting the duty cycle of the converter that connects the PV array to the GTI. During the transients, changes in the GTI dc-link voltage affect the harvested power since the PV array power depends on its terminal voltage. Thus, a control mechanism should be utilized to stabilize the PV array terminal voltage by dynamically adjusting the converter duty cycle when the GTI dc-link voltage fluctuates. A topology to achieve this goal is demonstrated in Fig. 4.2. Capacitor $C_{pv,i}$ between the PV array and the GTI helps decouple the GTI's dynamics from that of the PV array and provide more stability.

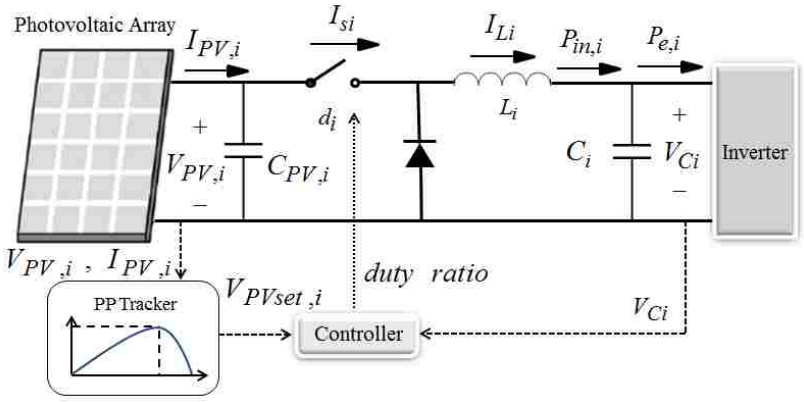


Fig. 4.2 PPT and dc/dc buck converter control system.

The set point for $V_{pv,i}$ is indicated by the MPPT block. The MPPT block command changes with the sun irradiation level. Although the maximum power point is usually the goal,

stability can be maintained around any power point. At each moment, any change in the GTI dc-link voltage ($V_{Ci}$) changes the PV array output power (capacitor input power $P_{in,i}$) and requires the converter duty cycle to adjust such that $P_{in,i}$ tracks the reference power through maintaining a constant voltage at the PV array terminals. Thus, a proper model and controller for buck converter in the presence of the PV array characteristics is developed in this section.

By adding the dynamics of a dc-dc buck converter in discontinuous-current mode (DCM) operation to the GTI dynamics, the renewable generator dynamical model is represented as

$$\dot{\gamma}_i = \lambda_i ; \quad \dot{\lambda}_i = (1/C_i)(P_{in,i} - P_{e,i})$$

$$\dot{E}'_{qri} = \frac{1}{T_{dr0i}}\left(-(x_{dri}/x'_{dri})E'_{qri} + ((x_{dri} - x'_{dri})/x'_{dri})V_i \cos(\gamma_i - \theta_i) + E_{fdri}\right)$$

$$\dot{I}_{Li} = 1/L_i\,(d_i V_{pv,i} - V_{Ci}) \tag{11}$$

$$\dot{V}_{pv,i} = 1/C_{pv,i}\,(I_{pv,i} - d_i\, I_L)$$

where $L_i$ is the dc-dc converter inductance, $d_i$ is the converter duty cycle, and $V_{pv,i}$ and $I_{Li}$ are the converter input voltage and inductor current, respectively. $I_{pv,i}$ is the photovoltaic array output current (shown in Fig. 4.2) which is a function of PV array output voltage $V_{pv,i}$ in the following form [26]

$$I_{pv,i} = \kappa(V_{pv,i}) = n_{pi} I_{ph} - n_{pi} I_{rs}(e^{\mu_i V_{pv,i}} - 1) \tag{12}$$

where $\mu_i = q/(n_{si}\phi KT)$ with the Boltzmann's constant $K = 1.3805 \times 10^{-23}\, J/K$, electronic charge $q = 1.6 \times 10^{-19}\, C$, cell temperature $T$, and the p-n junction characteristic factor $\phi$ (between 1 to 5.) In addition, $n_{pi}$ and $n_{si}$ are the numbers of the parallel branches and branch series solar cells,

respectively, $I_{ph}$ is the solar cell generated current, and $I_{rs}$ denotes the reverse saturation current.

### 4.3 Decentralized Controller Design

So far, a control mechanism is presented that is capable of mimicking a synchronous generator with excitation control through appropriate GTI amplitude modulation index and phase angle control. Also, the developed renewable generator model incorporates the dc-dc converter that connects the dc source to the GTI. To this end, any excitation-like controller may be employed with the proposed control mechanism to achieve subsystem (renewable generator) and overall grid stability. An example is given in Remark 3. It is desired that the controller/stabilizer provide the entire grid stability through individual subsystem control using only local measurements with assured performance. In addition, considerations on the dc-dc converter must be taken into account to address internal stability of the renewable generator in contrast with synchronous generators that have full state observability. These considerations are discussed in the following sections.

In this section, a decentralized representation of the renewable generator is obtained. The GTI dynamics are represented in Brunovsky canonical form and an adaptive state feedback controller is utilized to stabilize the inverter dc-link voltage through adjusting the inverter amplitude modulation factor and phase angle. The adaptive neural networks (NNs) [27] are employed to approximate the unknown nonlinearities. In addition, feedback linearization is utilized to mitigate the oscillations of the solar power caused by the grid disturbances.

The work of [18], [19] propose stable adaptive neural network decentralized controllers for interconnected systems; however, extra filters are required besides the neural network controller. By contrast, [16] utilizes quadratic error terms in the neural network update laws for

interconnected systems in backstepping form and achieves asymptotic stability; however, additional filters are still required. One of the main contributions of this work is achieving asymptotic stability in the grid while avoiding the extra filters introduced in the past literature [16] and the simulation results have been compared to this method. Subsequently, the controller is simplified.

A. Grid-Tie Inverter Decentralized Controller

One can define the individual renewable generator states represented by (11) in vector form as

$$\xi_i = [\xi_{1i}, \xi_{2i}, \xi_{3i}, \xi_{4i}, \xi_{5i}] = [\Delta\gamma_i, \lambda_i, E'_{qri}, V_{pv,i}, I_{Li}]$$

where $\Delta\gamma_i = \gamma_i - \gamma_{oi}$ and $\gamma_{oi}$ is the inverter output voltage phase angle in steady-state condition. In order to represent the renewable generator dynamics in Brunovsky canonical form, a new set of state variables are defined as

$$x_{1i} = \Delta\gamma_i \;;\; x_{2i} = \lambda_i \tag{13}$$

$$x_{3i} = \frac{P_{in,i} - P_{ei}}{C_i} = 1/C_i \,(V_{Ci}\, I_{Li} - E'_{qri} I_{qi} - (x_{qi} - x'_{di}) I_{qi} I_{di})$$

for $i = 1, \ldots, n_1$ where

$$I_{qi} = B_i V_i \sin(\gamma_i - \theta_i);\; I_{di} = B_i \left(E'_{qri} - V_i \cos(\gamma_i - \theta_i)\right)$$

and

$$\dot{x}_{i3} = \frac{1}{C_i}(\dot{P}_{in,i} - \dot{P}_{ei}) = \frac{1}{C_i}[\dot{V}_{Ci}\, I_{Li} + V_{Ci}\, \dot{I}_{Li} - \frac{I_{qi}}{T_{dr0i}} \begin{pmatrix} -(x_{dri}/x'_{dri}) E'_{qri} + ((x_{dri} - x'_{dri})/x'_{dri}) V_i \cos(\gamma_i - \theta_i) \\ + E_{fdri} \end{pmatrix}$$
$$- E'_{qri} \dot{I}_{qi} - (x_{qi} - x'_{di})(\dot{I}_{qi} I_{di} + I_{qi} \dot{I}_{di})] \tag{14}$$

where $i = 1, \ldots, n_1$ is the renewable generator number. With the inclusion of $n_2 = n - n_1$ synchronous generators that are driven by similar dynamics to (13), the total number of the subsystems (generators) is $n = n_1 + n_2$.

Terms $\dot{I}_{qi}$ and $\dot{I}_{di}$ in (13) generally depend on the entire grid state vector that contains the states of all synchronous and renewable generators in the grid since the time derivatives involve the entire grid states [16]. Thus, they are considered interconnection terms for the *i*-th subsystem (for $i = 1, \ldots, n$.) By substituting $\dot{V}_{Ci}$ and $\dot{I}_{Li}$ from (4) and (11) and conducting input-output feedback linearization, (13) can be rewritten as

$$\begin{aligned} &\dot{x}_{1i} = x_{2i} \,;\; \dot{x}_{2i} = x_{3i} \\ &\dot{x}_{3i} = f_i(\xi_i) + g_i(\xi_i)\, u_i + \Delta_i(X) \end{aligned} \tag{15}$$

where $x_i = [x_{1i},\, x_{2i}, x_{3i}]^T$ , $X = [x_1, \ldots, x_n]^T$ , $f_i(\xi_i)$ is called internal dynamics, $g_i(\xi_i)$ is the input gain, and $u_i$ is the subsystem state feedback control input to be designed for $i = 1, \ldots, n_1$. According to renewable generator model (13), $g_i(\xi_i) = -I_{qi} / (C_i\, T_{dr0i})$ and $u_i = E_{fdri}$. The unknown interconnections are $\Delta_i(X) = 1/C_i\,[-E'_{qi}\dot{I}_{qi} - (x_{qi} - x'_{di}) \times (\dot{I}_{qi} I_{di} + I_{qi}\dot{I}_{di})]$ and is a function of the entire grid states. A model similar to (15) can be derived for synchronous generators when one-axis model is utilized [16]; thus, dynamics (15) are applied to all the subsystems (generators) including renewable generators and synchronous generators.

It is desired to design a controller that stabilizes $x_i$ at the origin ( $x_i = 0$ ) for $i = 1, \ldots, n$. Thus, filtered error is defined as

$$r_i = [\lambda_i \;\; 1]^T x_i \tag{16}$$

where $\lambda_i = [\lambda_{1i} \ \lambda_{2i}]$ is chosen in such a way that polynomial $\chi(s) = \lambda_{1i} + \lambda_{2i} s + s^2$ is Hurwitz. This way, when filtered error goes to zero, it causes the grid errors converge to zero. The derivative of the filtered error is

$$\dot{r}_i = [\lambda_i \ 1]^T \dot{x}_i = f_i(\xi_i) + g_i(\xi_i) u_i + a_i(\xi_i) + \Delta_i(X) \tag{17}$$

where $a_i(\xi_i) = [0 \ \lambda_i]^T x_i$.

Before discussing the control design methodology the following brief introduction and assumptions are introduced:

A general function $f(x) \in \Re$ where $x \in \Re^m$ can be written as $f(x) = W^T \Phi(\bar{V}^T x) + \varepsilon(x)$ [16], [27] in the compact set $\Lambda \in \Re^m$ (neural network approximation domain) with $\varepsilon(x)$ denotes neural network functional reconstruction error vector, $h_i(\xi_i)$ and $\bar{V} \in R^{m \times N}$ represent target neural network weight matrices.

*Assumption 1*- Functions $g_i(\xi_i)$ are away from zero for $1 \le i \le n$. That is, $0 < g_{\min,i} \le g_i(\xi_i)$. Also, it is assumed that $|\dot{g}_i| \le g_{d\max,i}$, where $g_{\min,i}$ and $g_{d\max,i}$ are positive constants. This is a valid assumption for the ac grid since the rate of change in GTI current $I_{qi}$ is physically limited in the electric grid. Also, since the transients occur around a significantly high GTI steady-state current, it is reasonable to assume that GTI current $I_{qi}$ is always away from zero.

*Assumption 2* [19]- The interconnection terms are bounded by a function of the filtered error such that $|\Delta_i(X)| \le \sum_{j=1}^{n} \eta_{ij} \|r_j\|_2$ where $\eta_{ij}$ is a positive constant for $1 \le i \le n$. Since the interconnection effects vanish when state errors converge to zero, this assumption is applicable to the interconnected power grids.

The stabilizing control input $u_i$ should be chosen in such a way that makes the filtered error asymptotically stable in the form of $\dot{r}_i = -K_i r_i$ (with $K_i > 0$) in the absence of the interconnection terms. Thus, one can define the stabilizing controller as

$$u_i = u_i^* = u_{id} - K_i r_i \tag{18}$$

where

$$u_{id} = -\frac{f_i(\xi_i) + a_i(\xi_i)}{g_i(\xi_i)} - h_i(\xi_i) r_i . \tag{19}$$

and $h_i(.)$ is a nonlinear function to be designed to overcome the effects of the interconnection terms. The interconnection terms are in general uncertain and difficult to obtain due to unavailable grid states. Thus, term $h_i(\xi_i)$ is an unknown nonlinear function. In order to synthetize desired controller $u_{id}$, the neural network function approximation property [27] is employed to approximate $u_{id}$ using the available states as

$$u_{id} = -\frac{f_i(\xi_i) + a_i(\xi_i)}{g_i(\xi_i)} + r_i W_i^{*T} \Phi_i(x_i, \xi_i) + r_i \varepsilon_i(x_i, \xi_i) \tag{20}$$

where $W_i^*$ is the target neural network weight matrix, $\Phi_i(.)$ is a set of basis functions [27], and $\varepsilon_i(.)$ is the neural network function approximation error that satisfies $\|\varepsilon_i(.)\| \le \varepsilon_{Mi}$ [27] in the compact set $\Lambda$ comprising all possible variations of variables $x_i$. In practice, the target neural network weight matrix $W_i^*$ is not available and needs to be estimated by $\hat{W}_i$ resulting in the weight estimation error $\tilde{W}_i = \hat{W}_i - W_i^*$. Thus, $u_{id}$ is approximated as $\hat{u}_{id}$, and controller $u_i$ in (18) becomes

$$u_i = \hat{u}_{id} - K_i r_i = -\frac{f_i(\xi_i) + a_i(\xi_i)}{g_i(\xi_i)} + r_i \hat{W}_i^T \Phi_i - K_i r_i \ . \tag{21}$$

Since the target neural network weights are unknown, an adaptive update mechanism is employed to train the neural network online and without any prior training phase. Define the neural network weight update law as

$$\dot{\hat{W}}_i^T = -\rho_i \, r_i^2 \hat{W}_i^T + \rho_i r_i^2 \Phi_i \tag{22}$$

where $\rho_i$ is a positive constant. Employing a quadratic term of the error in neural network weight update law ensures the locally asymptotic stability of the filtered error dynamic without using additional filters in the controller used in the past literature [16], [19]. The block diagram of the adaptive neural network controller is depicted in Fig. 4.3.

The stability of the nonlinear interconnected system in the presence of unknown interconnection terms $\Delta_i(X)$ with the proposed adaptive neural network controller for $1 \le i \le n$ is proven and given in Appendix C by showing the stability of the filtered errors $r_i$ and weight estimation errors $\tilde{W}_i$ for all $1 \le i \le n$.

*Remark 4*. In order to simplify the design, controller in the form of $u_i = r_i \hat{W}_i^T \Phi_i - K_i \, r_i$ can also be implemented with the neural network update law (22). In this case, the knowledge of the renewable generator or synchronous generator dynamics $f_i(.)$ and $g_i(.)$ is not needed. However, asymptotic stability of the errors cannot be proven; that is, only boundedness of the errors can only be proven. Thus, the state errors will stabilize but may not reach their original values. By selecting proper control gains and neural network adaptation rate this effect can be minimized to a reasonable extent. The proof of boundedness in this case is very similar and is not included.

*Remark 5*. Dynamics represented in (15) are of order three while renewable generator original dynamics (11) are of order five. The two *unobservable* dynamics in (15) are known as *internal dynamics* [27]. When the observable states $x_i = [x_{1i}, \, x_{2i}, x_{3i}]^T$ converge to zero by employing a

proper controller, the internal dynamics (*zero dynamics*,) must be stable to assure the overall grid stability resulting in a *minimum-phase* system [27]. In the proposed design, the dc-dc converter dynamics $V_{pv,i}$ and $I_{Li}$ are the subsystem zero dynamics and must be stable when the observable states $x_i = [x_{1i}, x_{2i}, x_{3i}]^T$ converge to zero. In order to achieve stable zero dynamics, the dc-dc converter must be equipped with an appropriate controller, as will be explained in the following.

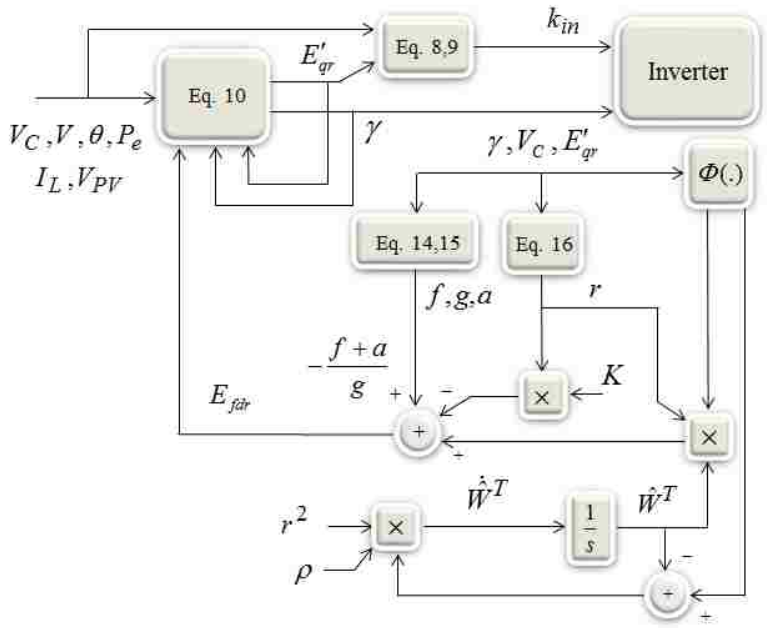


Fig. 4.3 GTI neural network controller.

B. Solar Power dc-dc Converter Controller Design

*A* dc-dc converter stabilizer is aimed in this part for the PV-connected converter. Although the controller employs the solar array specifications, the method is not restricted to solar power and can be applied to other dc power sources such as rectified wind power, fuel cells, etc.

In discontinuous-current mode (DCM) operation of a dc-dc buck converter (Fig. 4.4,) the relationship between the maximum inductor current $I_{L,\max,i}$ and the duty cycle is

$$I_{L,\max,i} = d_i T_s (V_{pv,i} - V_{Ci}) / L_i \tag{23}$$

where $T_s$ is the switching period, and $V_{pv,i}$ and $V_{Ci}$ are the input and output voltages of the $i$-th solar converter, respectively.

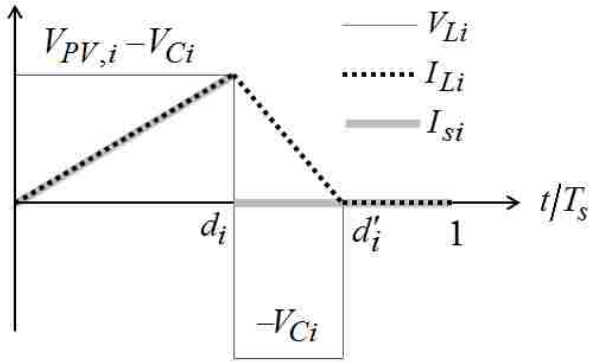


Fig. 4.4 DCM operation of buck converter.

The switch average current is calculated as

$$I_{s,ave,i} = d_i I_{L,\max,i} / 2 = d_i^2 T_s (V_{pv,i} - V_{Ci}) / (2L_i) . \tag{24}$$

Also, the input capacitor (Fig. 4.2) follows dynamic

$$C_{pv,i} \dot{V}_{pv,i} = I_{pv,i} - I_{s,ave,i} = \kappa(V_{pv,i}) - d_i^2 T_s (V_{pv,i} - V_{Ci}) / (2L_i) \tag{25}$$

where $I_{pv,i}$ is the photovoltaic array output current which is a function of PV array output voltage $V_{pv,i}$ in the following form [26]

$$I_{pv,i} = \kappa(V_{pv,i}) = n_{pi} I_{ph} - n_{pi} I_{rs} (e^{\mu_i V_{pv,i}} - 1) \tag{26}$$

as explained.

The solar output voltage can be decomposed as

$$V_{pv,i} = \bar{V}_{pv,i} + v_{pv,i} \tag{27}$$

where $\bar{V}_{pv,i}$ is the solar output voltage steady-state value and $v_{pv,i}$ is its error. Thus, (25) can be rewritten as

$$\dot{v}_{pv,i} = \kappa(\bar{V}_{pv,i} + v_{pv,i}) / C_{pv,i} - d_i{}^2 T_s \frac{V_{pv,i} + v_{pv,i} - V_{Ci}}{2L_i C_{pv,i}} \tag{28}$$

which is in nonlinear form

$$\dot{v}_{pv,i} = \alpha_i(v_{pv,i}) + \beta_i(v_{pv,i}, t)\, w_i \tag{29}$$

with $\alpha_i(x_i) = \kappa(\bar{V}_{pv,i} + v_{pv,i}) / C_{pv,i}$, $w_i = d_i{}^2$ as the control input, and $\beta_i(v_{pv,i}, t) = -T_s(\bar{V}_{pv,i} + v_{pv,i} - V_{Ci}) / (2L_i C_{pv,i})$. Using feedback linearization and taking the input as

$$w_i = 1/\beta_i(v_{pv,i}, t)(-\alpha_i(v_{pv,i}) - k_i\, v_{pv,i}) = [T_s(V_{pv,i} - V_{Ci})]^{-1} 2L_i C_{pv,i}(C_{pv,i}^{-1}\, \kappa(V_{pv,i}) - k_i\, v_{pv,i}) \tag{30}$$

where, $k_i$ is a design positive constant, one can obtain the asymptotically stable system states dynamics

$$\dot{v}_{pv,i} = -k_i\, v_{pv,i}\,. \tag{31}$$

By selecting a proper design constant $k_i$, the time constant of the exponentially decaying system (31) can be set significantly smaller than that of the GTI and the grid. Thus, the PV array terminal voltage $V_{pv,i}$ can be stabilized quickly resulting in a stable PV array output power.

**4.4 Simulation Results**

As mentioned earlier, all available excitation control methods for synchronous generator can be applied to the renewable generator equipped with the proposed GTI excitation-like mechanism. Here, the IEEE 14-bus, 5-generator power system shown in Fig. 4.5 is considered to demonstrate the effectiveness of the proposed renewable generator model (11) and decentralized controller (21). The renewable generator is connected to bus 5 while synchronous generators are located at buses 1 to 4. The synchronous generators and renewable generator are stabilized with the decentralized controller in Remark 4 as well as converter controller (30). Neural Networks are utilized to approximate the unknown functions required in the controller. The proposed

approach has been compared to the decentralized controller proposed in [16] as well as to the conventional droop control mechanism [1], [2], [28], [29].

A three-phase disturbance occurs at bus 6 at $t = 0.2s$ and is removed at $t = 0.4s$. Bus 5 is connected to a PV generator through a GTI and a dc-dc buck converter as shown in Fig. 4.1. The generators data are given in Table 4.1.

Table 4.1 Synchronous and renewable generators parameters

| Parameters | SGs | RG |
|---|---|---|
| $x'_d, x_d, x_q$ | 0.06 , 0.2 , 0.19 pu | 0.06 , 0.2 , 0.19 pu |
| $T_{d0}$ | 7 sec | 7 sec |
| $H_i = \omega_s M_i / 2$ | $H$=5 for $i$ = 1,4,5; $H$=1 for $i$ =2,3 | - |
| Inverters gain | - | $k_{in}$=0.8 in steady state |
| Capacitor Bank | - | $C = 0.026$ pu |

Two generation and load levels “low” and “high” (given in Table 4.2) are selected for the study to observe the robustness of the controllers.

All four synchronous generators are equipped with speed governors while the renewable generator maintains stable input power through the proposed dynamic converter gain (30). By employing the proposed modeling and decentralized controllers, the renewable generator’s inverter gain $k_{in}$ and angle $\gamma$, and converter duty cycle $d$ are tuned using model (11), and controllers (21) and (30). The power system loads are considered constants. The control objective is to stabilize the synchronous generators speed and the GTI dc-link capacitor voltage

and damp their oscillations caused by the disturbances. Simulations are performed using one-axis model for all synchronous generators

Table 4.2 Network loads and generations for low/high load level

| **Gen Bus No.** | P (p.u.) Active Power Generation Low/**High** | Q (p.u.) Reactive Power Generation Low/**High** | Load Bus No. | P (p.u.) Load Low/**High** | Q (p.u.) Load Low/**High** |
|---|---|---|---|---|---|
| **1 (SG)** | 0.7288<br>**0.7311** | 0.0920<br>**0.1872** | 6 | 0.1750<br>**0.4780** | -0.0390<br>**-0.0390** |
| **2 (SG)** | 0.0472<br>**0.6830** | -0.1136<br>**-0.1022** | 7 | 0.0000<br>**0.0000** | 0.0000<br>**0.0000** |
| **3 (SG)** | 0.1180<br>**0.4420** | - 0.420<br>**-0.420** | 8 | 0.0110<br>**0.0760** | 0.0160<br>**0.0160** |
| **4 (SG)** | 0.0540<br>**0.3120** | 0.2957<br>**0.5243** | 9 | 0.1530<br>**0.5950** | 0.1660<br>**0.1660** |
| **5 (RG)** | 0.1280<br>**0.6120** | 0.1830<br>**0.3134** | 10 | 0.0830<br>**0.3900** | 0.0580<br>**0.0580** |
| | | | 11 | 0.2210<br>**0.0350** | 0.0180<br>**0.0180** |
| | | | 12 | 0.1000<br>**0.6100** | 0.0160<br>**0.0160** |
| | | | 13 | 0.1150<br>**0.1350** | 0.0580<br>**0.0580** |
| | | | 14 | 0.1890<br>**0.3490** | 0.0500<br>**0.0500** |

.

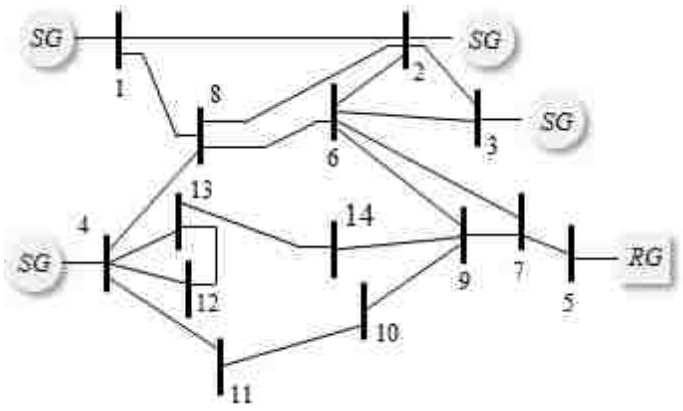


Fig. 4.5 IEEE 14-bus, 5-generator power system.

In the case of high penetration of the renewable energy sources, the renewable generator is a combination of a large number of small renewable energy sources and its dc-link capacitor is the equivalent capacitor of all the renewable generators'.

In Fig. 4.6, rotors speeds are depicted as variables $\omega_1$ to $\omega_4$ for four synchronous generators. Waveform $V_C$ is the renewable generator dc-link voltage. Satisfactory damping is observed for a medium size power network by using the proposed GTI and converter controllers. In addition, in Fig. 4.6, the damping effect of the decentralized DSC control method [16] is compared to that of the proposed controller applied to all the generators where the DCS controller design parameters are chosen as given in [16]. As the results demonstrate, the proposed controller is as effective as DSC stabilizer in damping the disturbance while it has a simpler structure. Figure 4.7 shows the inverter gain ($k_{in}$) for the renewable generator and the duty cycle ($d$) of the dc-dc buck converter when the proposed stabilizer is applied where the stabilizing efforts of the renewable generator controllers are in a reasonable range.

In Fig. 4.8 the system is tested under larger disturbances at different locations with high load levels of Table 4.2.

Figures 4.9 and 4.10 show the performance of dc-dc converter controller (30), which aims at delivering a constant power to the inverter. In the results of Figs. 4.6 through 4.8 the solar array operates at a voltage higher than the maximum power point (MPP). The solar array output voltage and power are shown in Fig. 4.9 where the proposed converter controller (30) mitigates the oscillations satisfactorily. Also, the PV system can operate at a lower voltage than the MPP voltage and still provide a constant power to the GTI during the transients using the proposed dc-dc converter controller. Figure 4.10 represents this case for an operating voltage below MPP. The advantage of operating in the latter region is the wider range of voltage variation; however, this region is less stable than the former.

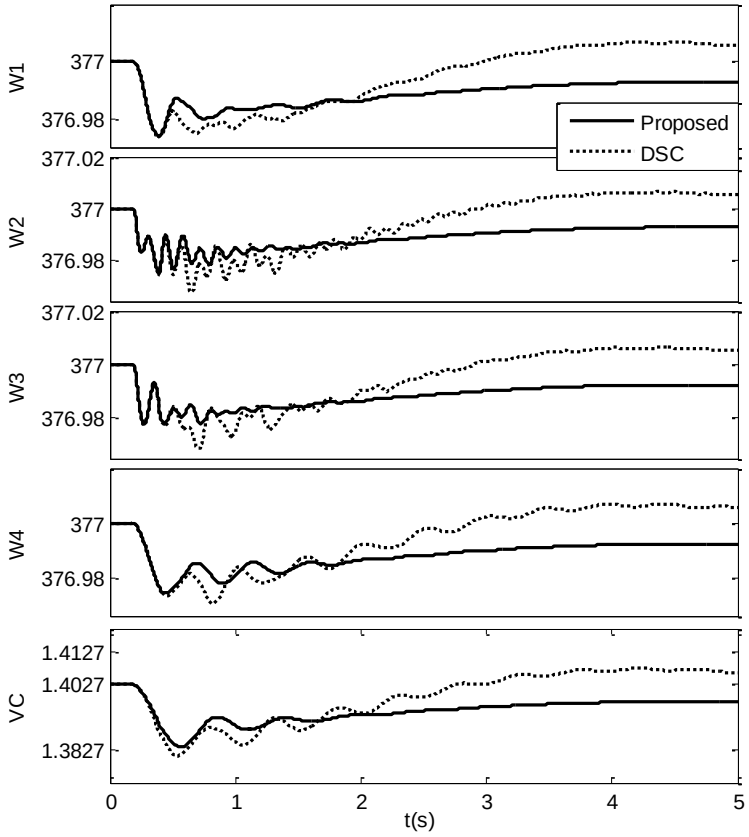


Fig. 4.6 Proposed stabilizer in comparison to DSC; $\omega_1$ to $\omega_4$ are the synchronous generators speed (rad/s), $V_C$ is the renewable generator capacitor voltage (pu); with fault at bus 6 and low load levels.

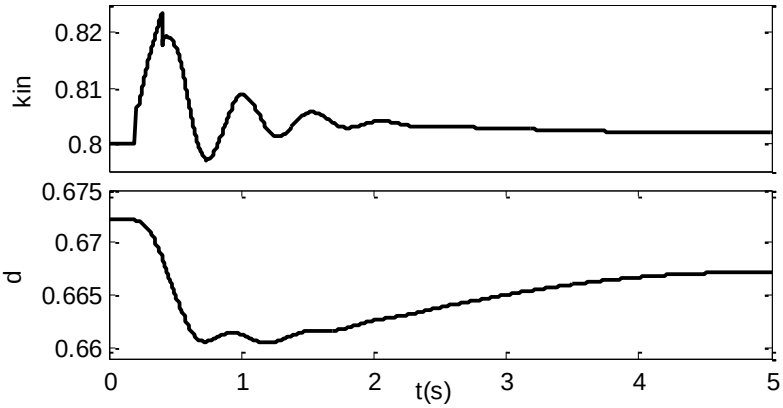


Fig. 4.7 GTI gains $k_{in}$ and buck converter duty cycle ($d$); proposed stabilizer with fault at bus 6 and low load levels.

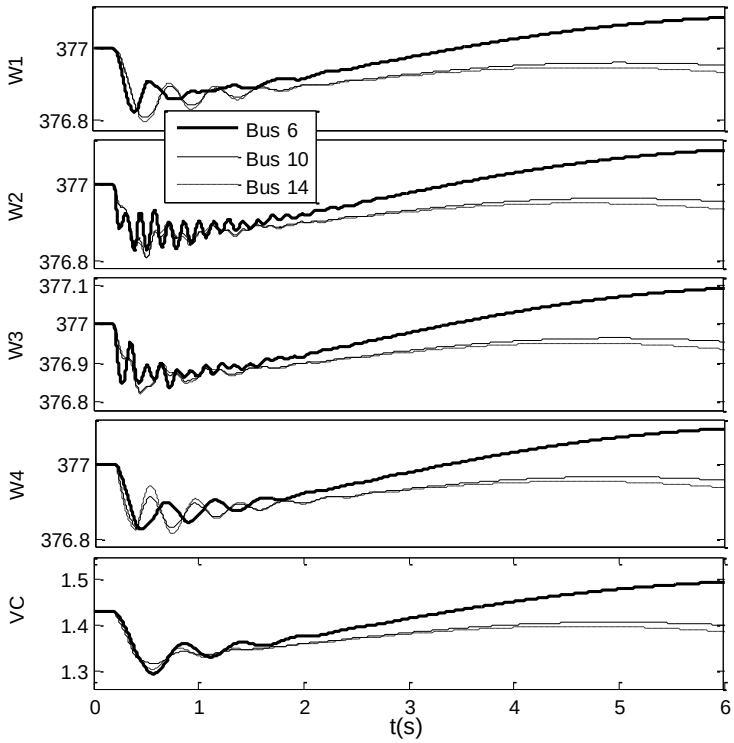


Fig. 4.8 Damping effects of the proposed stabilizer; $\omega_1$ to $\omega_4$ are the synchronous generators speed (rad/s), $V_C$ is the renewable generator capacitor voltage (pu); with faults at buses 6, 10, 14, high load levels, and severe disturbance.

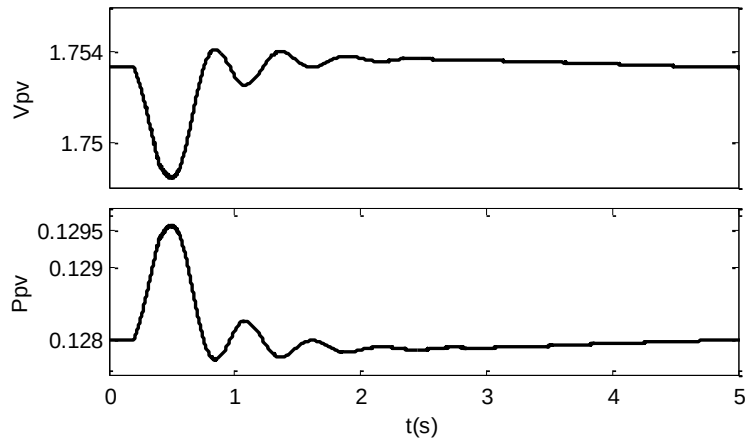


Fig. 4.9 Solar array buck converter input voltage and power (pu), with fault at bus 6 and low load levels when the solar voltage is higher than the maximum power point (MPP).

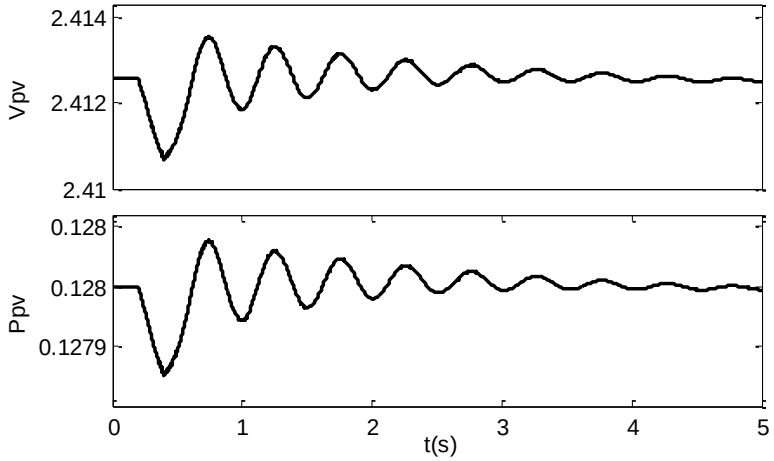


Fig. 4.10 Solar array buck converter input voltage and power (pu), with fault at bus 6 and low load levels when the solar voltage is lower than the maximum power point (MPP).

Next, the conventional droop control [1], [2], [28], [29] is applied to the GTI connected at bus 5 with parameters $K_p = 0.3$ and $K_I = 10$, while the dc-dc converter is controlled by controller (30). The performance of the proposed controller is then compared against the droop-based controller which uses P-ω and Q-V droop characteristics to generate frequency and voltage references for the inverter. The droop controller adjusts the inverter output voltage and phase angle to compensate for both active and reactive powers. According to Fig. 4.11, the droop controller has longer transients in stabilizing the generators speeds when compared to the

proposed controller. Moreover, in droop controller the dc-link capacitor voltage is not directly controlled which can lead to the capacitor voltage drift (when a large capacitor or battery storage is not utilized) as shown in Fig. 4.12 utilizing the dc-link capacitor of Table 4.1. Overall, the proposed adaptive neural network decentralized controller performs very well when compared to the available controllers.

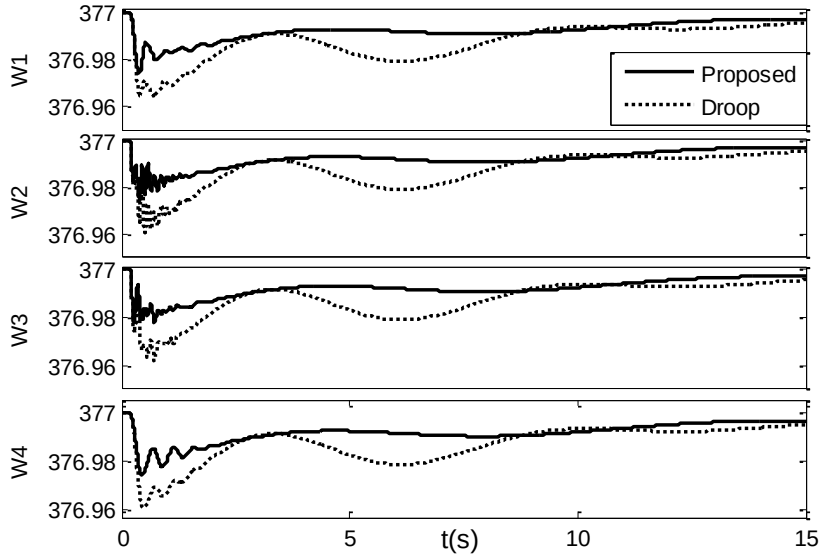


Fig. 4.11 Proposed stabilizer in comparison to droop controller; $\omega_1$ to $\omega_4$ are the synchronous generators speed (rad/s) with fault at bus 6 and low load levels.

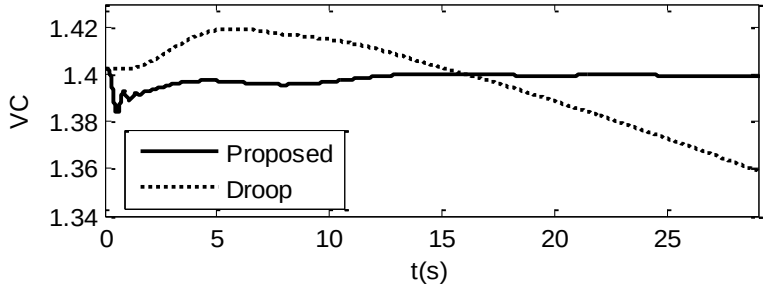


Fig. 4.12 Proposed stabilizer in comparison to droop controller; *VC* is the renewable generator dc-link capacitor voltage (pu) with fault at bus 6 and low load levels.

### 4.5 Conclusion

In this chapter the power system with penetration of renewable energy sources is modeled as a multi-generator power system and the inter-area oscillations is studied after a

disturbance has occurred. Through a novel modeling and decentralized control strategy for the renewable generators that dynamically controls the inverter gain and phase angle, as well as for the synchronous generators the overall grid stability is assured and proven in Appendix C. Simulation results on the IEEE 5-generator power system shows effectiveness of the proposed scheme in damping oscillations in the SG's frequencies and the GTI's capacitor voltage, that occur after disturbances. The proposed controller is shown to be more efficient compared to DSC and droop controllers.

### 4.6 References


[1] Y. A. R. I. Mohamed and E. F. El-Saadany, "Adaptive decentralized droop controller to preserve power sharing stability of paralleled inverters in distributed generation microgrids," *IEEE Transaction Power Electronics*, vol. 23, no. 6, pp. 2806–2816, 2008.

[2] J. C. Vasquez, J. M. Guerrero, A. Luna, P. Rodriguez, and R. Teodorescu, "Adaptive droop control applied to voltage-source inverters operating in grid-connected and islanded modes," *IEEE Transaction Industrial Electronics*, vol. 56, no. 10, pp. 4088–4096, 2009.

[3] A. Bidram, A. Davoudi, and R. S. Balog, "Control and circuit techniques to mitigate partial shading effects in photovoltaic arrays," *IEEE Journal of Photovoltaics*, vol. 2, no. 4, pp. 532–546, 2012.

[4] Y. C. Chen and A. D. Garcia, "A method to study the effect of renewable resource variability on power system dynamics," *IEEE Transaction Power Systems*, vol. 27, no. 4, pp. 1978–1989, 2012.

[5] D. Gautam, V. Vittal, and T. Harbour, "Impact of increased penetration of DFIG-based wind turbine generators on transient and small signal stability of power systems," *IEEE Transaction Power Systems*, vol. 24, no. 3,pp. 1426–1434, 2009.

[6] H.-P. Beck and R. Hesse, "Virtual synchronous machine," in *Proc. 9th Int. Conf. EPQU*, 2007, pp. 1–6

[7] Q.-C. Zhong and G. Weiss, "Synchronverters: Inverters that mimic synchronous generators," *IEEE Transaction Industrial Electronics*, vol. 58, no. 4, pp. 1259–1267, 2011.

[8] J. Driesen and K. Visscher, "Virtual synchronous generators," in *Proc. IEEE Power Energy Society General Meeting–Conversion and Delivery of Electrical Energy in the 21st Century*, July 2008, pp. 1–3.

[9] K. Visscher and S. W. H. De Haan, "Virtual synchronous machines (VSG's) for frequency stabilisation in future grids with a significant share of decentralized generation," in *Proc. IET-CIRED Semin. Smart-Grids Distrib.*, June 2008, pp. 1–4.

[10] S. D'Arco and J. A. Suul, "Virtual synchronous machines – classification of implementations and analysis of equivalence to droop controllers for microgrids," in *Proc. Power Tech. (POWERTECH), IEEE Grenoble*, pp. 1–7, 2013.

[11] M. P. N. van Wesenbeeck, S. W. H. de Haan, P. Varela, and K. Visscher, "Grid tied converter with virtual kinetic storage," *PowerTech, 2009 IEEE Bucharest*.

[12] V. Calderaro, G. Conio, V. Galdi, Giovanni Massa, and A. Piccolo, "Optimal decentralized voltage control for distribution systems with inverter-based distributed generators," *IEEE Transactions Power Systems*, vol. 29, no. 1, pp. 230–241, 2014.

[13] S. Xie, L. Xie, Y. Wang, and G. Guo, "Decentralized control of multi machine power systems with guaranteed performance", *Proc. of IEE Control Theory and Appls*, vol. 147, no. 3, pp. 355–365, 2000.

[14] W. Qiu, V. Vittal, and M. Khammash, "Decentralized power system stabilizer design using linear parameter varying approach", *IEEE Transaction Power Systems*, vol. 19, no. 4, pp. 1951–1960, 2004.

[15] G. E. Boukarim, S. Wang, J. H. Chow, G. N. Taranto and N. Martins, "A comparison of classical, robust, and decentralized control designs for multiple power system stabilizers," *IEEE Transaction Power Systems*, vol. 15, no. 4, pp. 1287–1292, 2000.

[16] S. Mehraeen, S. Jagannathan, and M. L. Crow, "Power system stabilization using adaptive neural network-based dynamic surface control," *IEEE Transaction Power Systems*, vol. 26, no. 2, pp. 669–680, 2011.

[17] B. Karimi, M.B. Menhaj, M. Karimi-Ghartemani, and I. Saboori, "Decentralized adaptive control of large-scale affine and nonaffine nonlinear systems," *IEEE Transaction Instrumentation and Measurement*, vol. 58, no. 8, pp. 2459–2467, 2009.

[18] J.T. Spooner and K.M. Passino, "Adaptive control of a class of decentralized nonlinear systems," *IEEE Transaction Automatic Control*, vol. 4 , no. 2, pp.280–284, 1996.

[19] S. Huang, K.K. Tan, and T.H. Lee, "Decentralized control design for large-scale systems with strong interconnections using neural networks," *IEEE Transaction Automatic Control*, vol. 48, no. 5, pp. 805–810, 2003.

[20] W. Liu, S. Jagannathan, G. K. Venayagamoorthy, D. C. Wunsch, M. L. Crow, L. Liu, and D. A. Cartes, "Neural network based decentralized controls of large scale power systems," *IEEE International Symposium on Intelligent Control,* pp. 676–681 Singapore, October 2007.

[21] P. W. Sauer and M. A. Pai, "*Power system dynamics and stability*," Stipes, 2000.

[22] A. Keyhani, "*Design of smart power grid renewable energy systems,*" John Wiley, 2011.

[23] R. C. N. Pilawa-Podgurski and D. J. Perreault, "Submodule integrated distributed maximum power point tracking for solar photovoltaic applications," *IEEE Transaction Power Electronics*, vol. 28, no. 6, pp. 2957–2967, 2013.

[24] G. R. Walker and P. C. Sernia, "Cascaded dc–dc converter connection of photovoltaic modules," *IEEE Transaction Power Electronics*, vol. 19, no. 4, pp. 1130–1139, 2004.

[25] N. Mohan, T. M. Undeland, and W. P. Robbins, *Power electronics: converters, applications, and design*, Wiley, 2002.

[26] C. S. Chiu and Y. L. Ouyang, "Robust maximum power tracking control of uncertain photovoltaic systems: A unified T-S fuzzy model-based approach," *IEEE Transaction Control Systems Technology*, vol. 19, no. 6, pp. 1516–1526, 2011.

[27] F. L. Lewis, S. Jagannathan, and A. Yesildirek, "Neural network control of robot. manipulators and nonlinear systems," Taylor & Francis, 1998.

[28] J. C. Vasquez, R. A. Mastromauro, J. M. Guerrero, and M. Liserre, "Voltage support provided by a droop-controlled multifunctional inverter," *IEEE Transaction Industrial Electronics*, vol. 56, no. 11, pp. 4510–4519, 2009.

[29] R. M. Kamel, A. Chaouachi and K. Nagasaka, "Three control strategies to improve the microgrid transient dynamic response during isolated mode: a comparative study," *IEEE Transaction Industrial Electronics,* vol. 60, no. 4, 2013

[30] J. M. Steele, "*The Cauchy-Schwarz master class: An introduction to the art of mathematical inequalities*," Maa Problem Books Series, The Mathematical Association of America, 2004.

# CHAPTER 5
# CONCLUSIONS AND FUTURE WORK

## 5.1 Conclusions

The interconnected ac/dc distribution system is represented as a class of interconnected, nonlinear systems with unknown dynamics.

The dc distribution system comprises several dc sources, here called subsystems, along with resistive and constant-power loads (CPLs.) Each subsystem includes a dc-dc converter (DDC) and exploits distributed energy resources (DERs) such as photovoltaic, wind, etc. Due to the power system frequent disturbances this system is prone to instability in the presence of the DDC dynamical components. On the other hand, designing a centralized controller may not be viable due to the distance between the subsystems (dc sources.)

In Chapter 2 the stability of the interconnected dc distribution system is enhanced through discrete-time decentralized adaptive nonlinear controller design that employs neural networks (NNs) to mitigate voltage and power oscillations after disturbances have occurred. The adaptive NN-based controller is introduced to overcome the unknown dynamics of each subsystem's converter and stabilize the entire grid, assuming that only the local measurements are available to each converter. The controller is tested in Matlab-Simulink to be evaluated in different load and source change conditions. The controller is able to mitigate the oscillations caused by different disturbances by adjusting the renewable sources power and stabilize the system in the new operating point. The controller is compared to droop controller and the results demonstrate more precise steady state response and significantly more noise rejection in the proposed method. In Chapter 3 output feedback controller is proposed which requires less information of the system than state feedback controller in which all state variables of the

subsystem are required. This controller is applied to IEEE 14-bus system in Simulink and its effectiveness has been evaluated in different conditions. This controller utilizes less information of the local system rather than the state feedback controller and estimates the unknown variables. As result, the output has more fluctuations in steady state and transient conditions in comparison to state feedback controller. The output has less fluctuation in comparison to droop controller.

In Chapter 4 the ac grid contained synchronous and renewable generators is investigated. A GTI is used to interface the renewable energy source to the grid in order to control the delivered power. In order to adjust the operating point of the PV generator, a dc-dc converter is incorporated to the system as an interface between the solar array and the GTI connecting the solar array to the power network. The interaction of the solar array dc-dc converter with the GTI is addressed. Simulation results show improved performance and stability of the proposed converter discrete-time controller over the conventional methods in the presence of the power system disturbance. The theoretical conjectures and simulation results of the controller imply that the converter input voltage and power as well as the inductor current are stabilized desirably at their initial set points, which verifies the accuracy of the converter discrete-time model and the effectiveness of the proposed discrete-time controller.

## 5.2 Recommendation of Future Work

The following recommendations are made for possible future research:

- Discrete-time adaptive neural network is a relatively new topic in the power system stability and control and hence further research be made on the update law and gain adjustment to improve its efficiency and effectiveness.

- The simulation scenarios be evaluated in the presence of protection equipment which have significant influence on the system operation specifically in severe disturbances.
- The system model be more general and developed to hybrid ac/dc distributed generation systems.
- The proposed controllers in both ac and dc systems be implemented in the lab and verified by experimental tests.

# APPENDIX A

Consider the overall Lyapunov function candidate $L = L_\theta + L_r$, where $L_\theta(k) = \sum_{i=1}^{n} \alpha_i^{-1} \tilde{\theta}_i^T(k)\tilde{\theta}_i(k)$ and $L_r(k) = \sum_{i=1}^{n} \left(r_i(k)/\sqrt{g_i(k-1)}\right)^2$. Using (20), the first difference of the Lyapunov function due to the first term is obtained as

$$\Delta L_\theta = \alpha_i^{-1} \left\| \tilde{\theta}_i(k) - \alpha_i \mu_i r_i(k+1) \right\|^2 - \alpha_i^{-1} \tilde{\theta}_i^T(k)\tilde{\theta}_i(k). \tag{A1}$$

Next, the first difference with respect to the second term in the Lyapunov function candidate is

$$\Delta L_r = \sum_{i=1}^{n} \left( \frac{r_i(k+1)}{\sqrt{g_i(\xi(k))}} \right)^2 - \sum_{i=1}^{n} \left( \frac{r_i(k)}{\sqrt{g_i(\xi(k-1))}} \right)^2. \tag{A2}$$

Substituting the filtered error (18) into (A2) and expanding the terms, one attains

$$\Delta L_r = \sum_{i=1}^{N} \Delta L_{r,i} = \sum_{i=1}^{n} \left( \sqrt{g_i(k)}(\tilde{\theta}_i^T \mu_i + \varepsilon_i + K_i r_i(k)) + \frac{\Delta_i(x(k))}{\sqrt{g_i(k)}} \right)^2 - \sum_{i=1}^{n} \left( \frac{r_i(k)}{\sqrt{g_i(k-1)}} \right)^2. \tag{A3}$$

Expanding the first difference of the overall Lyapunov function candidate $\Delta L = \Delta L_\theta + \Delta L_r$ results in

$$\Delta L \le \sum_{i=1}^{n} [g_i(k)\mu_i{}^T \tilde{\theta}_i(k)\tilde{\theta}_i(k)^T \mu_i + g_i(k)\varepsilon_i{}^2 + g_i(k)K_i{}^2 r_i(k) + \Delta_i(k)^2\, g_i(k)^{-1} + 2g_i(k)\tilde{\theta}_i(k)^T \mu_i \varepsilon_i$$

$$2g_i(k)\tilde{\theta}_i(k)^T \mu_i K_i r_i(k) + 2\tilde{\theta}_i(k)^T \mu_i \Delta_i + 2g_i(k)\varepsilon_i K_i r_i(k) + 2\varepsilon_i \Delta_i(k) + 2K_i r_i(k)\Delta_i(k)] - \sum_{i=1}^{n} \left( \frac{r_i(k)}{g_i(k-1)} \right)^2$$

$$+ \sum_{i=1}^{n} \left\{ \begin{array}{l} \alpha_i{}^{-1} \tilde{\theta}_i^T(k)\tilde{\theta}_i(k) + \alpha_i \mu_i{}^T \mu_i \left[ g_i(k) \left( \tilde{\theta}_i^T(k)\mu_i + \varepsilon_i + K_i\, r_i(k) \right) + \Delta_i(k) \right]^2 \\ -2\tilde{\theta}_i^T(k)\mu_i \left[ g_i(k) \left( \tilde{\theta}_i^T(k)\mu_i + \varepsilon_i + K_i\, r_i(k) \right) + \Delta_i(k) \right] \end{array} \right\} - \sum_{i=1}^{n} \alpha_i^{-1} \{\tilde{\theta}_i^T(k)\tilde{\theta}_i(k)\}. \tag{A4}$$

By applying Cauchy-Schwarz inequality [34] $(a_1 + a_2 + \cdots + a_n)^2 \le n(a_1{}^2 + a_2{}^2 + \cdots + a_n{}^2)$ and $\mu_i{}^T \tilde{\theta}_i \tilde{\theta}_i^T \mu_i = \tilde{\theta}_i^T \mu_i \mu_i{}^T \tilde{\theta}_i$, it yields

$$\Delta L \le \sum_{i=1}^{n}\begin{pmatrix}(2+g_i^{-1}(k)+4\alpha_i\|\mu_i\|^2)\Delta_i^{\,2}+(1+2g_i(k)+4\alpha_i\|\mu_i\|^2 g_i(k)^2)\varepsilon_i^{\,2}\\ +(1+2g_i(k)+4\alpha_i\|\mu_i\|^2 g_i(k)^2)K_i^{\,2}r_i^{\,2}\end{pmatrix}$$

$$-\sum_{i=1}^{n}\left(\frac{r_i(k)}{\sqrt{g_i(k-1)}}\right)^2-\sum_{i=1}^{n}\left(g_i(k)-4\alpha_i\|\mu_i\|^2 g_i(k)^2\right)\tilde{\theta}_i(k)^T\mu_i\mu_i^T\tilde{\theta}_i(k). \tag{A5}$$

Note that using Assumption 1, one has $\sum_{i=1}^{n}\beta_i|\Delta_i(x)|^2 \le$

$\sum_{i=1}^{n}\beta_i((n+1)\delta_{i0}^{\,2}+(n+1)\sum_{j=1}^{n}\gamma_{ij}^{\,2}r_j^{\,2})=\sum_{i=1}^{n}\beta_i(n+1)\delta_{i0}^{\,2}+\sum_{i=1}^{n}\sum_{j=1}^{n}\beta_j(n+1)\gamma_{ji}^{\,2}r_i^{\,2}$, where $\beta_i=\beta_i(x_i)$ is

an arbitrary real-valued function of $x_i$ for all $1\le i\le n$. Thus, (A5) becomes

$$\Delta L \le -\sum_{i=1}^{n}\begin{pmatrix}g_i(k-1)^{-1}-\sum_{j=1}^{n}\left[2+g_j(k)^{-1}+4\alpha_j\|\mu_j\|^2\right](n+1)\gamma_{ji}^{\,2}\\ -\left(1+2g_i(k)+4\alpha_i\|\mu_i\|^2 g_i(k)^2\right)K_i^{\,2}\end{pmatrix}r_i(k)^2-\sum_{i=1}^{n}\left(g_i(k)-4\alpha_i\|\mu_i\|^2 g_i(k)^2\right)\|\mu_i\|_{\max}^2\left\|\tilde{\theta}_i(k)\right\|^2$$

$$+\sum_{i=1}^{n}\left(\left(1+2g_i(k)+4\alpha_i\|\mu_i\|^2 g_i(k)^2\right)\varepsilon_i^{\,2}+\left(2+g_i(k)^{-1}+4\alpha_i\|\mu_i\|^2\right)(n+1)\delta_{0i}^{\,2}\right)$$

$$\le\sum_{i=1}^{n}-(C_{ir}r_i(k)^2+C_{i\theta}\left\|\tilde{\theta}_i(k)\right\|^2)-C_\varepsilon \tag{A6}$$

where

$$C_\varepsilon=\sum_{i=1}^{n}\left(\begin{pmatrix}1+2g_{i,\max}\\ +4\alpha_i\|\mu_i\|_{\max}^2\, g_{i,\max}^2\end{pmatrix}\varepsilon_{i,\max}^{\,2}+\left(2+g_{i,\min}^{\,-1}+4\alpha_i\|\mu_i\|_{\max}^2\right)(n+1)\delta_{0i}^{\,2}\right)$$

$$C_{ir}=g_{i,\max}^{\,-1}-\sum_{j=1}^{N}\left[2+g_{j,\min}^{\,-1}+4\alpha_j\left\|\mu_j\right\|_{\max}^2\right](n+1)\gamma_{ji}^{\,2}\;-\left(1+2g_{i,\max}+4\alpha_i\|\mu_i\|_{\max}^2\, g_{i,\max}^{\,2}\right)K_i^{\,2}$$

$$C_{i\theta}=\left(g_{i,\min}-4\alpha_i\|\mu_i\|_{\max}^2\, g_{i,\max}^{\,2}\right)\|\mu_i\|_{\max}^2. \tag{A7}$$

C Therefore, $\Delta L\le 0$ in (A6) provided the following conditions hold for all $1\le i\le n$

$$|r_i(k)|>\sqrt{C_\varepsilon/C_{ir}}\ \text{ or }\ \left\|\tilde{\theta}_i^T(k)\right\|>\sqrt{C_\varepsilon/C_{i\theta}}. \tag{A8}$$

This guaranties the boundedness of weight estimation errors, $\tilde{\theta}_i(k)$, and filtered error $r_i(k)$ which in turn show that states $\xi_i(k)$ are UUB according to the standard Lyapunov extension [35] for all $1 \le i \le n$ as explained. ■

Thus, the proposed NN controller guarantees that the closed-loop signals are UUB with the given bounds in (A7) and (A8). In order to have small errors, bound $C_\varepsilon$ must be reduced while $C_{ir}$ and $C_{i\theta}$ (for all $1 \le i \le n$) need to be increased. According to (A7), $C_\varepsilon$ depends on $\alpha_i$ and $\delta_{0i}$ whereas $C_{ir}$ and $C_{i\theta}$ depend on $K_i$, $\alpha_i$, and $\gamma_{ji}$ for all $1 \le i \le n$ and $1 \le j \le n$. Design gains $K_i$ and $\alpha_i$ are selected to be small positive constants while the interconnection bounds $\gamma_{ji}$ and $\delta_{0i}(1 \le i \le n; 1 \le j \le n)$ can be made small by utilizing high enough sampling frequency or adequately large output capacitors. Also, $C_\varepsilon$ can be further reduced by utilizing more NN hidden-layer neurons to obtain smaller NN function approximation error $\varepsilon_{i,\max}$ [29] (for all $1 \le i \le n$.) The NN approximation error can be made arbitrarily small provided an arbitrarily large number of hidden layer neurons are selected. However, to provide computational efficiency, here the NN hidden-layer neurons are limited to 10.

# APPENDIX B

The following theorem guaranties boundedness of the tracking errors, the NN weight estimation errors, and the state estimation errors.

*Theorem 2 (Decentralized NN Output Feedback Controller Stability):* Consider the nonlinear discrete-time interconnected system given by (4). Let the Assumptions 1 and 2 hold and that the desired trajectory $\xi_{md,i}$ (for all $1 \le i \le n$) and initial conditions for system (4) be bounded in the compact set $\Omega$. Let the subsystem states be estimated by observer (8) and unknown nonlinearities in each subsystem be approximated by a NN whose weight update is provided by (9). Also, let the control input be provided by a second NN whose update law is given by (15). Then, there exist a set of control gains $K_i$, $l_{1,i}$, $l_{2,i}$, $\alpha_{1,i}$, and $\alpha_{2,i}$ associated with the given NNs such that the tracking error $z_i(k)$, state estimation error $\tilde{\xi}_i(k)$ as well as the NNs weight estimation errors $\tilde{W}_{1,i}$ and $\tilde{W}_{2,i}$ are UUB for all $1 \le i \le n$.

Proof. Consider the overall Lyapunov function candidate $L = L_{\tilde{\xi}} + L_z + L_{W_1} + L_{W_2}$, where $L_{\tilde{\xi}}(k) = \sum_{i=1}^{n}\sum_{j=1}^{m}\eta_1 \tilde{\xi}_{j,i}(k)^2 + \sum_{i=1}^{n}\eta_1 \tilde{\xi}_{m,i}(k)^2$, $L_z(k) = \sum_{i=1}^{n}\sum_{j=1}^{m}\eta_2 \frac{j}{2} z_{j,i}(k)^2 + \sum_{i=1}^{n}\eta_2 \frac{m}{2} z_{m,i}(k)^2$, $L_{W_1}(k) = \sum_{i=1}^{n}\frac{\eta_3}{\alpha_{1,i}}\tilde{W}_{1,i}{}^T(k)\tilde{W}_{1,i}(k)$, and $L_{W_2}(k) = \sum_{i=1}^{n}\frac{\eta_4}{\alpha_{2,i}}\tilde{W}_{2,i}{}^T(k)\tilde{W}_{2,i}(k)$.

By using (17) and replacing the interconnection term $\Delta_i(\xi)^2$ using (7) in Assumption 1, Cauchy-Schwartz inequality [6] $(a_1 + a_2 + \cdots + a_n)^2 \le n(a_1{}^2 + a_2{}^2 + \cdots + a_n{}^2)$, and the fact that $\sum_{i=1}^{n}\sum_{j=1}^{n}\mu_{ij}{}^2\|z_j\|^2 = \sum_{i=1}^{n}\sum_{j=1}^{n}\mu_{ji}{}^2\|z_i\|^2$, the first term can be rewritten as

$$\Delta L_{\tilde{\xi}}(k) \le \sum_{i=1}^{n}\Big(-\eta_1 \tilde{\xi}_{1,i}{}^2(k) - \eta_1 \tilde{\xi}_{m,i}{}^2(k) + 6\eta_1 \left\|\tilde{W}_{1,i}(k)\varphi_i(\hat{M}_i(k))\right\|^2 + 6\eta_1 \|A_i\|^2$$

$$+ 6(n+1)\eta_1 \sigma_{0i}{}^2 + 6(n+1)\eta_1 \sum_{j=1}^{n} \mu_{ji}{}^2 \|z_i(k)\|^2\Big)$$

where $A_i = W_{1,i}^T \tilde{\varphi}_i - \varepsilon_{1,i}(M_i(k))$ and $\tilde{\varphi}_i = \varphi_i(\hat{M}_i(k)) - \varphi_i(\hat{M}_i(k))$.

Next, by substituting (14), $z_{m,i}(k+1) = \xi_{m,i}(k+1) - \xi_{md,i}(k+1)$, Cauchy-Schwartz inequality, and substituting the inter-connection terms the first difference of the Lyapunov function due to the second term becomes

$$\Delta L_z \le \sum_{i=1}^{n}\Big(-(\frac{\eta_2}{2} - 5m\eta_2(n+1)\sum_{j=1}^{n}\mu_{ji}{}^2)\|z_i(k)\|^2 - (\frac{m\eta_2}{2} - 5m\eta_2 g_i{}^2 K_i{}^2) z_{m,i}(k)^2$$
$$+ 5m\eta_2 (g_i{}^2 \left\|\tilde{W}_{2,i}^T \rho_i(\hat{Y}_i(k))\right\|^2 + \|S_i\|^2 + g_i{}^2 K_i{}^2 \tilde{\xi}_{m,i}(k)^2 + (n+1)\sigma_{i0}{}^2)$$

where $S_i = g_i(\bar{x}_i(k))\left(W_{2,i}^T \tilde{\rho}_i - \varepsilon_{2,i}(Y_i(k))\right)$ and $\tilde{\rho}_i = \rho_i(\hat{Y}_i(k)) - \rho_i(Y_i(k)$.

Moreover, by using (11) and Cauchy-Schwartz inequality the first difference of the Lyapunov function due to the third term becomes

$$\Delta L_{W1}(k) \le \eta_3 \sum_{i=1}^{n}\Big(3\alpha_{1,i}\left\|\varphi_i(\hat{M}_i(k))\right\|^2 \left\|\tilde{W}_{1,i}{}^T(k)\varphi_i(\hat{M}_i(k))\right\|^2 + 3\alpha_{1,i}\left\|\varphi_i(\hat{M}_i(k))\right\|^2 \left\|W_{1,i}{}^T(k)\varphi_i(\hat{M}_i(k))\right\|^2$$
$$+ 3\alpha_{1,i} l_{1,i}{}^2 \left\|\varphi_i(\hat{M}_i(k))\right\|^2 \tilde{\xi}_{1,i}{}^2 - \left\|\tilde{W}_{1,i}{}^T(k)\varphi_i(\hat{M}_i(k))\right\|^2 + 2\left\|W_{1,i}{}^T(k)\varphi_i(\hat{M}_i(k))\right\|^2 + 2 l_{1,i}{}^2 \tilde{\xi}_{1,i}{}^2\Big)$$

In addition, by using (16) and Cauchy-Schwartz inequality the first difference of the Lyapunov function due to the fourth term is given by

$$\Delta L_{W2}(k) \le \eta_4 \sum_{i=1}^{n}\Big(3\alpha_{2,i}\left\|\rho_i(\hat{Y}_i(k))\right\|^2 \left\|\tilde{W}_{2,i}{}^T(k)\rho_i(\hat{Y}_i(k))\right\|^2 + 3\alpha_{2,i}\left\|\rho_i(\hat{Y}_i(k))\right\|^2 \left\|W_{2,i}{}^T(k)\rho_i(\hat{Y}_i(k))\right\|^2$$
$$+ 3\alpha_{2,i} l_{2,i}{}^2 \left\|\rho_i(\hat{Y}_i(k))\right\|^2 z_{1,i}{}^2 - \left\|\tilde{W}_{2,i}{}^T(k)\rho_i(\hat{Y}_i(k))\right\|^2 + 2\left\|W_{2,i}{}^T(k)\rho_i(\hat{Y}_i(k))\right\|^2 + 2 l_{2,i}{}^2 z_{1,i}{}^2\Big)$$

The overall first difference of the Lyapunov function is

$$\Delta L = \Delta L_{\tilde{\xi}} + \Delta L_z + \Delta L_{W_1} + \Delta L_{W_2} \leq \tag{A1}$$

$$\sum_{i=1}^{n} -[B_{\tilde{\xi},i}\tilde{\xi}_{1,i}(k)^2 + B_{\tilde{\xi}m,i}\tilde{\xi}_{m,i}(k)^2 + B_{z,i}\|z_i(k)\|^2 + B_{zm,i}\|z_{m,i}(k)\|^2$$
$$+ B_{W_1,i}\|\tilde{W}_{1,i}{}^T(k)\varphi_i(\hat{M}_i(k))\|^2 + B_{W_2,i}\|\tilde{W}_{2,i}{}^T(k)\rho_i(\hat{Y}_i(k))\|^2 - B_{C,i}]$$

with

$$B_{\tilde{\xi},i} = \eta_1 - 3\alpha_{1,i}\eta_3 l_{1,i}{}^2\|\varphi_i(\hat{M}_i(k))\|_{\max}^2 - 2\eta_3 l_{1,i}{}^2$$

$$B_{\tilde{\xi}m,i} = \eta_1 - 5m\eta_2 K_i{}^2 g_{\max,i}^2$$

$$B_{z,i} = \frac{\eta_2}{2} - 5m\eta_2(n+1)\sum_{j=1}^{n}\mu_{ji}{}^2 - 6\eta_1(n+1)\sum_{j=1}^{n}\mu_{ji}{}^2 - 2\eta_4 l_{2,i}{}^2 - 3\eta_4\alpha_{2,i}l_{2,i}{}^2\|\rho_i(\hat{Y}_i(k))\|_{\max}^2$$

$$B_{zm,i} = \frac{m\eta_2}{2} - 5m\eta_2 K_i{}^2 g_{\max,i}^2$$

$$B_{W_1,i} = \eta_3 - 6\eta_1 - 3\eta_3\alpha_{i1}\|\varphi_i(\hat{M}_i(k))\|_{\max}^2$$

$$B_{W_2,i} = \eta_4 - 3\eta_4\alpha_{2,i}\|\rho_i(\hat{Y}_i(k))\|_{\max}^2 - 5m\eta_2 g_{\max,i}^2$$

$$B_{C,i} = (n+1)(6\eta_1 + 5m\eta_2)\sigma_{0i}{}^2 + 6\eta_1 A_{\max,i}^2 + 5m\eta_2 S_{\max,i}^2$$
$$+ (3\eta_3\alpha_{1,i}\|\varphi_i(\hat{M}_i(k))\|_{\max}^2 + 2\eta_3)\omega_{1,i}{}^2 + (3\eta_4\alpha_{2,i}\|\rho_i(\hat{Y}_i(k))\|_{\max}^2 + 2\eta_4)\omega_{2,i}{}^2$$

where $\omega_{1,i} = \max_{\Omega}\|W_{1,i}^T\varphi_i\|$, $\omega_{2,i} = \max_{\Omega}\|W_{2,i}^T\rho_i\|$, $S_{\max,i} = \max_{\Omega}\|S_i\|$,

and $A_{\max,i} = \max_{\Omega}\|A_i\|$.

The coefficients in (A1) are defined in the following by selecting $\eta_1 = 1$, $\eta_2 = 2$ , $\eta_3 = 7$, and

$\eta_4 > 10ng_{\max,i}^2$ as

$$B_{\tilde{\xi},i} = 1 - 21\alpha_{1,i} {l_{1,i}}^2 \left\| \varphi_i(\hat{M}_i(k)) \right\|_{\max}^2 - 6{l_{1,i}}^2$$

$$B_{\tilde{\xi}m,i} = 1 - 10m{K_i}^2 g_{\max,i}^2$$

$$B_{z,i} = 1 - 10m(n+1)\sum_{j=1}^{n} {\mu_{ji}}^2 - 6(n+1)\sum_{j=1}^{n} {\mu_{ji}}^2 - 2\eta_4 {l_{2,i}}^2 - 3\eta_4 \alpha_{2,i} {l_{2,i}}^2 \left\| \rho_i(\hat{Y}_i(k)) \right\|_{\max}^2$$

$$B_{zm,i} = m - 10m{K_i}^2 g_{\max,i}^2$$

$$B_{W_1,i} = 1 - 21\alpha_{i1} \left\| \varphi_i(\hat{M}_i(k)) \right\|_{\max}^2$$

$$B_{W_2,i} = \eta_4 - 3\eta_4 \alpha_{2,i} \left\| \rho_i(\hat{Y}_i(k)) \right\|_{\max}^2 - 10m g_{\max,i}^2$$

$$B_{C,i} = (n+1)(6+10m){\sigma_{0i}}^2 + 6A_{\max,i}^2 + 10mS_{\max,i}^2 + (21\alpha_{1,i} \left\| \varphi_i(\hat{M}_i(k)) \right\|_{\max}^2 + 14){\omega_{1,i}}^2$$
$$+ (3\eta_4 \alpha_{2,i} \left\| \rho_i(\hat{Y}_i(k)) \right\|_{\max}^2 + 2\eta_4){\omega_{2,i}}^2$$

Then, $\Delta L \le 0$ in (A1) provided the following conditions hold for all $1 \le i \le n$

$$\left|\tilde{\xi}_{1,i}(k)\right| > \sqrt{\frac{B_{C,i}}{B_{\tilde{\xi},i}}} \vee \left|\tilde{\xi}_{m,i}(k)\right| > \sqrt{\frac{B_{C,i}}{B_{\tilde{\xi}m,i}}} \vee \quad \left\|z_i(k)\right\| > \sqrt{\frac{B_{C,i}}{B_{z,i}}} \vee \left|z_{m,i}(k)\right| > \sqrt{\frac{B_{C,i}}{B_{zm,i}}} \vee \tag{A2}$$

$$\left\|\tilde{W}_{1,i}{}^T(k)\varphi_i(\hat{M}_i(k))\right\| > \sqrt{\frac{B_{C,i}}{B_{W_1,i}}} \vee \left\|\tilde{W}_{2,i}{}^T(k)\rho_i(\hat{Y}_i(k))\right\| > \sqrt{\frac{B_{C,i}}{B_{W_2,i}}}$$

where "$\vee$" denotes "or" operator.

The interconnection terms $\sigma_{0i}$ and $\mu_{ij}$ (for all $1 \le i \le n$ and $1 \le j \le m$) are weak in nature and can be made small by utilizing high enough sampling frequency or adequately large output capacitors. Consequently, the bound shown in (A2) can be reduced by selecting design gains $l_{1,i}$, $l_{2,i}$, $\alpha_{1,i}$, $\alpha_{2,i}$, and $K_i$ appropriately.

This guaranties the boundedness of weight estimation errors, $\tilde{W}_{1,i}(k), \tilde{W}_{2,i}(k)$, and tracking error $z_i(k)$ as well as the state estimation error $\tilde{\xi}_i(k)$ are UUB [7] with the given bounds in (19).

# APPENDIX C

By replacing $u_i$ from (21) in (17), the filtered error dynamic becomes

$$\dot{r}_i = f_i + g_i(-\frac{f_i + a_i}{g_i} + r_i \hat{W}_i^T \Phi_i - K_i r_i) + a_i + \Delta_i(X) \tag{A1}$$

by adding and subtracting $u_{id}$, (A1) can be rewritten as

$$\dot{r}_i = f_i + g_i(-\frac{f_i + a_i}{g_i} + r_i \hat{W}_i^T \Phi_i - K_i r_i + u_{di} - u_{di}) + a_i + \Delta_i(X). \tag{A2}$$

Next, from (19) and (20)

$$\dot{r}_i = f_i + g_i(-\frac{f_i + a_i}{g_i} + r_i \hat{W}_i^T \Phi_i - K_i r_i - \frac{f_i + a_i}{g_i} - h_i r_i + \frac{f_i + a_i}{g_i} - r_i W_i^{*T} \Phi_i - r_i \varepsilon_i) + a_i + \Delta_i(X)$$

$$= g_i(r_i \tilde{W}_i^T \Phi_i - K_i r_i - h_i r_i - r_i \varepsilon_i) + \Delta_i(X) \tag{A3}$$

Consider the overall Lyapunov function candidate $V = V_r + V_W$, where $V_r = \sum_{i=1}^{n} r_i^2 / 2g_i$ and

$V_W = \sum_{i=1}^{n} (\tilde{W}_i^T \tilde{W}_i) / (2\rho_i)$. The derivative of the first term in the Lyapunov function becomes

$$\dot{V}_{ri} = (r_i \dot{r}_i)/g_i - (\dot{g}_i r_i^2)/(2g_i^2) \tag{A4}$$

Replacing $\dot{r}_i$ from (A3)

$$\dot{V}_{ri} = -r_i^2 \tilde{W}_i^T \Phi_i - K_i r_i^2 - (\dot{g}_i r_i^2)/(2g_i^2) + (r_i \Delta_i)/g_i - h_i r_i^2 - r_i^2 \varepsilon_i$$
$$\leq -r_i^2 \tilde{W}_i^T \Phi_i - K_i r_i^2 + r_i^2 \varepsilon_{Mi} + |\dot{g}_i| r_i^2 / (2g_i^2) - h_i r_i^2 + |r_i \Delta_i| / g_i$$

$$\leq -r_i^2 \tilde{W}_i^T \Phi_i - K_i r_i^2 + r_i^2 \varepsilon_{Mi} - h_i r_i^2 + |\dot{g}_i| r_i^2 / (2g_i^2) + |r_i \Delta_i| / g_i \tag{A5}$$

Next, according to (A2) and (A3)

$$\dot{V}_{ri} \leq -r_i^2 (\tilde{W}_i^T \Phi_i + K_i - \varepsilon_{Mi} + h_i) + |\dot{g}_i| r_i^2 / (2g_i^2) + |r_i| / g_i \sum_{j=1}^{n} \eta_{ij} |r_j|$$

By applying Cauchy-Schwarz inequality [30] $(a_1 + a_2 + \cdots + a_n)^2 \leq n(a_1^2 + a_2^2 + \cdots + a_n^2)$, it yields

$$\dot{V}_{ri} \le -r_i^2 \tilde{W}_i^T \Phi_i - K_i r_i^2 + r_i^2 \varepsilon_{Mi} - h_i r_i^2 + g_{d\max,i} r_i^2 / 2g_i^2 + n r_i^2 / 2g_i^2 + 1/2 \sum_{j=1}^n \eta_{ij}^2 r_j^2$$

then $\sum_{i=1}^n \dot{V}_{ri}$ is written as

$$\sum_{i=1}^n \dot{V}_{ri} \le \sum_{i=1}^n [-r_i^2 \tilde{W}_i^T \Phi_i - K_i r_i^2 + r_i^2 \varepsilon_{Mi} - h_i r_i^2$$
$$+ r_i^2 / 2g_i^2 (g_{d\max,i} + n) +] + 1/2 \sum_{i=1}^n \sum_{j=1}^n \eta_{ij}^2 r_j^2 \qquad \text{.(A6)}$$

The last term can be rewritten as

$$\sum_{i=1}^n \sum_{j=1}^n \eta_{ij}^2 r_j^2 = \sum_{j=1}^n \sum_{i=1}^n \eta_{ji}^2 r_i^2 = \sum_{i=1}^n \sum_{j=1}^n \eta_{ji}^2 r_i^2$$

And consequently

$$\sum_{i=1}^n \dot{V}_{ri} \le \sum_{i=1}^n -r_i^2 (\tilde{W}_i^T \Phi_i + K_i - \varepsilon_{Mi} + h_i - \frac{g_{d\max,i} + n}{2g_i^2} - \frac{1}{2} \sum_{j=1}^n \eta_{ji}^2) \ .$$

Using the neural network weight update law (25) the derivative of the Lyapunov function due to the neural network weights is obtained as

$$\dot{V}_{Wi} = 1/2\rho_i (\tilde{W}_i^T \dot{\tilde{W}}_i + \dot{\tilde{W}}_i^T \tilde{W}_i) = \tilde{W}_i^T \dot{\tilde{W}}_i / \rho_i = \tilde{W}_i^T \dot{\hat{W}}_i / \rho_i$$

$$= \tilde{W}_i^T (-\rho_i r_i^2 \dot{\hat{W}}_i + \rho_i r_i^2 \Phi_i) / \rho_i = r_i^2 (\tilde{W}_i^T \Phi_i - \tilde{W}_i^T (W_i^* + \tilde{W}))$$

From the inequality $\tilde{W}_i^T W_i^* \le \tilde{W}_i^T \tilde{W}_i + W_i^{*T} W_i^*$

$$\dot{V}_{Wi} \le r_i^2 \tilde{W}_i^T \Phi_i - r_i^2 W_i^{*T} W_i^*$$

the derivative of the overall Lyapunov function candidate is

$$\dot{V} = \sum_{i=1}^n \dot{V}_{ri} + \sum_{i=1}^n \dot{V}_{Wi} \le \sum_{i=1}^n \ -r_i^2 (\tilde{W}_i^T \Phi_i + K_i - \varepsilon_{Mi} + h_i - \frac{g_{d\max,i} + n}{2g_i^2} - \frac{1}{2} \sum_{i=1}^n \eta_{ji}^2)$$
$$+ \sum_{i=1}^n r_i^2 (\tilde{W}_i^T \Phi_i - W_i^{*T} W_i^*)$$

Now define $h_i$ as $h_i = (g_{d\max,i} + n) / 2g_i^2 + 1/2 \sum_{i=1}^n \gamma_{ji}^2$ then $\dot{V} \le \sum_{i=1}^n -r_i^2 (K_i - \varepsilon_{Mi} + \left\| W_i^* \right\|_{\max}^2)$.

Therefore, semi-negative definite $\dot{V}$ (lacking the NN weight estimations errors) only guaranties boundedness of the states. Next, with the use of Barballat's lemma [27] the local asymptotic stability of the filtered error $r_i(k)$ can be proven, which in turn shows that states $\xi_i(k)$ are locally asymptotically stable according to the standard Lyapunov extension [27] for all $1 \leq i \leq n$.

# VITA

Shaghayegh Kazemlou was born in 1984 in Iran. She received the B.S. and M.S. degrees in electrical engineering from Sharif University of Technology, Tehran, Iran in 2007 and 2010, respectively, and the M.S. degree in electrical engineering from Louisiana State University, Baton Rouge, LA, USA, in 2013, where she is currently pursuing the Ph.D. degree. Her current research interests include renewable energies, power system stability, and nonlinear control of dynamic systems.